A Comparative Evaluation of Five Tire Traction Models

INTERIM DOCUMENT 6

by

John T. Tielking
Naveen K. Mital

January 1974

Highway Safety Research Institute / University of Michigan

BIBLIOGRAPHIC DATA SHEET	1. Report No. UM-HSRI-PF-74-2	2.	3. Recipient's Accession No.
4. Title and Subtitle A COMPARATIVE EVALUATION OF FIVE TIRE TRACTION MODELS			5. Report Date January 1974 6.
7. Author(s) J.T. Tielking and N.K. Mital			8. Performing Organization Rept. No. UM-HSRI-PF-74-2
9. Performing Organization Name and Address Highway Safety Research Institute University of Michigan Huron Parkway and Baxter Road Ann Arbor, Michigan 48105			10. Project/Task/Work Unit No. 11. Contract/Grant No.
12. Sponsoring Organization Name and Address Motor Vehicle Manufacturers Association 320 New Center Building Detroit, Michigan 48202			13. Type of Report & Period Covered 14.

15. Supplementary Notes

Interim Document 6: Tire Traction Characteristics Affecting Vehicle Performance

16. Abstracts

Five tire models which have the capability of simulating tire traction forces and aligning moment in response to combined longitudinal and lateral wheel slip (braking and steering) are evaluated in a new set of coordinates designed to simplify the closed-form algebraic traction force and moment expressions. The traction responses of the five tire models are compared and the effects of various assumptions made in the derivation of each model are discussed. A chapter is devoted to tire testing for model input data. Digital computer programs are included.

17. Key Words and Document Analysis. 17a. Descriptors

17b. Identifiers/Open-Ended Terms

17c. COSATI Field/Group

18. Availability Statement	19. Security Class (This Report)	21. No. of Pages
UNLIMITED	UNCLASSIFIED	162
	20. Security Class (This Page) UNCLASSIFIED	22. Price

A COMPARATIVE EVALUATION OF FIVE TIRE TRACTION MODELS

John T. Tielking
Naveen K. Mital

Project 329180

Tire Traction Characteristics
Affecting Vehicle Performance

Document 6

January 1974

Sponsored by

The Motor Vehicle Manufacturers Association

PREFACE

The study of tire traction models contained in this document was conducted as part of an ongoing tire research project entitled "Tire Traction Characteristics Affecting Vehicle Performance," sponsored by the Motor Vehicle Manufacturers Association. A primary objective of this research project is to develop a mathematical model capable of predicting the significant mechanical performance characteristics of the pneumatic tire from basic design and operating variables.

The research reported herein was conducted to gain a thorough understanding of the development and operation of recently published tire traction models. A systematic set of definitions for the operating variables describing tire orientation, motion, and shear force generation was developed in the framework of a system of tire and contact region coordinates defined to facilitate tire model study. Four published tire models are recast in this new coordinate system and rederived with the common set of operating variable definitions. A fifth tire model is derived by a change of pressure distribution. The tire model responses to a common set of tire characterizing data and operating variable ranges are compared and the effects of various assumptions made during model derivation are identified.

Because of the variations found in the response of the five tire models to the same input data, comparison with experimental data was not attempted in this document. The next stage of this tire research effort will be concerned with a quantitative validation of the various tire models with measured tire traction data.

TABLE OF CONTENTS

INTRODUCTION

The models analyzed in this document were recently developed for the simulation of tire traction characteristics produced by tire-road interfacial shear forces. Some of the models have the capability of simulating aligning moment in addition to the traction forces. Although the publication of a tire traction model always includes a comparison of its response with measured tire data, there is no discussion on the relative merits of the new model compared with previous ones. This should not be considered a defect in the literature as each model, in attempting to simulate certain aspects of tire behavior, contains a number of simplifying and sometimes indefensible assumptions. It should be recognized that a tire model is, of necessity, designed with a particular application in mind. This document is not written to declare one model superior over all others, but to present all of the models in a common format and to compare the response of each model to the others with the objective of identifying the effects of the various assumptions made during derivation. It is hoped that this document will facilitate the task of sifting through the literature to determine an adequate tire traction model for a particular application.

COORDINATE SYSTEMS

It is unfortunate that no standardized coordinate system suitable for tire traction work has been agreed upon. A tire axis system has been adopted by SAE [1][1] for inclusion in a

---

[1]Figures in brackets indicate literature references on page 107.

standardized vehicle dynamics terminology. This vehicle-oriented tire axis system ignores tire deformation and presumes a point rather than finite contact area. The SAE axis system, which originates at a hypothetical "center of tire contact," will be slightly modified in this document for use as a reference frame in the description of tire orientation, motion, and resultant traction force components.

For the study of tire traction, which involves a finite contact region whose location (with respect to the rigid wheel) and area are dependent upon tire operating variables, a separate coordinate system must be defined for the description of events taking place in the contact region. Since the contact region distortions associated with tire traction are very complex, it is important to adopt a contact coordinate system which will facilitate the derivation of traction equations and minimize their complexity. The contact coordinates which are introduced in Figure 1 result from a study of many tire models. They considerably simplify the description of tire contact distortion and shear force generation. The models analyzed in this document have been rederived in this new set of coordinates.

Figure 1 depicts an inclined tire rolling at a slip angle α. Point C, in Figure 1, lies on the road surface at the center of tire contact[2] as defined by SAE [1]. The wheel diameter passing through C is inclined from vertical at an angle γ.

---

[2]The center of tire contact is defined to be the intersection of the wheel plane and the vertical projection of the wheel axis onto the road plane.

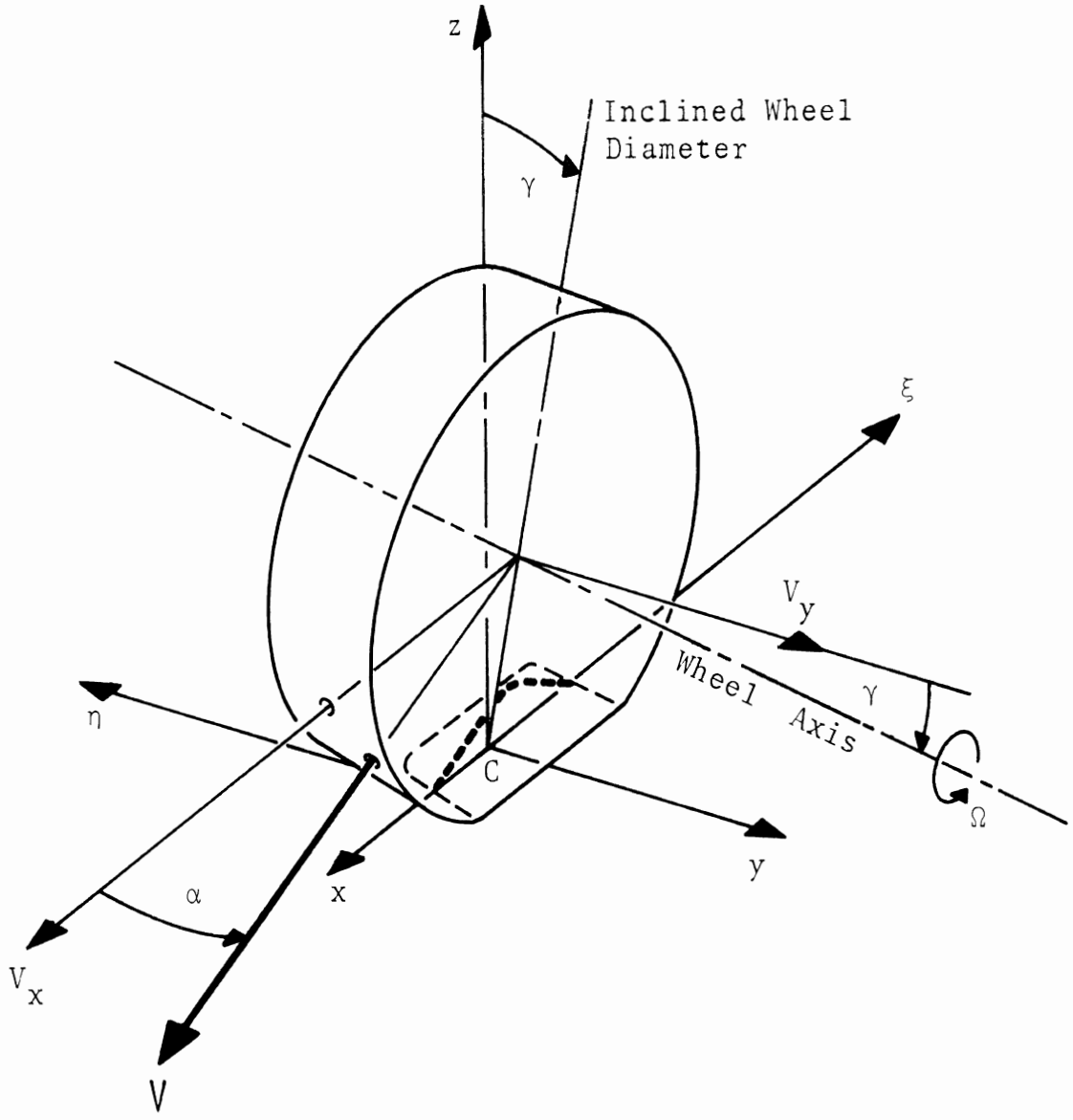

Figure 1. Tire coordinates (x,y,z) and contact coordinates (ξ,η).

Steady-state rolling of a uniform tire is presumed so that it will not be necessary to distinguish between moving and inertial coordinates. The tire coordinate system (x,y,z) originates at point C with x-y in the road plane and the z-axis vertical upward. The wheel velocity components V_x and V_y are positive in the directions of the x and y axes. The slip angle α, measured from the x-axis to the direction of travel, is positive as shown in Figure 1. Except for orientation (z-axis positive upward) the tire coordinate system (x,y,z) in Figure 1 is equivalent to the SAE tire axis system (X', Y', Z' in Fig. 1 of [1]). The slip angle α and the inclination angle γ are SAE positive.

The contact coordinates (ξ,η) originate on the carcass equator at the point directly above the leading edge of the free-rolling contact area. The ξ-axis runs rearward along the carcass equator and is allowed to deform with it. For the models considered in this document, the carcass equator is presumed flat and rigid in the contact region although able to translate laterally and longitudinally. The contact coordinates will translate with the carcass; the ξ-η plane remaining parallel with the road.

The deformation of the tread rubber with respect to the tire carcass will be described in the ξ,η coordinate system. The deformation of the carcass with respect to the center of tire contact is given by the relationship of the contact coordinates (ξ,η) to the tire coordinates (x,y). The use of an independent contact coordinate system (ξ,η) thus allows separation of the influence of the tread rubber from the influence of carcass compliance on tire traction.

GENERAL KINEMATICS

In Figure 1, the direction of wheel travel is indicated by the velocity vector $\mathbf{V}$. Lateral tire motion is produced by constraining the wheel plane to move at an angle α to the direction of travel. The travel velocity then has two components in the x,y coordinate system defined in the previous section. The longitudinal component, $V_x = |\mathbf{V}|\cos\alpha$, is composed of the wheel rolling velocity V_r and the velocity V_{cx} produced by longitudinal elastic slip and sliding in the contact region. The lateral component, $V_y = |\mathbf{V}|\sin\alpha$, is due entirely to lateral elastic slip or sliding and is generally termed the lateral slip velocity V_{cy}. The tire slip velocity vector, $\mathbf{V}_c$ shown in Figure 2, is defined by the slip velocity components V_{cx} and V_{cy}.

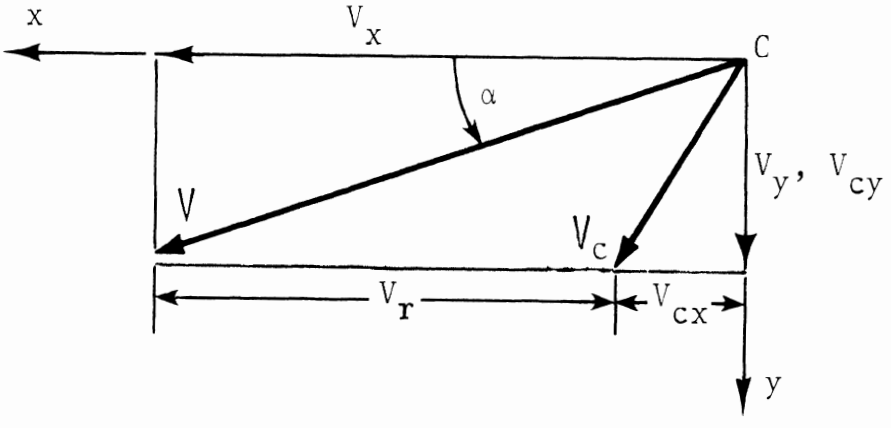

Figure 2. Kinematics of tire motion with braking applied.

It is important to distinguish between the terms slip and sliding as used in tire terminology. Slip is here defined as tire motion not due to rolling. Two independent phenomena contribute to slip. Perhaps the least-understood (in the kinematic sense) contribution is elastic deformation in the forward part of the contact region. The tire carcass and attached tread comprise a highly deformable structure. As braking is applied to the rolling tire, the contact region moves rearward and the tire material entering contact begins to elongate. The elongation of the contacting material contributes a slip speed V_{cx} which becomes a certain percentage of the longitudinal velocity V_x. In the forward part of the contact region, the elastic deformation is produced by the tread elements adhering to the road surface. However, a point is reached where the available friction force is insufficient to balance the elastic deformation force and sliding begins contributing to the slip speed as the elongation contribution is reduced. Pure sliding with velocity V_{cx} exists at the rear of the contact region. The contact deformations during braking are clearly seen in the photographs shown in Figures 7.2.60-62 of reference [2].

The preceding discussion concerns straight ahead motion. If the tire is moving at a slip angle α, as shown in Figure 1, a lateral component of velocity arises which is due purely to slip. The elastic deformation is indicated by the path of the tread equator contact line shown dotted in Figure 1. In the adhesion area, the equator contact line parallels the direction of motion.

As sliding begins, the tread equator begins to return to its undeformed position. The net result of this unsymmetric contact region distortion is lateral tire motion with velocity V_{cy}.

When the tire is free-rolling, the rolling velocity is equal to the wheel plane velocity V_x.

$$V_r = V_x \quad \text{(free-rolling)} \tag{1}$$

It is advantageous to define an effective rolling radius R_e as the ratio of the free-rolling velocity to the wheel spin velocity Ω.

$$R_e \equiv V_r/\Omega \quad \text{(free-rolling)} \tag{2}$$

Experiments show that the effective rolling radius lies somewhere between the static loaded and unloaded radii. With the definition of effective rolling radius, the rolling velocity for all braking and driving torque applications can be determined from the resulting spin velocity.

$$V_r = \Omega R_e \tag{3}$$

When braking is applied, the longitudinal velocity and the rolling velocity are reduced by a certain amount each instant in time. Due to elastic deformation and sliding in the contact region, V_x decreases by a lesser amount. The difference is the longitudinal slip velocity V_{cx} shown in Figure 2 at a certain instant in time.

$$V_{cx} = V_x - V_r \tag{4}$$

If driving torque is applied, elastic deformation and sliding cause the rolling velocity to exceed the longitudinal velocity and V_{cx} becomes negative.

It is convenient to define a parameter s_x as the fraction of longitudinal velocity which indicates the amount of braking or driving torque applied.

$$s_x \equiv V_{cx}/V_x \tag{5}$$

This parameter, called the longitudinal slip parameter, may exhibit the following range of values.

$$s_x \begin{cases} = 1 & \text{locked wheel} \\ < 1 & \text{braking traction} \\ = 0 & \text{free-rolling} \\ < 0 & \text{driving traction} \end{cases}$$

By use of Equations (4) and (3), the definition of s_x may be expressed as

$$s_x = 1 - V_r/V_x = 1 - \Omega R_e/V_x$$

Also useful is Equation (6) obtained by eliminating V_x from Equations (4) and (5).

$$\frac{V_{cx}}{V_r} = \frac{s_x}{1-s_x} \tag{6}$$

Analogous to the longitudinal slip parameter, the lateral slip parameter s_y is defined to be

$$s_y \equiv V_{cy}/V_x = \tan\alpha \tag{7}$$

where V_{cy} is the lateral slip velocity shown in Figure 2. Eliminating V_{cx} from Equations (4) and (5), and substituting the resulting expression for V_x in Equation (7) results in the following useful equation.

$$\frac{V_{cy}}{V_r} = \frac{s_y}{1-s_x} \tag{8}$$

The slip velocity magnitude $V_c = |\mathbf{V}_c|$ is computed from the components V_{cx} and V_{cy}.

$$V_c = \sqrt{V_{cx}^2 + V_{cy}^2}$$

Introducing Equations (6) and (8) into the above gives the slip velocity magnitude as a fraction of the rolling velocity.

$$\frac{V_c}{V_r} = \frac{\sqrt{s_x^2 + s_y^2}}{1 - s_x} \tag{9}$$

As the wheel is locked ($s_x \to 1$, $V_r \to 0$), the slip velocity approaches the travel velocity and full sliding develops in the contact region. At lockup:

$$V_{cx} = V_x \quad \text{(from Equation (4))}$$

$$V_{cy} = V_y \quad \text{(always)}$$

$$\mathbf{V}_s = \mathbf{V}_c = \mathbf{V}$$

where $\mathbf{V}_s$ is the sliding velocity vector.

MODEL DEFINITION

The models derived in this document represent the tire tread by an array of elastic rectangular blocks attached radially to an elastic or rigid ring. The ring represents the tire carcass and may be rigidly attached to the mounting rim or separated from the rim by a spring foundation which permits lateral and longitudinal carcass motion to be simulated. In Figure 3, the carcass

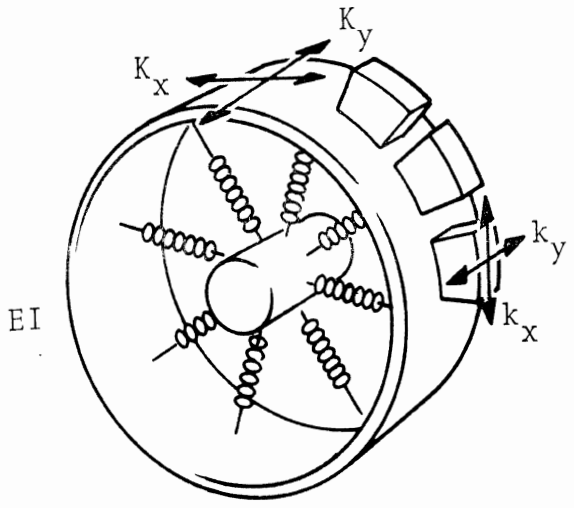

Figure 3. Tire model: rectangular tread elements attached to an elastically supported deformable ring of bending stiffness EI.

ring, which has bending stiffness EI, moves on foundation springs of stiffness K_x and K_y. The tread blocks have infinitesimal volume in the contact region but undergo finite shear deformations parallel to the road. Their longitudinal and lateral stiffnesses are k_x and k_y. The stiffness parameters K_x, K_y and k_x, k_y have the units of force/length[3].

The shear deformation of the single array[3] of tread elements is conviently described in the ξ,η contact coordinate system as shown in Figure 4.

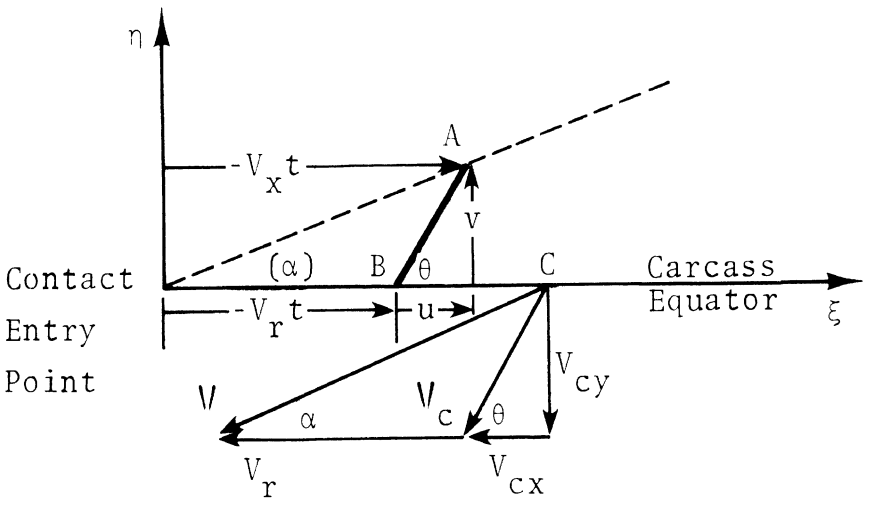

Figure 4. Braking/cornering deformation of tread element attached at B.

In time t, the base point B of a tread element will move into the contact region a longitudinal distance ξ determined by the rolling velocity V_r.

---

[3]Deformation (and shear stress) is averaged across the tire tread. The resulting kinematic and force expressions will depend only on ξ.

$$\xi = -V_r t \tag{10}$$

If there is braking, the contacting tip A, which moves relative to η with the wheel plane velocity V_x, will cover an additional distance u as indicated in Figure 4. The displacement of point A from the axis η is

$$\xi + u = -V_x t \tag{11}$$

Eliminating time from Equations (10) and (11) gives an expression for the longitudinal displacement u.

$$u = \left(\frac{V_x}{V_r} - 1\right)\xi \tag{12}$$

In terms of the longitudinal slip speed given by Equation (4),

$$u = \frac{V_{cx}}{V_r}\,\xi \tag{13}$$

The relative lateral velocity of contacting tip A is V_{cy}. In time t, this point is displaced laterally a distance $v = -V_{cy}t$. Using Equation (10) to eliminate time gives an expression for the lateral displacement v.

$$v = \frac{V_{cy}}{V_r}\,\xi \tag{14}$$

Note that u and v depend only on the contact coordinate ξ.

The preceding analysis presumes that point A does not slide with respect to the road surface. From experimental observation, the contacting tip should describe a path parallel to the wheel traveling velocity vector $\mathbf{V}$. That it will do this is easily shown by writing the tangent angle of the dashed line path in Figure 4.

$$\tan(\ ) = \frac{v}{\xi + u}$$

$$= \frac{V_{cy}/V_r}{1 + V_{cx}/V_r} = \frac{V_{cy}}{V_r + V_{cx}}$$

$$= \frac{V_{cy}}{V_x} = \tan\alpha$$

When the tangent of the angle θ made by AB with the carcass equator is written with Equations (13) and (14),

$$\tan\theta = \frac{v}{u} = \frac{V_{cy}}{V_{cx}},$$

it is seen that the deformed tread element AB in adhesion with the road is parallel to the slip velocity vector $\mathbf{V}_c$.

In the adhesion region, the deformations u and v are produced by static friction with a limiting coefficient μ_o. The components q_x and q_y of the static friction force required to produce these displacements depend upon the longitudinal and lateral stiffnesses of the element.

$$q_x = k_x u \tag{15}$$

$$q_y = k_y v \tag{16}$$

Since $\frac{q_y}{q_x} = \frac{k_y V_{cy}}{k_x V_{cx}}$, the static friction force vector will not oppose the slip speed vector V_c unless the tread element stiffnesses are equal ($k_x = k_y$).

The right-hand sides of Equations (15) and (16) represent the components of linear elastic force developed in a tread element. At any point in the adhesion region, the magnitude of the static friction force required to balance the elastic force is

$$q = \sqrt{q_x^2 + q_y^2} \tag{17}$$

The maximum static friction available from a particular tire-road combination depends upon the limiting friction coefficient μ_o and the vertical contact pressure distribution $q_z(\xi)$ which is assumed to be uniform in the η direction. The friction force requirement, computed by Equation (17), increases linearly as shown in Figure 5 until

$$q\Big|_{\xi=\xi_a} = \mu_o q_z\Big|_{\xi=\xi_a}$$

which defines the limit, ξ_a, of the adhesion region. The tread element displacements

$$u = \frac{V_{cx}}{V_r}\,\xi_a \tag{18}$$

$$v = \frac{V_{cy}}{V_r}\,\xi_a \tag{19}$$

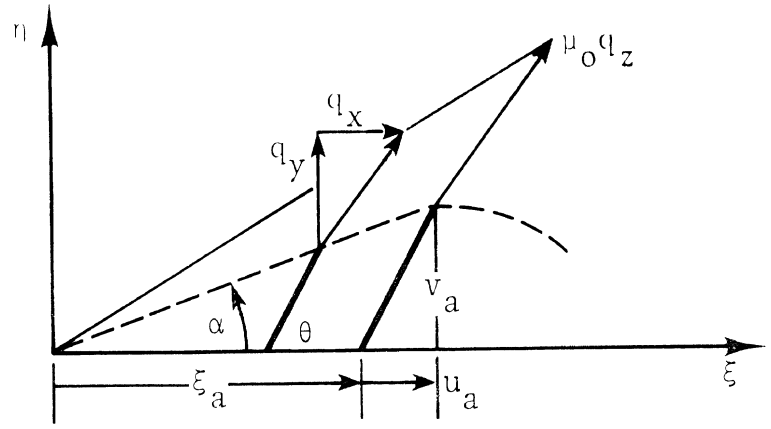

Figure 5. Maximum static friction force $\mu_o q_z(\xi_a)$ on tread element at ξ_a, the limit of adhesion.

are maximum at the adhesion limit which is located by evaluating Equation (17) at ξ_a.

$$\sqrt{q_x^2 + q_y^2}\,\Big|_{\xi=\xi_a} = \mu_o q_z\,\Big|_{\xi=\xi_a}$$

Substituting (18) and (19) into (15) and (16) and the resulting expressions for q_x and q_y into the above, allows the adhesion limit to be expressed as

$$\xi_a = \frac{\mu_o V_r}{\sqrt{(k_x V_{cx})^2 + (k_y V_{cy})^2}}\, q_z\,\Big|_{\xi=\xi_a} \qquad (20)$$

For a uniform contact pressure distribution, p = const.,

$$q_z\Big|_{\xi=\xi_a} = p$$

is used in Equation (20). For nonuniform contact pressures given by closed form expressions (such as parabolic), it may be possible to solve Equation (20) for ξ_a by rearrangement. In the case of arbitrary contact pressures, iteration of Equation (20) will be necessary to obtain the adhesion limit ξ_a.

The preceding analysis is common to all linear element tire models since deformation behavior in the adhesion region is well known from observations of a tire rolling over a glass plate. By presuming linear elastic tire behavior the shear force generated at the road surface in the adhesion portion of the contact region can be easily computed. The situation is considerably more complicated in the sliding region where the sliding friction force rather than adhesive constraint governs the tire deformation. In the sliding region, one must presume a friction force and then compute the resulting displacements based on structure stiffnesses. This is directly opposite to the straightforward procedure followed in the adhesion region. The success or failure of a tire model is in direct proportion to skill in approximating sliding region behavior.

FORCE AND MOMENT EQUATIONS

The advantages of using the two coordinate systems (tire and contact) described earlier will now become apparent. The length of the contact region as well as its location with respect to the tire mounting rim varies with the tire operating conditions. It is convenient to define the non-slip[4] contact length L on the carcass equator to which the ξ,η coordinates are attached. By presuming uniform behavior laterally (across the finite contact width), the distributed contact shear forces q_x and q_y are defined as functions of ξ only which is taken as the independent variable. The resultant traction force components, F_x and F_y, transmitted to the tire mounting rim, are now obtained via the following integrals:

$$F_x = -w \int_0^L q_x d\xi \ , \tag{21}$$

$$F_y = -w \int_0^L q_y d\xi \ , \tag{22}$$

where w is the contact width.[5] The minus signs appear in Equations (21) and (22) because F_x and F_y (applied to the tire by the road) are referred to the tire coordinate system.

---

[4]This is the contact length of the free-rolling tire at zero slip angle.

[5]The contact region is seldom rectangular; L and w are representative dimensions.

If the rigid carcass is elastically supported, as presumed by some tire models, the preceding traction forces may cause longitudinal and lateral translations

$$\tilde{u} = - \frac{F_x}{K_x} , \tag{23}$$

$$\tilde{v} = - \frac{F_y}{K_y} , \tag{24}$$

which depend upon the carcass foundation stiffnesses K_x and K_y. The carcass translation for combined braking and cornering is shown in Figure 6.

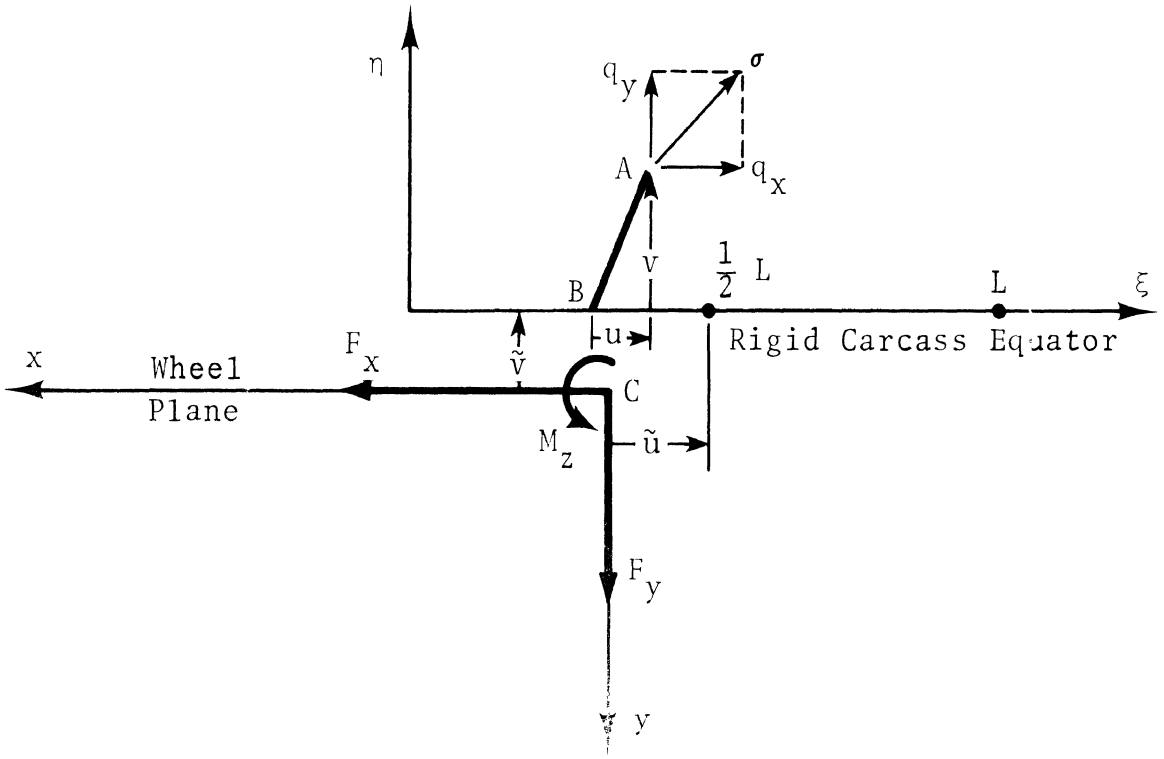

Figure 6. Sign convention for traction forces and moment.

Following the sign convention given in Figure 6, the aligning moment expression may be written

$$M_z = -w \int_0^L [q_x(v+\tilde{v}) - q_y(u+\tilde{u}+\xi-\frac{L}{2})]d\xi$$

which, with the aid of Equations (21-24), becomes

$$M_z = -w \int_0^L [q_x v - q_y(u+\xi-\frac{L}{2})]d\xi + F_x F_y(\frac{1}{K_x} - \frac{1}{K_y}) \qquad (25)$$

Due to the nonuniform distribution of the shear forces q_x and q_y, and the carcass translations $\tilde{u}$ and $\tilde{v}$, the resultant traction forces are not necessarily colinear with the x and y axes as shown in Figure 6. The traction forces F_x and F_y may be offset certain distances ℓ_x and ℓ_y from the wheel center as shown in Figure 7.

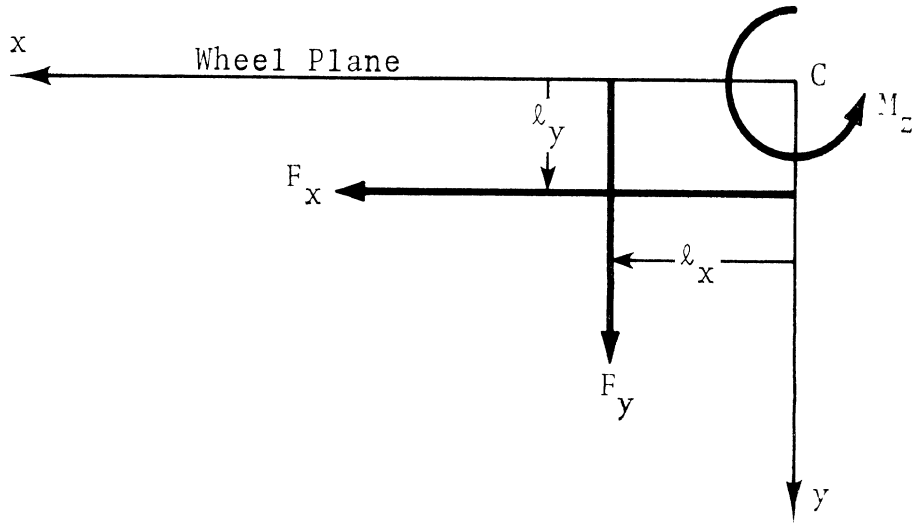

Figure 7. Positive sign convention for traction force offsets ℓ_x and ℓ_y.

Moment equilibrium about the center of tire contact is expressed by

$$M_z = F_y \ell_x - F_x \ell_y \tag{26}$$

For straight ahead operation, $F_y = \ell_y = 0$ and no aligning moment is generated. For free-rolling at a slip angle, $F_x = 0$ which reduces the moment equation to

$$M_z = F_y \ell_x \tag{27}$$

The length ℓ_x is frequently called the "pneumatic trail." It can be positive or negative depending on the tire operating conditions.

In the adhesion region, $\xi \leq \xi_a$, the shear forces q_x and q_y are considered by all tire models in this document to be linearly distributed according to Equations (15-16) derived earlier

$$q_x = k_x \frac{V_{cx}}{V_r} \xi \tag{15}$$

$$q_y = k_y \frac{V_{cy}}{V_r} \xi \tag{16}$$

and the displacements by Equations (13-14)

$$u = \frac{V_{cx}}{V_r} \xi \tag{13}$$

$$v = \frac{V_{cy}}{V_r} \xi \tag{14}$$

The shear forces and displacements in the sliding region, $\xi > \xi_a$, are approximated in a different manner by each of the following models discussed individually.

HSRI-NBS-I [3]

This model presumes tread element deformation in the sliding region to be uniform with the magnitude attained at the adhesion limit $\xi = \xi_a$. Thus

$$u_s = u_a = \frac{V_{cx}}{V_r} \xi_a \tag{28}$$

$$v_s = v_a = \frac{V_{cy}}{V_r} \xi_a \tag{29}$$

where u_s and v_s are the displacement components in the sliding region.

To sustain these displacements, the shear-stress components in the sliding region are required to be $q_x = k_x u_s$ and $q_y = k_y v_s$. The stress distribution over the entire contact region, shown in Figure 8, implies a single friction coefficient μ. This model considers μ to be a linearly decreasing function of sliding speed according to

$$\mu = \mu_o (1 - A_s V_s) \tag{30}$$

where A_s is an experimentally determined speed sensitivity coefficient and

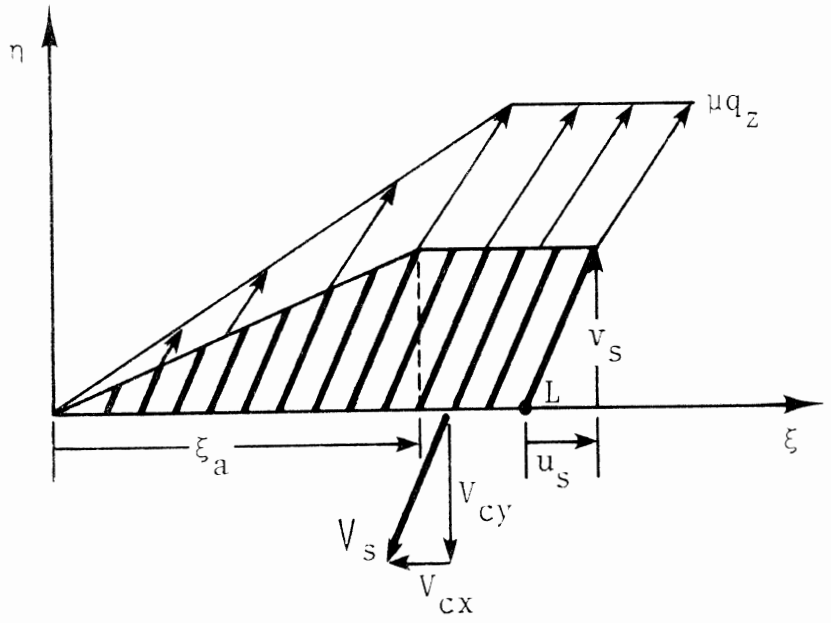

Figure 8. Deformation and stress presumed by HSRI-NBS-I model.

$$V_s = V_c = \sqrt{V_{cx}^2 + V_{cy}^2}$$

It should be noted that here no distinction is made between slip and sliding speed or static and dynamic friction. This is a necessary consequence of prescribing the deformation (Equations (28) and (29)) beyond the adhesion limit. The adhesion limit is computed by using μ from Equation (30) instead of μ_o in Equation (20).

$$\xi_a = \frac{\mu V_r}{\sqrt{(k_x V_{cx})^2 + (k_y V_{cy})^2}} q_z \Big|_{\xi=\xi_a} \qquad (31)$$

The traction forces F_x and F_y are computed by substituting the shear-stress distributions

$$q_x = \begin{cases} k_x \dfrac{V_{cx}}{V_r} \xi & \xi \leq \xi_a \\ k_x \dfrac{V_{cx}}{V_r} \xi_a & \xi > \xi_a \end{cases}$$

$$q_y = \begin{cases} k_y \dfrac{V_{cy}}{V_r} \xi & \xi \leq \xi_a \\ k_y \dfrac{V_{cy}}{V_r} \xi_a & \xi > \xi_a \end{cases}$$

into the force equations (21) and (22). The traction force in the longitudinal direction is

$$F_x = -w\, k_x \frac{V_{cx}}{V_r} \left(\int_0^{\xi_a} \xi d\xi + \int_{\xi_a}^{L} \xi_a d\xi \right)$$

After integrating,

$$F_x = -w\, k_x \frac{V_{cx}}{V_r} \xi_a \left(L - \frac{1}{2}\xi_a\right) \tag{32}$$

If the rolling and slip velocities are such that Equation (31) yields $\xi_a \geq L$, there is complete adhesion over the entire contact region and

$$F_x = -w\, k_x \frac{V_{cx}}{V_r} \frac{L^2}{2} \tag{33}$$

In the lateral direction, the integration of Equation (22) gives

$$F_y = -w\, k_y \frac{V_{cy}}{V_r} \xi_a \left(L - \frac{1}{2}\xi_a\right) \tag{34}$$

If adhesion is complete,

$$F_y = -w\, k_y \frac{V_{cy}}{V_r} \frac{L^2}{2} \tag{35}$$

Adhesion will be complete for small values of V_{cx} and V_{cy}. The use of Equations (6) and (8) permits the adhesive traction forces, (33) and (35), to be written in the following way.

$$F_x = -w\, k_x \frac{s_x}{1 - s_x} \frac{L^2}{2} \tag{36}$$

$$F_y = -w\, k_y \frac{s_y}{1 - s_x} \frac{L^2}{2} \tag{37}$$

The braking and cornering traction stiffnesses, C_s and C_α, are defined for complete adhesion according to

$$C_s \equiv \left|\frac{\partial F_x}{\partial s_x}\right|_{\substack{s_x=0 \\ s_y=0 \ (\alpha=0)}} \tag{38}$$

and

$$C_\alpha \equiv \left| \frac{\partial F_y}{\partial \alpha} \right|_{\substack{s_x=0 \\ s_y=0 \ (\alpha=0)}} \tag{39}$$

Carrying out the required operations on Equations (36) and (37) yields

$$C_s = \frac{1}{2} k_x w L^2 \tag{40}$$

$$C_\alpha = \frac{1}{2} k_y w L^2 \tag{41}$$

These parameters, which represent the slopes of the traction force curves passing through the zero slip point, are easily determined from experimental tire data. It is convenient to express the traction forces in terms of C_s and C_α.

$$F_x = \begin{cases} -C_s \dfrac{s_x}{1 - s_x} & \xi_a \geq L \\ -C_s \dfrac{s_x}{1 - s_x} \dfrac{\xi_a}{L} \left(2 - \dfrac{\xi_a}{L}\right) & \xi_a < L \end{cases} \tag{42}$$

$$F_y = \begin{cases} -C_\alpha \dfrac{s_y}{1 - s_x} & \xi_a \geq L \\ -C_\alpha \dfrac{s_y}{1 - s_x} \dfrac{\xi_a}{L} \left(2 - \dfrac{\xi_a}{L}\right) & \xi_a < L \end{cases} \tag{43}$$

The HSRI-NBS-I model presumes the vertical contact pressure distribution, q_z, to be uniform over the contact region. Thus, at the adhesion limit,

$$q_z(\xi_a) = F_z/wL \tag{44}$$

where F_z is the tire load. The use of this assumption and Equations (6), (8), (40), and (41) allows Equation (31) to be written as the adhesion fraction

$$\frac{\xi_a}{L} = \frac{1}{2}\mu F_z(1 - s_x)[(s_x C_s)^2 + (s_y C_\alpha)^2]^{-\frac{1}{2}} \tag{45}$$

where the friction coeffficient μ varies with sliding speed as given by Equation (30).

For braking at a positive slip angle α, as illustrated in Figure 1, the slip parameters s_x and $s_y = \tan\alpha$ are positive. The traction forces computed by Equations (42) and (43) will be negative and generally oppose the direction of travel, decelerating the vehicle.

For locked wheel braking (s_x=1), the adhesion fraction (45) vanishes and the traction forces become (on combining (45) with (42) and (43))

$$F_x = -C_s \mu F_z[C_s^2 + (s_y C_\alpha)^2]^{-\frac{1}{2}} \tag{46}$$

$$F_y = -C_\alpha s_y \mu F_z[C_s^2 + (s_y C_\alpha)^2]^{-\frac{1}{2}} \tag{47}$$

For straight ahead (s_y=0) locked wheel braking, the lateral force vanishes and the longitudinal force becomes simply

$$F_x = -\mu F_z \tag{48}$$

During locked wheel travel, the sliding velocity equals the travel velocity V. The friction coefficient, considered to vary with sliding velocity, is then

$$\mu = \mu_o(1 - A_s|V|) \tag{49}$$

The sliding region approximations made in the development of this model do not allow a reasonable equation for aligning moment to be derived by integration of Equation (25). The traction force calculations, (42) and (43), however, agree well with experimental data.

HSRI-NBS-II [4]

This model uses the limiting coefficient of static friction, μ_o, to define the limit of the adhesion region. The limit of adhesion is given by Equation (20), written below in terms of the slip parameters s_x and s_y.

$$\xi_a = \frac{\mu_o (1-s_x)}{\sqrt{(k_x s_x)^2 + (k_y s_y)^2}} q_z\Big|_{\xi=\xi_a} \tag{50}$$

In the sliding region, the available friction drops to the level of the dynamic coefficient μ which is considered to be linearly

related to sliding speed by Equation (30) used with the HSRI-NBS-I model.

$$\mu = \mu_o(1 - A_s V_s) \tag{30}$$

Instead of prescribing tread deformation in the sliding region, as was done in deriving the HSRI-NBS-I model, the shear stress in the sliding region will be recognized as having the magnitude μq_z and a direction[6] opposing that of the sliding velocity. The tread deformation in the sliding region then depends on the longitudinal and lateral tread stiffnesses k_x and k_y.

$$u_s = \frac{q_x}{k_x} \qquad \text{(sliding)} \qquad v_s = \frac{q_y}{k_y} \tag{51}$$

where, referring to Figure 9,

[6]Due to tread pattern and preferential pavement surface direction, the sliding shear force may not be directed exactly opposite to the sliding velocity. This phenomenon can be accounted for by using anisotropic friction coefficients μ_x and μ_y as is done by the Sakai model discussed later.

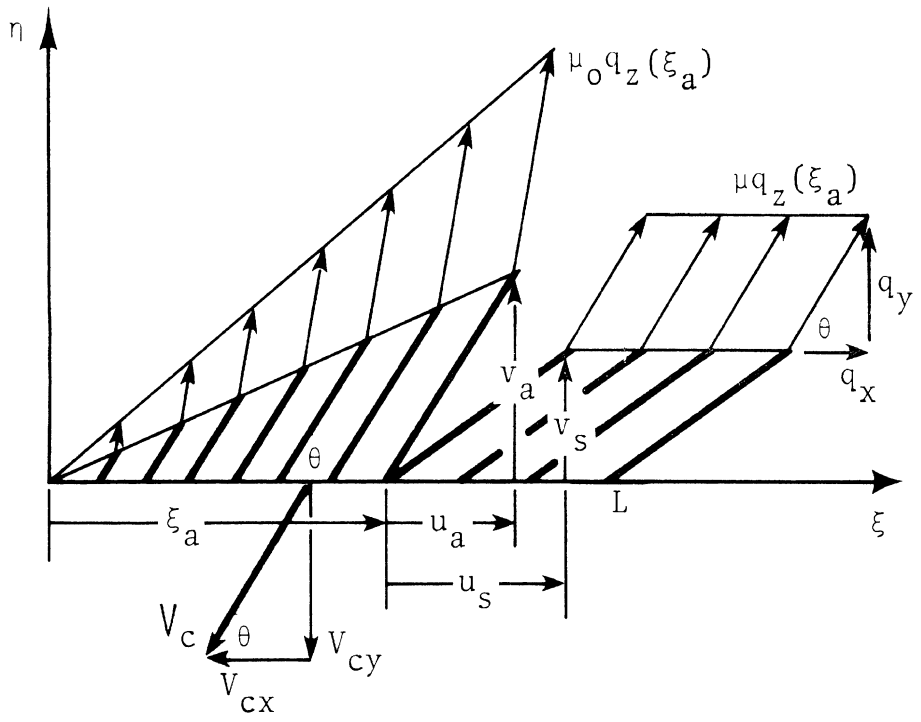

Figure 9. Deformation and stresses in HSRI-NBS-II model with instantaneous transition.

$$q_x = \mu q_z \cos\theta = \frac{V_{cx}}{V_s} \mu q_z$$

$$q_y = \mu q_z \sin\theta = \frac{V_{cy}}{V_s} \mu q_z \qquad \text{(full sliding, } V_c = V_s\text{)} \qquad (52)$$

For $k_x < k_y$ and $V_{cx} < V_{cy}$, the deformation and stresses will be as shown in Figure 9.

The abrupt shift from adhesion to sliding produces a displacement discontinuity at $\xi=\xi_a$ (see Fig. 9). This discontinuity is unacceptable and indicates the existence of a finite transition region between adhesion and fully developed sliding. The accommodation of the transition region is a major contribution of the HSRI-NBS-II model.

In passing through the transition region, a deformed tread element gradually changes its length and orientation. The shear force vector similarly changes its length and orientation in passing from geometrically constrained static friction to limiting dynamic friction generated during fully developed sliding. Finite transition behavior for $k_x > k_y$ is illustrated in Figure 10.

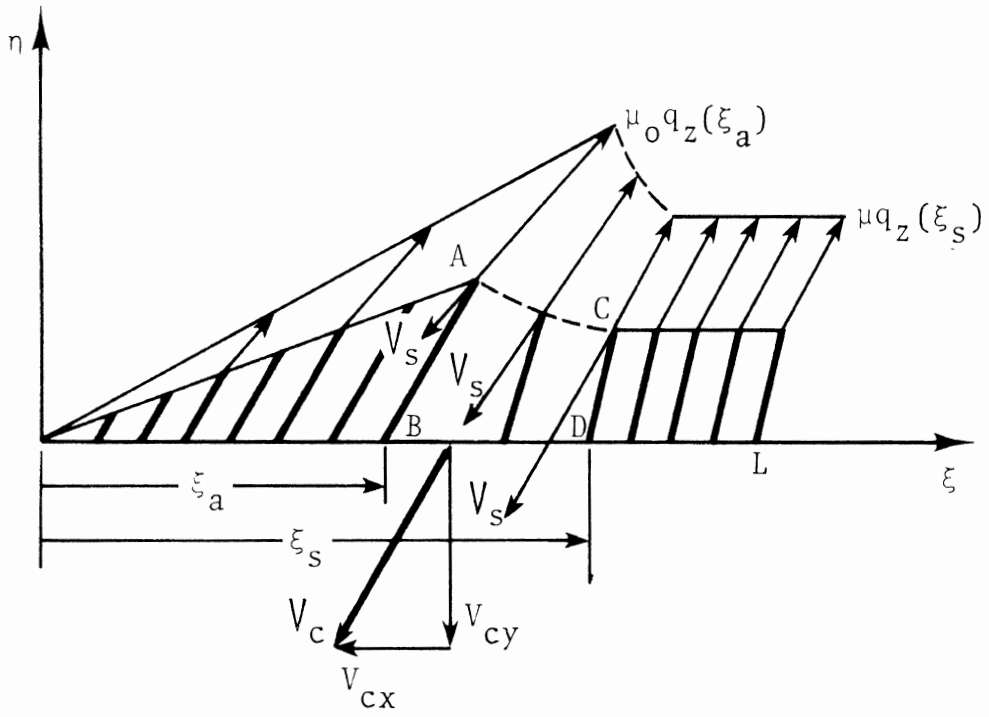

Figure 10. HSRI-NBS-II model with finite transition.

At the adhesion limit, $\xi=\xi_a$, the incipient sliding speed $V_s = 0^+$ will be assumed to oppose the direction of the maximum static shear force $\mu_o q_z(\xi_a)$. During transition, the sliding speed builds up and tends to oppose the direction of the local dynamic friction force. At the transition limit, $\xi=\xi_s$, sliding is fully

developed and $V_s = V_c$. An approximation to the transition length $t = \xi_s - \xi_a$ is made in the following way.

Triangle AC'D', shown in Figure 11, is formed by translating the first fully sliding element CD forward in the direction of wheel travel until C is at C' on the line of action of $\mu_o q_z$. In this position, it can be shown that D will be at D' on the line extending the last adhesion element AB. The formation of triangle AC'D' is proven by

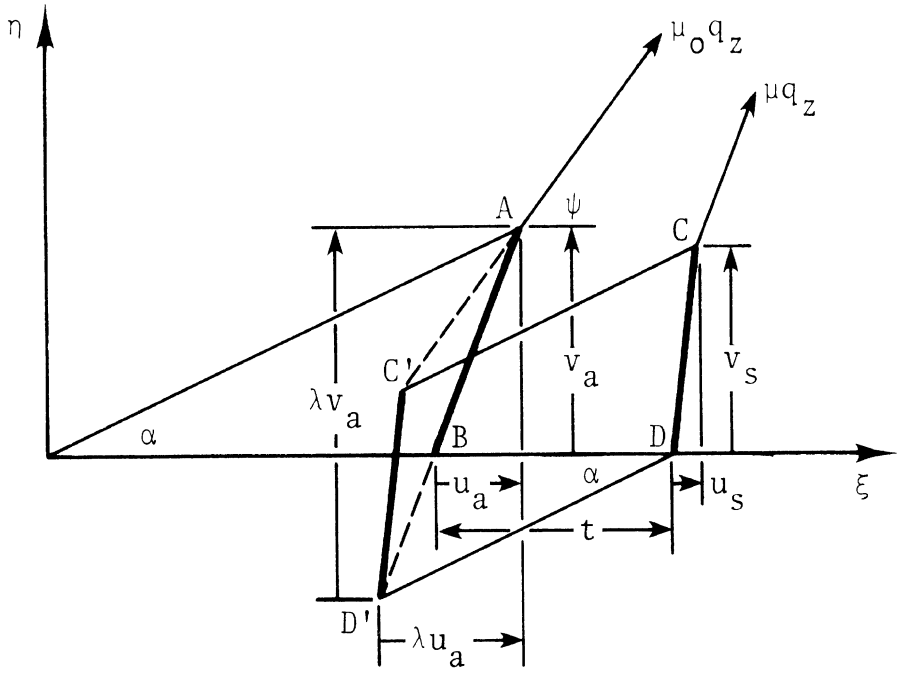

Figure 11. Translation of fully sliding element CD for a definition of the transition region.

showing that the interior angles at A, C' and D' add up to 180°.

Angle at A: $\left(\tan^{-1}\frac{v_a}{u_a} - \tan^{-1}\frac{k_y v_a}{k_x u_a}\right)$

Angle at C': $180° - \left(\tan^{-1}\frac{v_s}{u_s} - \tan^{-1}\frac{k_y v_a}{k_x u_a}\right)$

Angle at D': $\left(\tan^{-1}\frac{v_s}{u_s} - \tan^{-1}\frac{v_a}{u_a}\right)$

Sum of angles: $180°$

The factor λ, which indicates the separation of the vertices at A and D', may be determined from the slope of side AC'.

Slope of AC' at A: $\frac{k_y v_a}{k_x u_a}$

Slope of AC' at C': $\frac{\lambda v_a - v_s}{\lambda u_a - u_s}$

After equating these expressions and solving for λ,

$$\lambda = \frac{k_x u_a v_s - k_y u_s v_a}{(k_x - k_y) u_a v_a} \tag{53}$$

From Equations (13) and (14),

$$u_a = \frac{V_{cx}}{V_r}\xi_a \qquad v_a = \frac{V_{cy}}{V_r}\xi_a$$

with ξ_a given by Equation (20), and from Equations (51) and (52),

$$u_s = \frac{V_{cx}}{V_s} \frac{\mu q_z}{k_x} (\xi_s) \qquad v_s = \frac{V_{cy}}{V_s} \frac{\mu q_z}{k_y} (\xi_s)$$

λ is found to be independent of rolling velocity V_r.

$$\lambda = \frac{\mu q_z(\xi_s)}{\mu_o q_z(\xi_a)} \left| \frac{1}{k_x} + \frac{1}{k_y} \right| \frac{\sqrt{(k_x V_{cx})^2 + (k_y V_{cy})^2}}{V_s} \tag{54}$$

In this expression, $V_s = V_c = \sqrt{(V_{cx})^2 + (V_{cy})^2}$ since the translated element is in fully developed sliding. Referring to Figure 11, the transition length is seen to be

$$t = (\lambda - 1)(v_a \cot\alpha - u_a) = (\lambda - 1)\xi_a \tag{55}$$

The limit of the transition region is

$$\xi_s = \xi_a + t = \lambda \xi_a \tag{56}$$

Multiplying Equation (54) for λ by Equation (50) for ξ_a results in an expression for the transition limit

$$\xi_s = \mu q_z(\xi_s)(1-s_x)\left(\frac{1}{k_x} + \frac{1}{k_y}\right) \frac{\sqrt{(k_x V_{cx})^2 + (k_y V_{cy})^2}}{V_s \sqrt{(k_x s_x)^2 + (k_y s_y)^2}} \tag{57}$$

which can be simplified by the use of Equations (6) and (8) to yield

$$\xi_s = \mu q_z(\xi_s) \frac{V_r}{V_s} \left(\frac{1}{k_x} + \frac{1}{k_y}\right) \tag{58}$$

Recognizing that $V_s = V_c$, Equation (9) can be used to write the sliding boundary in terms of the slip parameters.

$$\xi_s = \mu q_z(\xi_s)(1-s_x)\left(\frac{1}{k_x} + \frac{1}{k_y}\right)\left[(s_x)^2 + (s_y)^2\right]^{-1/2} \qquad (59)$$

This expression should be compared with Equation (50) as rewritten below.

$$\xi_a = \mu_o q_z(\xi_a)(1-s_x)\left[(k_x s_x)^2 + (k_y s_y)^2\right]^{-1/2} \qquad (60)$$

A transition region must be considered only if the operating variables are such that $\xi_s > \xi_a$. If $\xi_s \leq \xi_a$, instantaneous transition from adhesion to steady-state sliding will be assumed. If $\xi_a \geq L$, the entire contact region is in adhesion and there is no difference between the HSRI-NBS-II and HSRI-NBS-I models. It is possible to find $\xi_s \geq L$ in which case (if $\xi_a < L$) the transition region extends to the end of contact and there is no fully developed sliding. Only for $\xi_a < \xi_s < L$ will all three regions exist, each contributing to the traction forces and aligning moment.

The transition region displacements, u_t and v_t, are presumed to be linearly decreasing during the transition from adhesion to fully developed sliding (Figure 12). The displacement components, linear in ξ, are now written by referring to Figure 12.

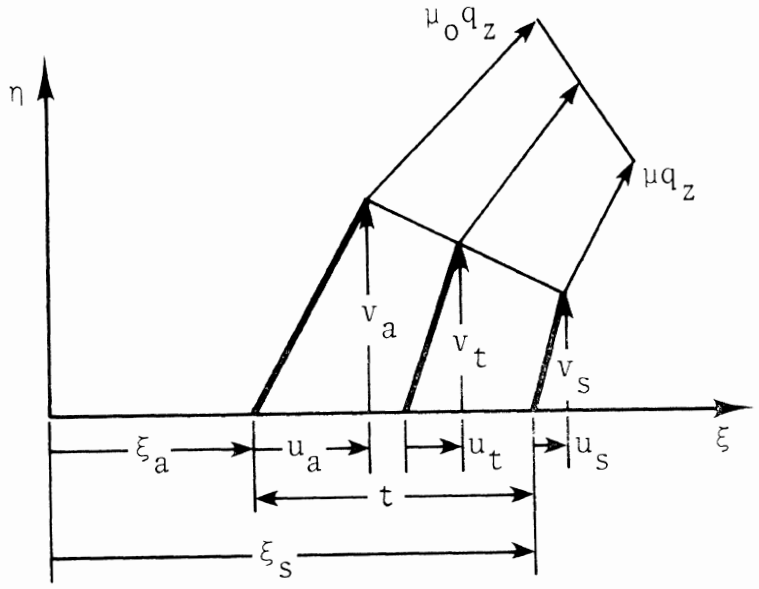

Figure 12. Linear approximation of deformation and stress in the transition region.

$$u_t = [(\xi_s - \xi)u_a + (\xi - \xi_a)u_s]/t$$
$$v_t = [(\xi_s - \xi)v_a + (\xi - \xi_a)v_s]/t \qquad (61)$$

Having prescribed the transition region displacements, the transition region shear stress components must be

$$q_x = k_x u_t$$
$$q_y = k_y v_t \qquad \text{(transition)} \qquad (62)$$

These will decrease linearly to the sliding stress components given by Equations (52).

The shear stress distribution over the entire contact region may now be assembled. If the tire operating conditions are such that all three regions exist ($\xi_a < \xi_s < L$), then

$$q_x = \begin{cases} k_x \frac{V_{cx}}{V_r} \xi & 0 \le \xi \le \xi_a \\ \frac{V_{cx}}{t} \left[\left(\frac{k_x \xi_s}{V_r} - \frac{\mu q_z(\xi_s)}{V_s} \right) \xi_a + \left(\frac{\mu q_z(\xi_s)}{V_s} - \frac{k_x \xi_a}{V_r} \right) \xi \right] & \xi_a \le \xi \le \xi_s \\ \frac{V_{cx}}{V_s} \mu q_z(\xi) & \xi_s \le \xi \le L \end{cases} \tag{63}$$

and

$$q_y = \begin{cases} k_y \frac{V_{cy}}{V_r} \xi & 0 \le \xi \le \xi_a \\ \frac{V_{cy}}{t} \left[\left(\frac{k_y \xi_s}{V_r} - \frac{\mu q_z(\xi_s)}{V_s} \right) \xi_a + \left(\frac{\mu q_z(\xi_s)}{V_s} - \frac{k_y \xi_a}{V_r} \right) \xi \right] & \xi_a \le \xi \le \xi_s \\ \frac{V_{cy}}{V_s} \mu q_z(\xi) & \xi_s \le \xi \le L \end{cases}$$

The traction forces, F_x and F_y, are computed by substituting the above shear stresses into the force integrals (21) and (22). The contribution from each region may be computed separately. For example:

$$\text{(adhesion)} \qquad F_{xa} = -w \int_0^{\xi_a} q_x d\xi$$

$$\text{(transition)} \qquad F_{xt} = -w \int_{\xi_a}^{\xi_s} q_x d\xi$$

$$\text{(sliding)} \qquad F_{xs} = -w \int_{\xi_s}^{L} q_x d\xi$$

The resultant traction forces are obtained by summing the contributions from each region, viz.,

$$F_x = F_{xa} + F_{xt} + F_{xs} \tag{64}$$

$$F_y = F_{ya} + F_{yt} + F_{ys} \tag{65}$$

where, for a uniform contact pressure distribution $q_z = F_z/wL$,

$$\left.\begin{aligned} F_{xa} &= -C_s \frac{V_{cx}}{V_r}\left(\frac{\xi_a}{L}\right)^2 \quad (\text{if } \xi_a > L, \text{ set } \xi_a = L) \\ F_{xt} &= -\left[C_s \frac{V_{cx}}{V_r}\frac{\xi_a}{L} + \frac{1}{2}\mu F_z \frac{V_{cx}}{V_s}\right]\left(\frac{\xi_s}{L} - \frac{\xi_a}{L}\right) \\ F_{xs} &= -\mu F_z \frac{V_{cx}}{V_s}\left(1 - \frac{\xi_s}{L}\right) \end{aligned}\right\} \tag{66}$$

$$\left.\begin{aligned} F_{ya} &= -C_\alpha \frac{V_{cy}}{V_r}\left(\frac{\xi_a}{L}\right)^2 \quad (\text{if } \xi_a > L, \text{ set } \xi_a = L) \\ F_{yt} &= -\left[C_\alpha \frac{V_{cy}}{V_r}\frac{\xi_a}{L} + \frac{1}{2}\mu F_z \frac{V_{cy}}{V_s}\right]\left(\frac{\xi_s}{L} - \frac{\xi_a}{L}\right) \\ F_{ys} &= -\mu F_z \frac{V_{cy}}{V_s}\left(1 - \frac{\xi_s}{L}\right) \end{aligned}\right\} \tag{67}$$

The traction stiffnesses, C_s and C_α, given by Equations (40) and (41) have been used to simplify the above expressions. The transition forces F_{xt} and F_{yt} are zero if $\xi_a > \xi_s$ (then set $\xi_s = \xi_a$). The fully developed sliding forces F_{xs} and F_{ys} are zero if $\xi_s \geq L$ (then set $\xi_s = L$). The traction forces may be

expressed in terms of slip parameters by using Equations (59) and (60) for ξ_s and ξ_a, and the following expressions

$$\frac{V_{cx}}{V_r} = \frac{s_x}{1 - s_x} \qquad \frac{V_{cx}}{V_s} = \frac{s_x}{\sqrt{s_x^2 + s_y^2}}$$

$$\frac{V_{cy}}{V_r} = \frac{s_y}{1 - s_x} \qquad \frac{V_{cy}}{V_s} = \frac{s_y}{\sqrt{s_x^2 + s_y^2}}$$

For small values of slip, the contact will be entirely adhesive. In this case,

$$\begin{aligned} F_x &= F_{xa} = -C_s \frac{s_x}{1 - s_x} \\ F_y &= F_{ya} = -C_\alpha \frac{s_y}{1 - s_x} \end{aligned} \tag{68}$$

which is the result given by the HSRI-NBS-I model.

For locked wheel braking ($s_x = 1$), the adhesion and transition regions vanish. Setting $\xi_a = \xi_s = 0$ in Equations (66) and (67), the locked wheel traction forces are found to be

$$\begin{aligned} F_x &= F_{xs}\Big|_{s_x=1} = -\mu F_z \frac{1}{\sqrt{1 + s_y^2}} \\ F_y &= F_{ys}\Big|_{s_x=1} = -\mu F_z \frac{s_y}{\sqrt{1 + s_y^2}} \end{aligned} \tag{69}$$

where $F_z = wLq_z$ is the tire load distributed uniformly over the contact region. These expressions differ considerably from Equations (46) and (47) derived from the HSRI-NBS-I model in locked wheel braking. The braking and cornering stiffnesses C_s and C_α do not appear in Equations (69) because the sliding region displacements do not govern the sliding shear forces as is presumed by the HSRI-NBS-I model. It is currently a matter of conjecture how much tire stiffness actually influences the dynamic friction force produced by sliding at a slip angle. For straight ahead (s_y=0) locked wheel travel, F_y vanishes and $F_x = -\mu F_z$ which should be predicted by all tire models.

The HSRI-NBS-II model produces a somewhat reasonable aligning moment simulation. The aligning moment, computed from Equation (25), depends on the displacement distribution expressions

$$u = \begin{cases} \dfrac{V_{cx}}{V_r}\,\xi & 0 \le \xi \le \xi_a \\ \dfrac{V_{cx}}{t}\left[\left(\dfrac{\xi_s}{V_r} - \dfrac{\mu q_z(\xi_s)}{k_x V_s}\right)\xi_a + \left(\dfrac{\mu q_z(\xi_s)}{k_x V_s} - \dfrac{\xi_a}{V_r}\right)\xi\right] & \xi_a \le \xi \le \xi_s \\ V_{cx}\,\dfrac{\mu q_z(\xi)}{k_x V_s} & \xi_s \le \xi \le L \end{cases} \tag{70}$$

$$v = \begin{cases} \dfrac{V_{cy}}{V_r}\,\xi & 0 \le \xi \le \xi_a \\ \dfrac{V_{cy}}{t}\left[\left(\dfrac{\xi_s}{V_r} - \dfrac{\mu q_z(\xi_s)}{k_y V_s}\right)\xi_a + \left(\dfrac{\mu q_z(\xi_s)}{k_y V_s} - \dfrac{\xi_a}{V_r}\right)\xi\right] & \xi_a \le \xi \le \xi_s \\ V_{cy}\,\dfrac{\mu q_z(\xi)}{k_y V_s} & \xi_s \le \xi \le L \end{cases}$$

as well as the shear force distribution given by Equations (63). The total aligning moment is given by Equation (25) as rewritten below.

$$M_z = M_{za} + M_{zt} + M_{zs} + F_x F_y \left(\frac{1}{K_x} - \frac{1}{K_y}\right) \tag{71}$$

where

$$M_{za} = -w \int_0^{\xi_a} \left[q_x v - q_y \left(u + \xi - \frac{L}{2}\right)\right] d\xi$$

$$M_{zt} = -w \int_{\xi_a}^{\xi_s} \left[q_x v - q_y \left(u + \xi - \frac{L}{2}\right)\right] d\xi$$

$$M_{zs} = -w \int_{\xi_s}^{L} \left[q_x v - q_y \left(u + \xi - \frac{L}{2}\right)\right] d\xi$$

After performing the integrations with the assumption of a uniform contact pressure distribution, $q_z = F_z/wL$, the contribution of each region to the total aligning moment is found.

$$
\left.
\begin{aligned}
M_{za} &= -\frac{L}{3}\left[2(C_s - C_\alpha)\,\frac{V_{cx}}{V_r}\,\frac{\xi_a}{L} - \frac{1}{2}C_\alpha\,\left(4\,\frac{\xi_a}{L} - 3\right)\right]\frac{V_{cy}}{V_r}\left(\frac{\xi_a}{L}\right)^2 \\
M_{zt} &= -\frac{L}{6}\left\{(C_s - C_\alpha)\left[4\,\frac{V_{cx}V_{cy}}{V_r^{\,2}}\left(\frac{\xi_a}{L}\right)^2\right.\right. \\
&\quad + \left(\frac{1}{C_s} + \frac{1}{C_\alpha}\right)\mu F_z\,\frac{V_{cx}V_{cy}}{V_r V_s}\,\frac{\xi_a}{L} + \frac{\mu^2 F_z^{\,2}}{C_s C_\alpha}\,\frac{V_{cx}V_{cy}}{V_s^{\,2}}\Bigg] \\
&\quad - \left[C_\alpha\,\frac{V_{cy}}{V_r}\,\frac{\xi_a}{L}\left(4\,\frac{\xi_a}{L} + 2\,\frac{\xi_s}{L} - 3\right)\right. \\
&\quad \left.\left. + \frac{1}{2}\,\mu F_z\,\frac{V_{cy}}{V_s}\left(2\,\frac{\xi_a}{L} + 4\,\frac{\xi_s}{L} - 3\right)\right]\right\}\left(\frac{\xi_s}{L} - \frac{\xi_a}{L}\right) \\
M_{zs} &= -\frac{L}{2}\,\mu F_z\left[\left(\frac{1}{C_\alpha} - \frac{1}{C_s}\right)\mu F_z\,\frac{V_{cx}}{V_s} - \frac{\xi_s}{L}\right]\frac{V_{cy}}{V_s}\left(1 - \frac{\xi_s}{L}\right)
\end{aligned}
\right\} \quad (72)
$$

The traction stiffnesses, C_s and C_α, given by Equations (40) and (41) have been used to simplify the above aligning moment expressions.

The transition region moment, M_{zt}, is zero if $\xi_a \geq \xi_s$ (then set $\xi_s = \xi_a$). The sliding moment is zero if $\xi_s \geq L$ (then set $\xi_s = L$). It is possible to have $\xi_a \geq L$, in which case there is neither a sliding nor a transition region and $\xi_a = L$, indicating complete adhesion, should be used in evaluating Equations (72). The aligning moment may be expressed in terms of the slip parameters in the same manner as the traction forces F_x and F_y.

For small values of slip, the contact is entirely adhesive and the aligning moment is given by

$$M_z = M_{za} + F_{xa}F_{ya}\left(\frac{1}{K_x} - \frac{1}{K_y}\right) \tag{73}$$

Introducing the slip parameters s_x and s_y into Equation (72) for M_{za} and using Equations (68), the HSRI-NBS-II aligning moment for entirely adhesive contact is

$$M_z = -\frac{L}{6}\left[4(C_s - C_\alpha)\frac{s_x}{1 - s_x} - C_\alpha\right]\frac{s_y}{1 - s_x}$$

$$+ C_s C_\alpha\left(\frac{1}{K_x} - \frac{1}{K_y}\right)\frac{s_x s_y}{(1 - s_x)^2} \tag{74}$$

For locked wheel braking ($s_x = 1$), $\xi_s = \xi_a = 0$ and Equation (71) reduces to

$$M_z = M_{zs} + F_{xs}F_{ys}\left(\frac{1}{K_x} - \frac{1}{K_y}\right) \tag{75}$$

Using Equations (69) and (72) written in terms of slip parameters results in the HSRI-NBS-II aligning moment for fully sliding contact.

$$M_z = -(\mu F_z)^2\left[\frac{L}{2}\left(\frac{1}{C_\alpha} - \frac{1}{C_s}\right) + \left(\frac{1}{K_y} - \frac{1}{K_x}\right)\right]\frac{s_y}{1 + s_y^2} \tag{76}$$

For the free-rolling tire at a small slip angle α, the aligning moment given by Equation (74) reduces to (with $s_y = \tan\alpha \approx \alpha$)

$$M_z = \frac{1}{6} C_\alpha \alpha \tag{77}$$

The lateral force, in this situation, is given by the second of Equations (68).

$$F_y = -C_\alpha \alpha \tag{78}$$

It is now possible to compute a definite value for the free-rolling pneumatic trail ℓ_x by substituting Equations (77) and (78) into Equation (27).

$$\ell_x = \frac{M_z}{F_y} = -\frac{L}{6} \qquad \text{(free-rolling)} \tag{79}$$

The HSRI-NBS-II model thus predicts the free-rolling pneumatic trail to be one-sixth of the non-slip contact length. The lateral traction force resultant is located behind the wheel center as shown in Figure 13 and tends to align the wheel with the direction of travel.

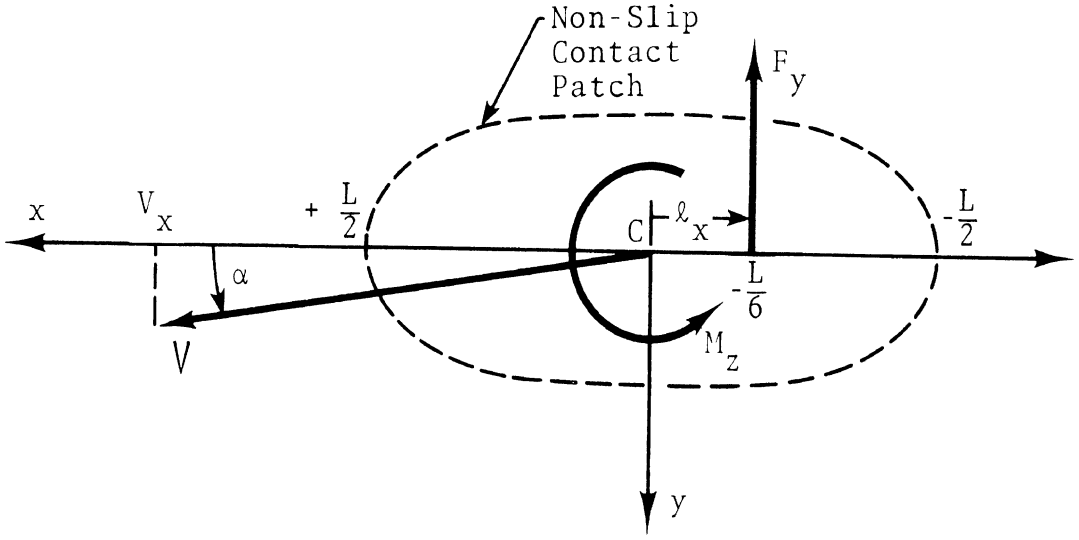

Figure 13. Free-rolling pneumatic trail ℓ_x for linear tire traction models at small slip angle α.

This result, valid for any[7] free-rolling lateral motion which retains completely adhesive contact, is common to all models which treat the tire as a linearly elastic structure.

GOODYEAR MODEL [5]

This model considers the entire contact region to have the constant coefficient of friction μ_o. A nonuniform pressure distribution is presumed and the adhesion limit as given by Equation (20), written below in terms of slip parameters,

$$\xi_a = \frac{\mu_o q_z(\xi_a)(1 - s_x)}{\sqrt{(k_x s_x)^2 + (k_y s_y)^2}} \tag{80}$$

will depend on the particular pressure distribution, $q_z(\xi)$, assumed. The pressure distribution may be approximated analytically or taken graphically from traction test results.

A technique is presented in the Goodyear paper [5] for consolidating the traction data taken over the complete range of tire operating conditions. This technique utilizes the moduli of two vectors, F and S, defined below.

---

[7] The requirement $\tan\alpha \approx \alpha$ isn't necessary for the derivation of Equation (79).

A vector S, called the slip-modulus vector, is employed to describe the slip operating conditions. Using s_x and s_y as defined by Equations (5) and (7)[8], the slip-modulus vector is

$$S = \frac{1}{k_y} [k_x s_x i + k_y s_y j]/(1 - s_x) \tag{81}$$

where i and j are unit vectors in the positive x and y directions, respectively. The magnitude of the slip-modulus vector is $S = |S|$.

The shear force distribution σ is considered as a vector with components q_x and q_y

$$\sigma = -(q_x i + q_y j)$$

which opposes S as shown in Figure 14.

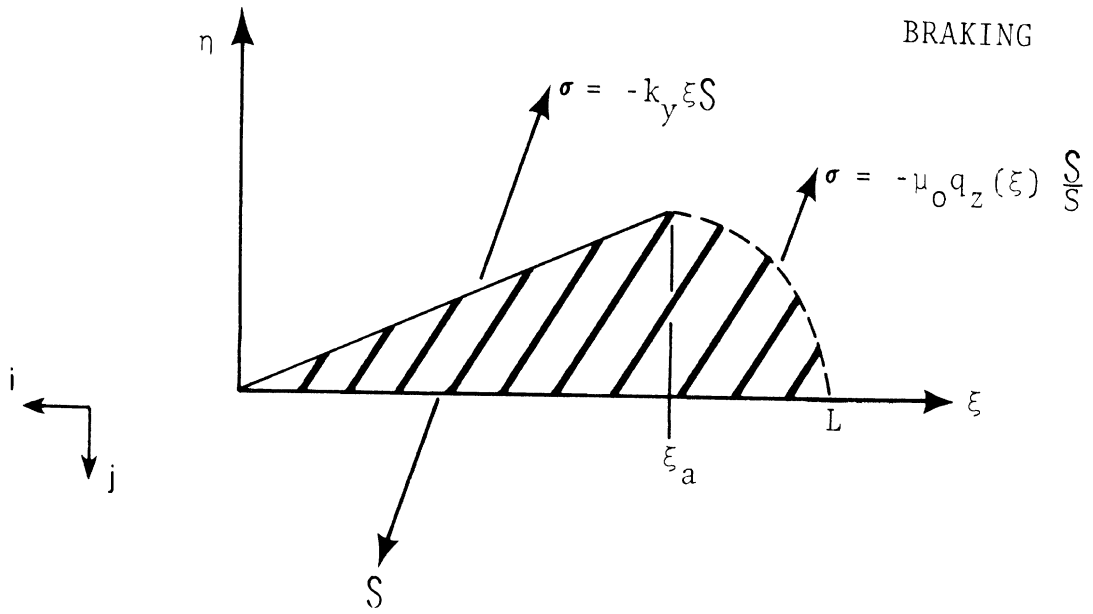

Figure 14. Goodyear model. Deformation and shear force distribution.

[8] s_x and s_y are defined differently in [5].

The shear force distribution is assumed to vary linearly with ξ in the adhesion region according to

$$\sigma = - k_y \xi \underline{S} \ .$$

In the sliding region, $\xi > \xi_a$, σ is assumed to vary with the arbitrary pressure distribution $q_z(\xi)$, viz.,

$$\sigma = - \mu_o \, q_z(\xi) \, \frac{\underline{S}}{S}$$

while maintaining the direction opposing the slip-modulus vector $\underline{S}$.

Assuming that the shear force distribution vector always opposes the slip-modulus vector allows the traction force vector $\underline{F}$ to be determined by the following integration over the contact length.

$$\underline{F} = w \int_o^L \sigma \, d\xi$$

$$\underline{F} = -w\left[\frac{1}{2} k_y \xi_a^{\,2} + \frac{\mu_o}{S} \int_{\xi_a}^{L} q_z(\xi) d\xi\right]\underline{S} \qquad (82)$$

The preceding equation expresses the dependence of the traction force vector, defined as

$$\underline{F} = F_x \underline{i} + F_y \underline{j}$$

on the slip-modulus vector $\mathbf{S}$ given by Equation (81). This analytical dependence of $\mathbf{F}$ upon $\mathbf{S}$ involves an arbitrary expression for the vertical contact pressure distribution $q_z(\xi)$.

The relationship between $\mathbf{F}$ and $\mathbf{S}$ can be determined experimentally by measuring longitudinal and lateral forces over a wide range of operating conditions. For a particular tire, this data can be consolidated into a single characteristic plot of $F = |\mathbf{F}|$ versus $S = |\mathbf{S}|$ (Figure 15).

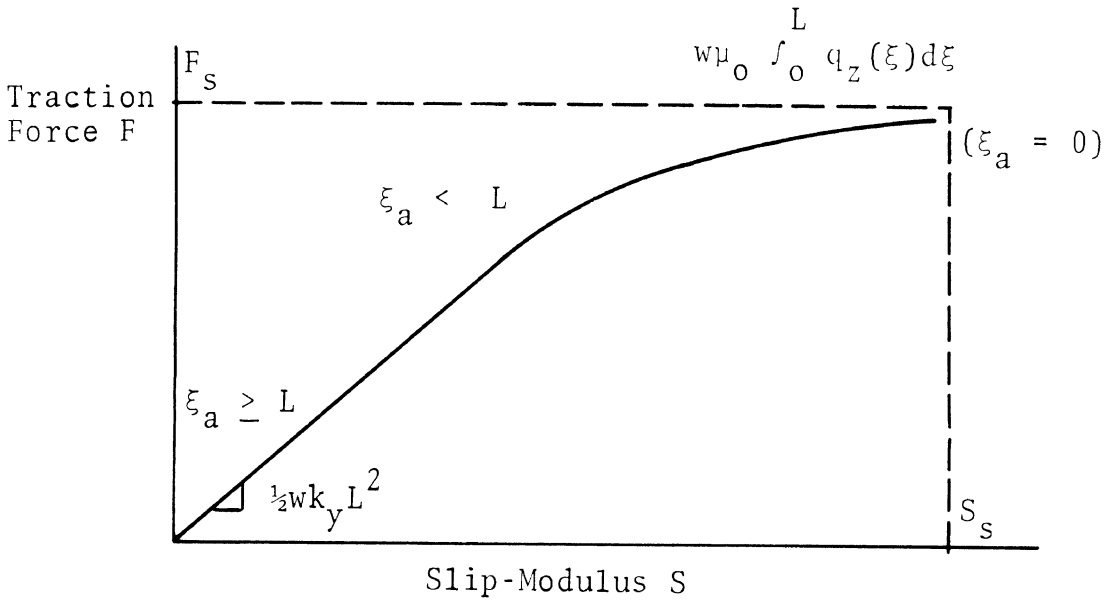

Figure 15. Consolidated traction data for a hypothetical tire.

The linear region in Figure 15 indicates complete adhesion with the force given by the first term of Equation (82). As sliding begins to appear ($\xi_a < L$), the plot becomes nonlinear with the influence of the second term of (82). When sliding dominates ($\xi_a = 0$), the limiting traction force, F_s, is attained and given by the second term of Equation (82).

When enough traction data has been taken to define the relationship illustrated in Figure 15, a graphical construction can be made to determine the interaction between the longitudinal and lateral force components. Usually this is developed as a plot of F_y versus F_x at a particular slip angle as shown in Figure 16.

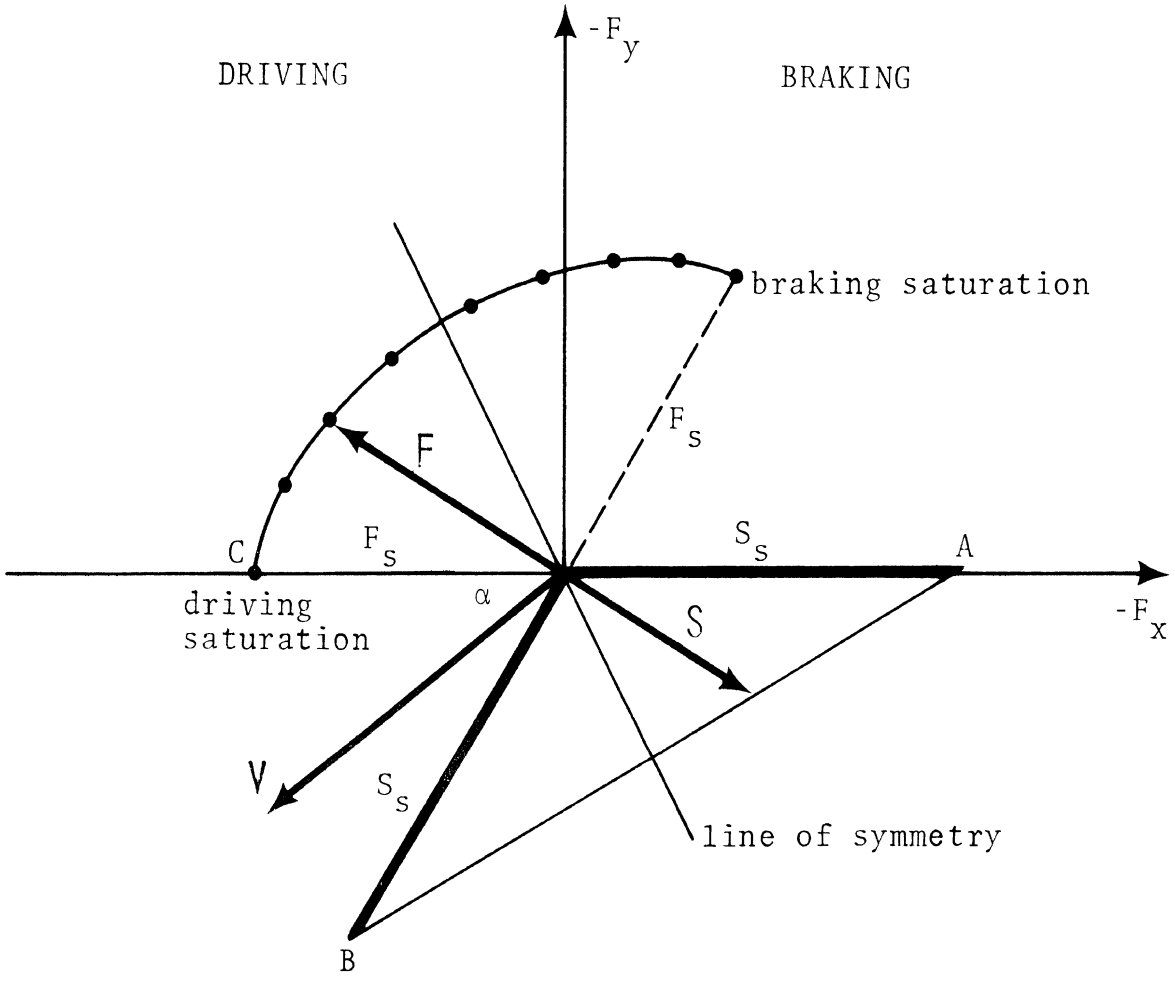

Figure 16. Construction of traction force component plot for slip angle α from consolidated data of Figure 15.

The construction for a particular slip angle α begins by determining the saturation slip value S_s where the limiting traction force F_s is attained. For driving traction, S_s is laid off on the negative x-axis and the force F_s on the positive x-axis. As the operating conditions shift from driving to braking, the vector $\mathbf{S}$ rotates clockwise while sweeping out the straight line AB (Figure 16). The traction force vector $\mathbf{F}$, always opposing $\mathbf{S}$, sweeps out the desired plot according to the magnitude relationship given in Figure 15. When S_s is again reached (now in braking), the plot is terminated. A line of symmetry is found to pass through the origin and the midpoint of AB.

As the slip angle α decreases, point B describes a circular arc toward the x-axis as shown in Figure 17. Point A does not move;

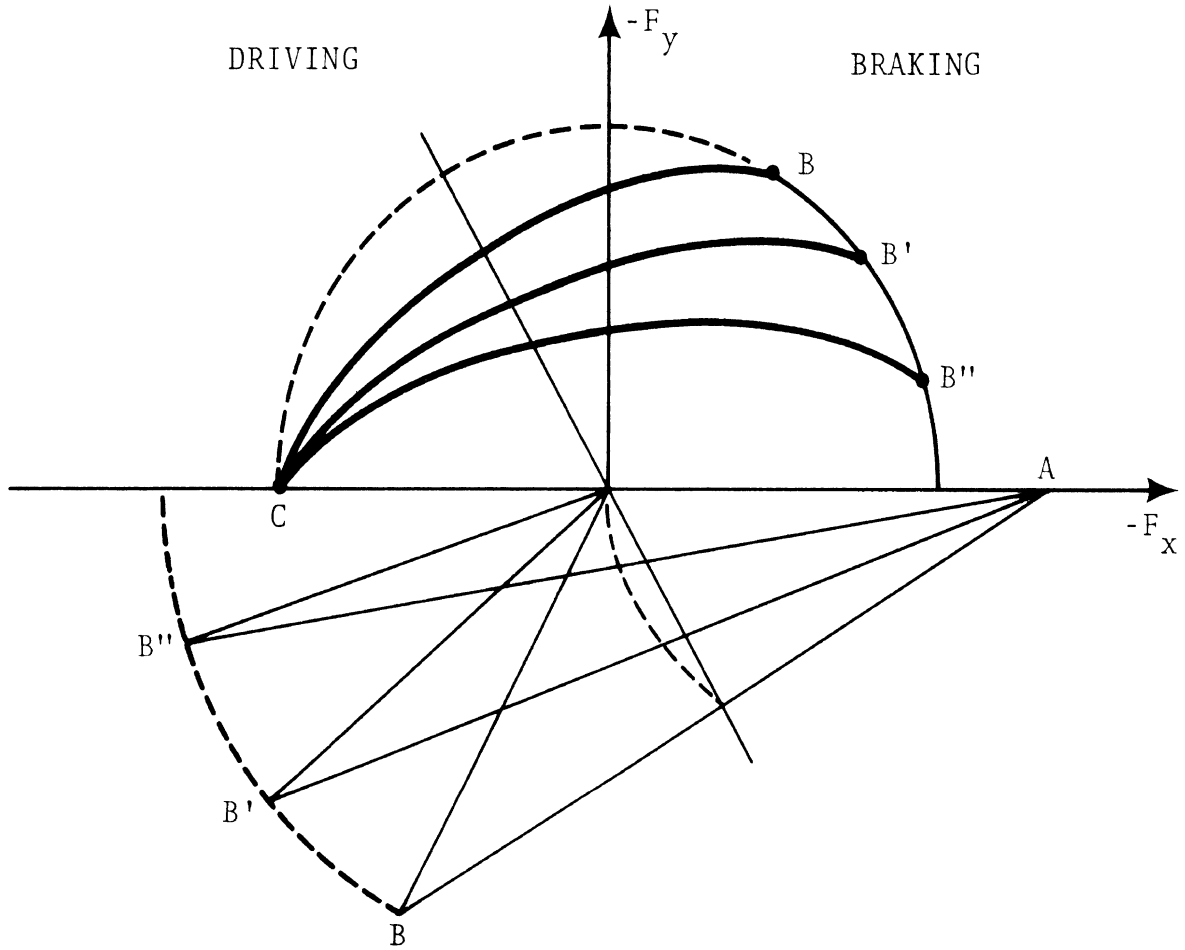

Figure 17. Traction force component plots at three slip angles.

consequently, all plots will begin at the driving saturation point C.

The traction equation (82) contains one unknown factor: the contact pressure distribution $q_z(\xi)$. When sufficient experimental data is available to characterize traction behavior as in Figure 15, Equation (82), viewed as an integral equation, may be solved for the integral $q_z(\xi)$. This is conveniently done by a graphical procedure outlined in [5]. The analysis of data from several tire traction testing programs indicates that the pressure distribution determined in this manner is roughly parabolic.

Closed form expressions for the traction force components F_x and F_y are not presented in the original publication [5]. The expressions for F_x and F_y are obtained from Equation (82) after the pressure distribution $q_z(\xi)$ is determined from the analysis of experimental traction data for a particular tire.

If a uniform pressure distribution is assumed such that

$$q_z = \frac{F_z}{wL}$$

the traction equations derived from the Goodyear model are identical to the traction equations of the HSRI-NBS-I model with the speed sensitivity coefficient, A_s, set equal to zero.

To investigate the influence of a nonuniform pressure distribution on the traction forces, the traction vector equation

(82), derived from the Goodyear model, will be evaluated with the assumption of a parabolic pressure distribution, viz.,

$$q_z(\xi) = \frac{6F_z}{wL}\left(1 - \frac{\xi}{L}\right)\frac{\xi}{L} \tag{83}$$

At the adhesion limit, $\xi = \xi_a$, the contact pressure is

$$q_z(\xi_a) = \frac{6F_z}{wL}\left(1 - \frac{\xi_a}{L}\right)\frac{\xi_a}{L} \tag{84}$$

The substitution of Equation (84) into Equation (80) enables the following explicit equation for the adhesion fraction, $\frac{\xi_a}{L}$, to be written.

$$\frac{\xi_a}{L} = 1 - \frac{1}{3}\frac{C_\alpha S}{\mu_o F_z} \tag{85}$$

where

$$C_\alpha S = \frac{\sqrt{(C_s s_x)^2 + (C_\alpha s_y)^2}}{(1 - s_x)} \tag{86}$$

is derived from the magnitude of the slip modulus vector (81).

Equations (85) and (86) show that complete adhesion ($\xi_a = L$) exists only for $s_x = s_y = 0$, the straight ahead free-rolling condition. Full sliding ($\xi_a = 0$), however, takes place when the operating conditions are such that $C_\alpha S = 3\mu_o F_z$ which occurs before wheel lock. This is quite different from the behavior of the HSRI-NBS-I model (see Equation (45)) where full sliding takes

place only when the wheel is locked ($s_x = 1$) although complete adhesion can exist at operating conditions other than straight ahead free-rolling.

Substituting (83) into the second term of (82), and integrating, yields the following traction force vector equation derived on the assumption of a parabolic pressure distribution.

$$F = \begin{cases} -\frac{1}{3} C_\alpha [1 + \frac{\xi_a}{L} + (\frac{\xi_a}{L})^2] S & 0 < \xi_a < L \\ -\mu_o F_z \frac{S}{S} & \xi_a = 0 \end{cases} \qquad (87)$$

Only two ranges, adhesion plus sliding and full sliding, are written because complete adhesion occurs only in the special case of straight ahead free-rolling ($s_x = s_y = 0$) when no traction forces are generated. The second expression of (87) is obtained by setting $\xi_a = 0$ in Equation (85).

The preceding analysis shows that the assumption of a non-uniform contact pressure distribution, such as parabolic, which vanishes at the exit point of the contact region produces the requirement for traction force generation to always be associated with a certain amount of sliding near the exit point of the contact region. Such a requirement does not exist in the HSRI models which, with the assumption of uniform contact pressure, permit traction force to be generated in completely adhesive contact.

The use of the slip modulus vector S, given by Equation (81), enables the components of the traction force vector F to be written as follows.

$$F_x = \begin{cases} -\frac{1}{3} C_s \frac{s_x}{1 - s_x} \left[1 + \frac{\xi_a}{L} + \left(\frac{\xi_a}{L} \right)^2 \right] & 0 < \xi_a < L \\ -\mu_o F_z \frac{C_s s_x}{\sqrt{(C_s s_x)^2 + (C_\alpha s_y)^2}} & \xi_a = 0 \end{cases} \tag{88}$$

$$F_y = \begin{cases} -\frac{1}{3} C_\alpha \frac{s_y}{1 - s_x} \left[1 + \frac{\xi_a}{L} + \left(\frac{\xi_a}{L} \right)^2 \right] & 0 < \xi_a < L \\ -\mu_o F_z \frac{C_\alpha s_y}{\sqrt{(C_s s_x)^2 + (C_\alpha s_y)^2}} & \xi_a = 0 \end{cases} \tag{89}$$

These traction force component equations should be compared with Equations (42), (43), (46), and (47) for the HSRI-NBS-I model and with Equations (64) and (65) for the HSRI-NBS-II model. Note that the full sliding ($\xi_a = 0$) traction forces depend on the traction stiffnesses C_s and C_α. This behavior is a consequence of constraining the shear force distribution to oppose the slip modulus vector S in the sliding region.

Since the Goodyear model does not separate the tread stiffness from the carcass stiffness, the aligning moment is computed from Equation (25) rewritten below with $1/K_x = 1/K_y = 0$.

$$M_z = -w \int_0^L [q_x v - q_y (u + \xi - \tfrac{L}{2})] d\xi \tag{90}$$

The shear force components, obtained from the following shear force vector equation, viz.,

$$\sigma = \begin{cases} -k_y \xi S & 0 \leq \xi \leq \xi_a \\ -\mu_o q_z(\xi) \dfrac{S}{\bar{S}} & \xi_a \leq \xi \leq L \end{cases} \tag{91}$$

are

$$q_x = \begin{cases} k_x \dfrac{s_x}{1 - s_x} \xi & 0 \leq \xi \leq \xi_a \\ k_x \dfrac{s_x}{1 - s_x} \dfrac{(L - \xi)}{(L - \xi_a)} \xi & \xi_a \leq \xi \leq L \end{cases}$$

$$q_y = \begin{cases} k_y \dfrac{s_y}{1 - s_x} \xi & 0 \leq \xi \leq \xi_a \\ k_y \dfrac{s_y}{1 - s_x} \dfrac{(L - \xi)}{(L - \xi_a)} \xi & \xi_a \leq \xi \leq L \end{cases} \tag{92}$$

(Equation (85) was used in simplifying the above expressions.) Since the contacting tread rubber is assumed to be linearly elastic (as expressed by the longitudinal and lateral stiffnesses, k_x and k_y) the displacements throughout the contact region are given by

$$u = \frac{q_x}{k_x}$$

$$v = \frac{q_y}{k_y} \tag{93}$$

After substituting (92) and (93) into (90) and performing the integration, the aligning moment as derived with the assumption of a parabolic pressure distribution is found to be

$$M_z = -\frac{L}{6}\left\{\frac{2}{5}(C_s - C_\alpha)\left[1 + 2\frac{\xi_a}{L} + 3\left(\frac{\xi_a}{L}\right)^2 + 4\left(\frac{\xi_a}{L}\right)^3\right]\frac{s_x}{1 - s_x}\right.$$

$$\left. - C_\alpha\left(\frac{\xi_a}{L}\right)^3\right\}\frac{s_y}{1 - s_x} \qquad 0 < \xi_a < L \qquad (94)$$

Equation (94) shows the moment to have an implicit dependence on tire load, F_z, through the adhesion limit, ξ_a, given by Equation (85).

Setting $\xi_a = 0$ in (94) gives the aligning moment generated in fully developed sliding (which occurs <u>before</u> $s_x = 1$).

$$M_z = -\frac{L}{15}(C_s - C_\alpha)\frac{s_x s_y}{(1 - s_x)^2} \qquad \xi_a = 0 \qquad (95)$$

The vanishing of the adhesion region before wheel lock, a consequence of assuming a contact pressure distribution which vanishes at the contact entry and exit points, renders the Goodyear tire model incapable of simulating locked wheel aligning moment. At a particular slip angle (s_y) it is incorrect to compute the aligning moment at values of s_x beyond those which cause the adhesion limit to vanish. A derivation and discussion of the upper bounds on s_x and s_y imposed by the assumption of parabolic contact pressure is given in Appendix III. The upper bounds are found to depend on tire load.

SAKAI MODEL [6]

Several major advances in traction force simulation are incorporated in this model. Based on an idea of W. Bergman [7], the Sakai model contains a mechanism for simulating the influence of braking and driving tractive forces (longitudinal forces) on lateral force generation. The analysis, however, differs from that

of Bergman in that Sakai views Bergman's "effective tractive effort" as acting along the deflected tread surface (in the direction of motion for driving, against the direction of motion for braking). The Bergman effective tractive effort acts in the wheel plane.

Figure 18 shows the adhesive shear forces assumed by Sakai to be acting on a tread element deflected by braking at a slip angle α. The Sakai effective tractive effort is the tangential

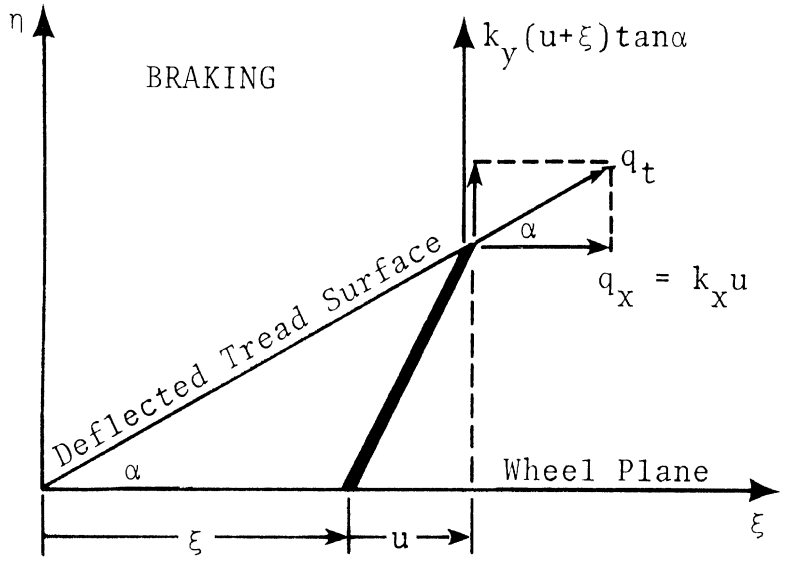

Figure 18. Adhesion region longitudinal and lateral forces acting on the Sakai model. The tangential tractive effort q_t.

force q_t generated along the deflected tread surface when braking is applied to a tire operating at a slip angle.

$$q_t = q_x \sec\alpha \tag{96}$$

The physical Sakai model has the tread elements attached to an elastically supported beam as shown in Figure 19.

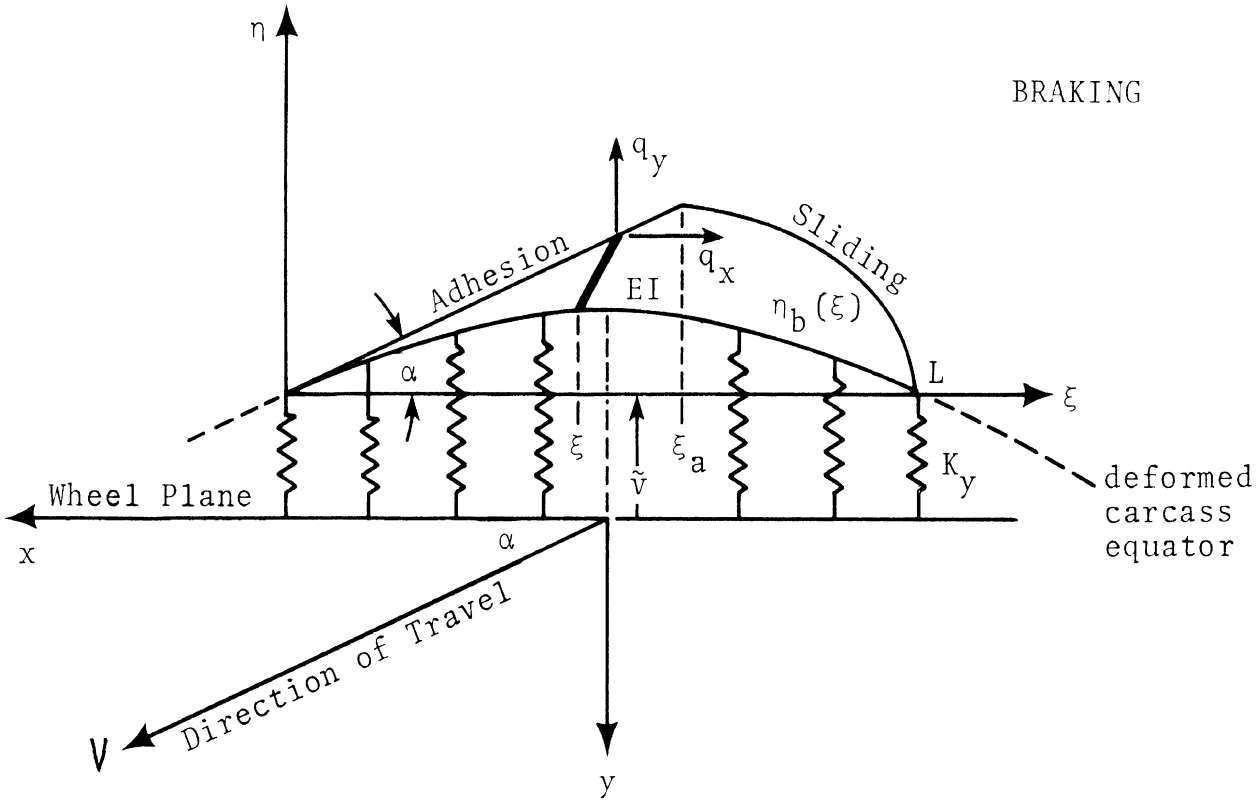

Figure 19. Physical Sakai model.

The elastic beam deflection in the contact region ($0 \leq \xi \leq L$) is approximated by the parabolic curve

$$\eta_b = \frac{F_y}{k_y b}\left(1 - \frac{\xi}{L}\right)\frac{\xi}{L} \tag{97}$$

where b (length units) is the deformation constant of the elastically supported beam. The constant b, experimentally determined, depends on both the beam stiffness EI and the beam foundation modulus K_y.

In the adhesion region, the tread element deformation expressions are given by Equations (13) and (14) written in terms of slip parameters by use of Equations (6) and (8).

$$u = \frac{s_x}{1 - s_x} \xi \tag{98}$$

$$v = \frac{s_y}{1 - s_x} \xi - \eta_b(\xi) \tag{99}$$

The stresses are linearly related to the deformations by the tread element stiffnesses k_x and k_y. The lateral stress, however, is increased by the lateral component of the tangential tractive force q_t defined earlier.

$$q_x = k_x \frac{s_x}{1 - s_x} \xi \tag{100}$$

$$q_y = k_y \left[\frac{s_y}{1 - s_x} \xi - \eta_b(\xi)\right] + k_x \frac{s_x s_y}{1 - s_x} \xi \tag{101}$$

or

$$q_y = (k_y + k_x s_x) \frac{s_y}{1 - s_x} \xi - k_y \eta_b(\xi) \tag{102}$$

As in the Goodyear model, a parabolic contact pressure distribution is assumed according to Equation (83), repeated below.

$$q_z = \frac{6F_z}{wL} \left(1 - \frac{\xi}{L}\right) \frac{\xi}{L} \tag{83}$$

The adhesion limit, ξ_a, is determined by equating the resultant elastic stress at this point to the maximum static friction force $\mu_o q_z(\xi_a)$, determined from the parabolic pressure distribution (83).

$$\sqrt{q_x^2 + q_y^2}\Big|_{\xi=\xi_a} = \mu_o q_z\Big|_{\xi=\xi_a} \tag{103}$$

Equation (100) and the first term[9] of Equation (101) are used in the left side of (103). After some algebraic manipulation, the adhesion limit is found to be

$$\frac{\xi_a}{L} = 1 - \frac{(k_y s_y \frac{F_y}{b} - \sqrt{Z})L}{\left[\left(\frac{F_y}{b}\right)^2 - \left(\frac{6\mu_o F_z}{wL}\right)^2\right](1 - s_x)} \tag{104}$$

where

$$Z = (k_y s_y)^2 \left(\frac{6\mu_o F_z}{wL}\right)^2 - (k_x s_x)^2 \left[\left(\frac{F_y}{b}\right)^2 - \left(\frac{6\mu_o F_z}{wL}\right)^2\right]$$

If the influence of F_y is neglected (rigid beam tread base), the adhesion fraction reduces to

$$\frac{\xi_a}{L} = 1 - \frac{\sqrt{(C_s s_x)^2 + (C_\alpha s_y)^2}}{3\mu_o F_z (1 - s_x)} \tag{105}$$

---

[9] Sakai neglects the last term of (101) as being small compared with the first term for the purpose of computing the adhesion limit.

where C_s and C_α are the braking and cornering stiffnesses defined earlier by Equations (40) and (41). Equation (105) is identical to Equation (85) derived with the Goodyear model. Complete adhesion ($\xi_a = L$) occurs only for the straight ahead, free-rolling tire.

At the adhesion limit, the static friction coefficient μ_o immediately drops to μ and the sliding shear stress shifts in direction to oppose the sliding velocity V_s. As shown in Figure 20, V_{cx}/V_s and V_{cy}/V_s are the cosine and sine of the slide angle θ.

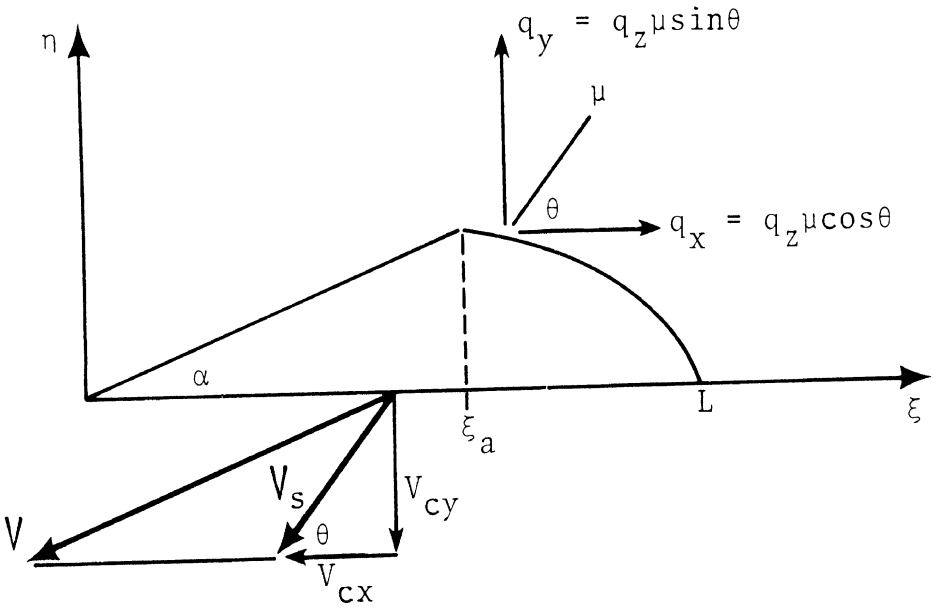

Figure 20. Sliding friction shear forces (braking).

By use of (6), (8), and (9), the slide angle may be expressed in terms of the slip parameters s_x and s_y.

$$\frac{V_{cx}}{V_s} = \cos\theta = \frac{s_x}{\sqrt{s_x^2 + s_y^2}}$$

(sliding region, $V_s = V_c$)

$$\frac{V_{cy}}{V_s} = \sin\theta = \frac{s_y}{\sqrt{s_x^2 + s_y^2}}$$

The sliding friction μ is assumed by Sakai to be slightly orthotropic with constant components μ_x and μ_y. In the consideration of this treatment of sliding friction, it should be recalled that the HSRI models consider the sliding friction μ to be isotropic with magnitude dependent on the sliding velocity V_s. The Goodyear model considers the friction to be isotropic and constant throughout the contact region.

Prescribing the stress in the sliding region to have a line of action different from the stress in the adhesion region leads to a displacement discontinuity at the adhesion limit. This was recognized in the HSRI-NBS-II model and a transition region employed to permit gradual shift into full sliding. The Sakai model does not recognize a transition region. The displacement discontinuity present at ξ_a may be computed as follows where u_1, v_1 are displacements just before the adhesion limit and u_2, v_2 are the displacements just beyond the adhesion limit. From (98),

$$u_1 = \frac{s_x}{1 - s_x} \xi_a \qquad (106)$$

Just beyond the adhesion limit,

$$u_2 = \frac{q_x}{k_x}$$

From Figure 20 and Equation (83),

$$u_2 = \frac{\mu_x}{k_x} \frac{6F_z}{wL^2} \left(1 - \frac{\xi_a}{L}\right) \frac{V_{cx}}{V_s} \xi_a$$

Introducing Equations (6), (9), and (105) into the above,

$$u_2 = \frac{\mu_x}{\mu_o} \sqrt{\frac{s_x^2 + \left(\frac{C_\alpha}{C_s} s_y\right)^2}{s_x^2 + s_y^2}} \left(\frac{s_x}{1 - s_x}\right) \xi_a \qquad (107)$$

The longitudinal displacement discontinuity, $\Delta u = u_2 - u_1$, is computed by subtracting Equation (106) from Equation (107).

From (99), with $\eta_b(\xi)$ neglected,

$$v_1 = \frac{s_y}{1 - s_x} \xi_a \qquad (108)$$

After the adhesion limit,

$$v_2 = \frac{q_y}{k_y}$$

From Figure 20 and Equation (83),

$$v_2 = \frac{\mu_y}{k_y} \frac{6F_z}{wL^2} \left(1 - \frac{\xi_a}{L}\right) \frac{V_{cy}}{V_s} \xi_a$$

Introducing Equations (6), (9), and (105) into the above,

$$v_2 = \frac{\mu_y}{\mu_o} \sqrt{\frac{\left(\frac{C_s}{C_\alpha} s_x\right)^2 + s_y^2}{s_x^2 + s_y^2}} \left(\frac{s_y}{1 - s_x}\right) \xi_a \qquad (109)$$

The lateral displacement discontinuity, $\Delta v = v_2 - v_1$, is computed by subtracting Equation (108) from Equation (109).

The displacement discontinuity vanishes at zero slip angle ($s_y = 0$) if $\mu_x = \mu_o$. Since $\mu_x \simeq \mu_y \simeq \mu_o$ in most situations, the magnitude of the discontinuity depends primarily on how much the stiffness ratio

$$\frac{C_s}{C_\alpha} = \frac{k_x}{k_y}$$

deviates from unity. Traction test results have shown the stiffness ratio to be approximately 4 for a bias tire and approximately 2 for a radial tire.

The Sakai traction forces are computed according to Equations (21) and (22) with the following shear force distributions.

$$q_x = \begin{cases} k_x \dfrac{s_x}{1 - s_x}\,\xi & 0 \le \xi < \xi_a \\ \mu_x \dfrac{V_{cx}}{V_s}\dfrac{6F_z}{wL}\left(1 - \dfrac{\xi}{L}\right)\dfrac{\xi}{L} & \xi_a < \xi \le L \end{cases} \tag{110}$$

$$q_y = \begin{cases} (k_y + k_x s_x)\dfrac{s_y}{1 - s_x}\,\xi & 0 \le \xi < \xi_a \\ \mu_y \dfrac{V_{cy}}{V_s}\dfrac{6F_z}{wL}\left(1 - \dfrac{\xi}{L}\right)\dfrac{\xi}{L} & \xi_a \le \xi < L \end{cases}$$

The discontinuity at $\xi = \xi_a$ in the longitudinal shear force distribution, q_x, vanishes when $C_s = C_\alpha$ and $\mu_x = \mu_o$. The use of the effective tractive effort concept produces a permanent discontinuity at $\xi = \xi_a$ in the lateral shear force distribution. The beam deformation, $\eta_b(\xi)$, has been neglected in the expression for q_y.

After performing the integrations and introducing the traction stiffness parameters (C_s and C_α), the Sakai model traction forces may be written as follows

$$F_x = \begin{cases} -C_s \dfrac{s_x}{1 - s_x}\left(\dfrac{\xi_a}{L}\right)^2 - \mu_x F_z \dfrac{s_x}{\sqrt{s_x^2 + s_y^2}}\left[1 - 3\left(\dfrac{\xi_a}{L}\right)^2 + 2\left(\dfrac{\xi_a}{L}\right)^3\right] & 0 < \xi_a < L \\ -\mu_x F_z \dfrac{s_x}{\sqrt{s_x^2 + s_y^2}} & \xi_a = 0 \end{cases} \tag{111}$$

$$F_y = \begin{cases} -(C_\alpha + C_s s_x)\frac{s_y}{1 - s_x}\left(\frac{\xi_a}{L}\right)^2 - \mu_y F_z \frac{s_y}{\sqrt{s_x^2 + s_y^2}}\left[1 - 3\left(\frac{\xi_a}{L}\right)^2 + 2\left(\frac{\xi_a}{L}\right)^3\right] & 0 < \xi_a < L \\ -\mu_y F_z \frac{s_y}{\sqrt{s_x^2 + s_y^2}} & \xi_a = 0 \end{cases} \tag{112}$$

As for the Goodyear model with a parabolic pressure distribution, only two ranges, adhesion plus sliding and full sliding, are written because complete adhesion is possible only in the special case of straight-ahead free-rolling ($s_x = s_y = 0$). Unlike the Goodyear model, the full sliding ($\xi_a = 0$) traction forces do not depend on the traction stiffness parameters. This is a consequence of allowing the sliding shear stress to oppose the sliding velocity instead of the direction of the "slip-modulus vector" employed in the definition of the Goodyear model. The Sakai traction force equations (111-112) should be compared with Equations (42), (43), (46), and (47) for the HSRI-NBS-I model, Equations (64) and (65) for the HSRI-NBS-II model, and Equations (88) and (89) for the Goodyear model.

Since the Sakai model permits the rigid tread base to translate laterally on an elastic foundation of modulus K_y, the aligning moment is computed according to Equation (25) as rewritten below with $1/K_x = 0$.

$$M_z = -w \int_o^L [q_x v - q_y(u + \xi - \frac{L}{2})]d\xi - F_x F_y / K_y \qquad (113)$$

The shear stress distributions, q_x and q_y, are given by Equations (110). For the express purpose of evaluating Equation (113), the following simplified set of displacement distributions, u and v, are assumed which ignore the longitudinal displacement u entirely and consider the lateral displacement v in the sliding region to decrease linearly to zero at the contact exit point.

$$u = 0 \qquad 0 \leq \xi \leq L$$

$$v = \begin{cases} s_y \xi & 0 \leq \xi \leq \xi_a \\ s_y \xi_a \dfrac{L - \xi}{L - \xi_a} & \xi_a \leq \xi \leq L \end{cases} \qquad (114)$$

Figure 21 illustrates the tread element deformation assumed for the moment computation. The linearly decreasing displacement in the sliding region is a more realistic approximation than the uniform sliding region displacement assumed by the HSRI-NBS-I model (see Figure 8). Note also that displacement continuity is maintained for the moment computation although the shear stresses, q_x and q_y, still contain the discontinuity across which the traction forces were computed.

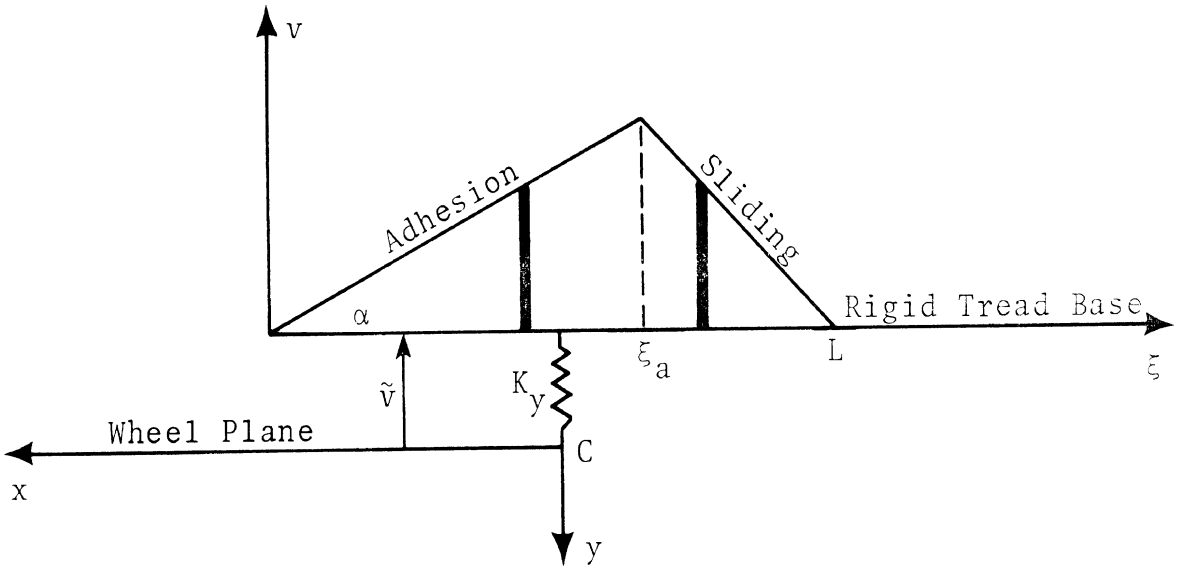

Figure 21. Displacements assumed by the Sakai model for the computation of aligning moment.

Denoting the adhesion region contribution to the aligning moment by M' and taking the shear force and displacement distributions from (110) and (114), the first integral of (113) is evaluated as follows.

$$M' = -w \int_0^{\xi_a} [k_x \frac{s_x s_y}{1 - s_x} \xi^2 - (k_y + k_x s_x) \frac{s_y}{1 - s_x} \xi(\xi - \frac{L}{2})] d\xi$$

$$= -w \int_0^{\xi_a} [\frac{L}{2}(k_y + k_x s_x)\xi - k_y \xi^2] d\xi \frac{s_y}{1 - s_x}$$

After performing the integration and introducing the traction stiffnesses C_s and C_α,

$$M' = -\frac{L}{6}\left[3(C_\alpha + C_s s_x) - 4C_\alpha \frac{\xi_a}{L}\right]\left(\frac{\xi_a}{L}\right)^2 \frac{s_y}{1 - s_x} \qquad (115)$$

Denoting the sliding region contribution to the aligning moment by M'', the second integral of (113) is evaluated as follows.

$$M'' = -6F_z \int_{\xi_a}^{L} \left[\mu_x \frac{V_{cy}}{V_s} s_y \left(\frac{\xi_a}{L - \xi_a}\right)\left(1 - \frac{\xi}{L}\right)^2 \frac{\xi}{L} - \mu_y \frac{V_{cy}}{V_s}\left(1 - \frac{\xi}{L}\right)\frac{\xi}{L}\left(\xi - \frac{L}{2}\right)\right] d\xi$$

$$= -6F_z \int_{\xi_a}^{L} \left[\mu_x s_x \left(\frac{\xi_a}{L - \xi_a}\right)\left(1 - \frac{\xi}{L}\right)^2 \frac{\xi}{L} - \mu_y \left(1 - \frac{\xi}{L}\right)\left(\frac{\xi^2}{L} - \frac{\xi}{2}\right)\right] d\xi \frac{s_y}{\sqrt{s_x^2 + s_y^2}}$$

After performing the integration,

$$M'' = -\frac{L}{2}\left[\mu_x s_x \left(1 + 3\frac{\xi_a}{L}\right) - 3\mu_y \frac{\xi_a}{L}\right] F_z \frac{s_y}{\sqrt{s_x^2 + s_y^2}} \qquad (116)$$

The aligning moment equation (113) is now

$$M_z = M' + M'' - F_x F_y / K_y$$

where M' and M'' are given by Equations (115) and (116). The complete expression for the Sakai aligning moment is

$$M_z = -\frac{L}{6}\left[3(C_\alpha + C_s s_x) - 4C_\alpha \frac{\xi_a}{L}\right]\left(\frac{\xi_a}{L}\right)^2 \frac{s_y}{1 - s_x}$$

$$-\frac{L}{2}\left[\mu_x s_x \left(1 + 3\frac{\xi_a}{L}\right) - 3\mu_y \frac{\xi_a}{L}\right] F_z \frac{s_y}{\sqrt{s_x^2 + s_y^2}} \left(1 - \frac{\xi_a}{L}\right)^2 \frac{\xi_a}{L}$$

$$- F_x F_y / K_y \qquad (117)$$

where the traction forces, F_x and F_y, are given by Equations (111) and (112).

Setting $\xi_a = 0$ in Equation (117) yields the aligning moment generated by the Sakai model in fully developed sliding.

$$M_z = -\frac{\mu_x \mu_y F_z^2}{K_y} \frac{s_x s_y}{s_x^2 + s_y^2} \qquad (118)$$

HSRI-NBS-III

Favorable experience gained during the study of the Goodyear and Sakai tire models, which assume a parabolic contact pressure distribution, has led to the incorporation of a parabolic pressure distribution, q_z, in a rederivation of the force and moment equations of the HSRI-NBS-II model. This modification, which

substantially changes the traction characteristics obtained from the HSRI-NBS-II model with uniform contact pressure, is the basis of the HSRI-NBS-III tire traction model.

The parabolic contact pressure distribution is defined to vanish at the entry ($\xi = 0$) and exit ($\xi = L$) points of the contact region. The parabolic expression, Equation (83) used in analysis of the Goodyear model, is

$$q_z(\xi) = \frac{6F_z}{wL}\left(1 - \frac{\xi}{L}\right)\frac{\xi}{L} \tag{83}$$

where

$$F_z = w\int_0^L q_z(\xi)d\xi$$

is the tire load.

The adhesion limit is obtained by substituting Equation (83) evaluated at $\xi = \xi_a$, into Equation (60). After rearrangement, the result obtained is the adhesion fraction previously derived for the Sakai model

$$\frac{\xi_a}{L} = 1 - \frac{\sqrt{(C_s s_x)^2 + (C_\alpha s_y)^2}}{3\mu_o F_z(1 - s_x)} \tag{105}$$

with C_s and C_α the braking and cornering stiffnesses defined by Equations (40) and (41).

The limit of the transition region is obtained by substituting Equation (83), evaluated at $\xi = \xi_s$, into Equation (59). After rearrangement, the result is written as the transition limit fraction

$$\frac{\xi_s}{L} = 1 - \left(\frac{C_s C_\alpha}{C_s + C_\alpha}\right) \frac{\sqrt{s_x^2 + s_y^2}}{3\mu F_z (1 - s_x)} \tag{119}$$

It is evident from Equation (105) that complete adhesion ($\xi_a = L$) will occur only for straight-ahead ($s_y = 0$), free-rolling ($s_x = 0$) tire operation. As Equation (119) shows that $\xi_s < L$ for all conditions other than straight-ahead free-rolling, and $\xi_a \leq \xi_s$, the HSRI-NBS-III model will always exhibit a certain amount of sliding in the contact region.

The traction forces, F_x and F_y, are obtained by using the parabolic pressure distribution in evaluating the terms of Equations (64) and (65). The adhesion region terms, F_{xa} and F_{ya}, are unchanged as they do not depend on the tire load, F_z.

In the transition region, the shear stress distribution is assumed to be parabolic in accordance with the vertical contact pressure. It is therefore necessary to prescribe parabolic functions for the displacements, $u_t(\xi)$ and $v_t(\xi)$ in the transition region.

$$\begin{pmatrix} u_t \\ v_t \end{pmatrix} = a_o + a_1 \xi + a_2 \xi^2$$

The coefficients, a_o, a_1, a_2, are chosen such that

$$u_t(\xi_a) = u_a \qquad v_t(\xi_a) = v_a$$
$$u_t(\xi_s) = u_s \qquad v_t(\xi_s) = v_s$$
$$u_t(L) = 0 \qquad v_t(L) = 0$$

where u_a, v_a, u_s, v_s are the displacements at the limits of the adhesion and transition regions. The parabolic transition region displacement functions, satisfying the above conditions, are

$$u_t = \frac{1}{t}\left[\frac{u_a}{L - \xi_a}(\xi_s - \xi) - \frac{u_s}{L - \xi_s}(\xi_a - \xi)\right](L - \xi)$$
$$v_t = \frac{1}{t}\left[\frac{v_a}{L - \xi_a}(\xi_s - \xi) - \frac{v_s}{L - \xi_s}(\xi_a - \xi)\right](L - \xi) \qquad (120)$$

The transition region force terms, F_{xt} and F_{yt}, are now obtained by integrating $q_x = k_x u_t$ and $q_y = k_y v_t$ over the transition region ($\xi_a \leq \xi < \xi_s$).

The sliding region force terms, F_{xs} and F_{ys}, are obtained by integrating

$$q_x = \frac{V_{cx}}{V_s}\mu\frac{6F_z}{wL}(1 - \frac{\xi}{L})\frac{\xi}{L}$$
$$q_y = \frac{V_{cy}}{V_s}\mu\frac{6F_z}{wL}(1 - \frac{\xi}{L})\frac{\xi}{L} \qquad (121)$$

over the sliding region ($\xi_s \leq \xi \leq L$).

After carrying out the indicated integrations, the HSRI-NBS-III tire model traction force components are

$$
\begin{aligned}
F_{xa} &= -C_s \frac{s_x}{1 - s_x} \left(\frac{\xi_a}{L}\right)^2 \\
F_{xt} &= -\left[\frac{1}{3} C_s \frac{s_x}{1 - s_x} \left(3 - 2\frac{\xi_a}{L} - \frac{\xi_s}{L}\right)\frac{\xi_a}{L} / \left(1 - \frac{\xi_a}{L}\right)\right. \\
&\quad \left. + \mu F_z \frac{s_x}{\sqrt{s_x^2 + s_y^2}} \left(3 - 2\frac{\xi_s}{L} - \frac{\xi_a}{L}\right)\frac{\xi_s}{L}\right] \left(\frac{\xi_s}{L} - \frac{\xi_a}{L}\right) \\
F_{xs} &= -\mu F_z \frac{s_x}{\sqrt{s_x^2 + s_y^2}} \left[1 - 3\left(\frac{\xi_s}{L}\right)^2 + 2\left(\frac{\xi_s}{L}\right)^3\right]
\end{aligned}
\tag{122}
$$

$$
\begin{aligned}
F_{ya} &= -C_\alpha \frac{s_y}{1 - s_x} \left(\frac{\xi_a}{L}\right)^2 \\
F_{yt} &= -\left[\frac{1}{3} C_\alpha \frac{s_y}{1 - s_x} \left(3 - 2\frac{\xi_a}{L} - \frac{\xi_s}{L}\right)\frac{\xi_a}{L} / \left(1 - \frac{\xi_a}{L}\right)\right. \\
&\quad \left. + \mu F_z \frac{s_y}{\sqrt{s_x^2 + s_y^2}} \left(3 - 2\frac{\xi_s}{L} - \frac{\xi_a}{L}\right)\frac{\xi_s}{L}\right] \left(\frac{\xi_s}{L} - \frac{\xi_a}{L}\right) \\
F_{ys} &= -\mu F_z \frac{s_y}{\sqrt{s_x^2 + s_y^2}} \left[1 - 3\left(\frac{\xi_s}{L}\right)^2 + 2\left(\frac{\xi_s}{L}\right)^3\right]
\end{aligned}
\tag{123}
$$

Referring to Equations (105) and (119), it is seen that the adhesion and transition regions vanish before wheel lock ($s_x = 1$). If the tire operating conditions are such that $\xi_a = 0$ but $\xi_s > 0$, the resulting traction forces, from Equations (122-3),

$$F_x = -\mu F_z \frac{s_x}{\sqrt{s_x^2 + s_y^2}}$$

$$F_y = -\mu F_z \frac{s_y}{\sqrt{s_x^2 + s_y^2}} \qquad (124)$$

are seen to be equivalent to the traction force expressions for full sliding contact ($\xi_a = \xi_s = 0$). Equations (124) should be compared with the analogous Equations (69) for the HSRI-NBS-II model. The longitudinal slip parameter, s_x, appears in Equations (124) because full sliding occurs before wheel lock.

The aligning moment, M_z, is obtained by using the parabolic pressure distribution in evaluating the terms of Equation (71). The adhesion region term, M_{za}, being independent of tire load, is unchanged.

The transition region term, M_{zt}, is found by a rather lengthy integration

$$M_{zt} = -w \int_{\xi_a}^{\xi_s} [q_x v - q_y (u + \xi - \frac{L}{2})] d\xi$$

with $u = u_t$ and $v = v_t$ where u_t, v_t are given by Equations (120) and $q_x = k_x u_t$, $q_y = k_y v_t$.

The sliding region term, M_{zs}, is found with the integration

$$M_{zs} = -w\int_{\xi_s}^{L} [q_x v - q_y(u + \xi - \frac{L}{2})]d\xi$$

where q_x and q_y are given by Equations (121) and $u = q_x/k_x$, $v = q_y/k_y$.

The resulting aligning moment terms, written with slip parameters s_x and s_y, are written as Equations (125), below.

$$M_{za} = -\frac{s_y L}{3(1-s_x)}\left[2(C_s - C_\alpha)\frac{s_x}{1-s_x}\frac{\xi_a}{L} - \frac{1}{2}C_\alpha(4\frac{\xi_a}{L} - 3)\right](\frac{\xi_a}{L})^2$$

$$M_{zt} = -s_y L\left[(C_s - C_\alpha)\left\{\frac{s_x}{(1-s_x)^2}(\frac{\xi_a}{L})^2\frac{1}{(1-\frac{\xi_a}{L})^2}\frac{1}{15}\left[6(\frac{\xi_a}{L})^2\right.\right.\right.$$

$$\left.\left.\left. + 3\frac{\xi_a}{L}\frac{\xi_s}{L} + (\frac{\xi_s}{L})^2 - 15\frac{\xi_a}{L} - 5\frac{\xi_s}{L} + 10\right]\right.$$

$$+ \frac{s_x \mu F_z}{(1-s_x)\sqrt{s_x^2+s_y^2}}\left(\frac{1}{C_s} + \frac{1}{C_\alpha}\right)\frac{\xi_a}{L}\frac{\xi_s}{L}\frac{1}{(1-\frac{\xi_a}{L})}\frac{1}{10}\left[3(\frac{\xi_s}{L})^2\right.$$

$$\left. + 3(\frac{\xi_a}{L})^2 + 4\frac{\xi_a}{L}\frac{\xi_s}{L} - 10(\frac{\xi_a}{L} + \frac{\xi_s}{L}) + 10\right]$$

$$+ \frac{s_x \mu^2 F_z^2}{(s_x^2 + s_y^2)C_s C_\alpha}\frac{3}{10}\left[6(\frac{\xi_s}{L})^2 + 3\frac{\xi_a}{L}\frac{\xi_s}{L} + (\frac{\xi_a}{L})^2\right.$$

$$\left.\left. - 15\frac{\xi_s}{L} - 5\frac{\xi_a}{L} + 10\right]\right\}$$

$$+ \frac{C_\alpha}{1-s_x} \frac{\xi_a}{L} \frac{1}{(1-\frac{\xi_a}{L})} \frac{1}{6} \left[3-3\frac{\xi_a}{L}(2-\frac{\xi_a}{L}) - \frac{\xi_s}{L}(3-\frac{\xi_s}{L}) + 2\frac{\xi_a}{L}\frac{\xi_s}{L}\right]$$

$$+ \frac{\mu F_z}{\sqrt{s_x^2 + s_y^2}} \frac{\xi_s}{L} \frac{1}{2} \left[3-3\frac{\xi_s}{L}(2-\frac{\xi_a}{L}) - \frac{\xi_a}{L}(3-\frac{\xi_a}{L}) + 2\frac{\xi_a}{L}\frac{\xi_s}{L}\right]\left(\frac{\xi_s}{L} - \frac{\xi_a}{L}\right)$$

$$M_{zs} = -s_y L \left\{\left(\frac{1}{C_\alpha} - \frac{1}{C_s}\right) \frac{s_x(\mu F_z)^2}{s_x^2 + s_y^2} \frac{3}{5}\left[1 + 3\frac{\xi_s}{L} + 6(\frac{\xi_s}{L})^2\right](1-\frac{\xi_s}{L})^2 \right.$$

$$\left. - \frac{\mu F_z}{\sqrt{s_x^2 + s_y^2}} \left[1 + \frac{\xi_s}{L} + (\frac{\xi_s}{L})^2\right]\right\}(1-\frac{\xi_s}{L}) \qquad (125)$$

This expression should be compared with Equation (76) derived for the HSRI-NBS-II model which employed the assumption of uniform contact pressure.

TIRE TESTING FOR MODEL INPUT DATA

The tire characterizing data required to operate the five tire models described in this document are gathered by laboratory and over-the-road tests of the actual tires to be represented by the models. It is frequently necessary to adjust certain of the measured tire data in order to obtain an improved simulation of tire traction characteristics. This practice, made necessary by the gross approximations inherent in all tire models, is common in the simulation of complex phenomena other than tire traction. The measurement techniques and data processing procedures used to obtain input data for the various tire models are discussed in this chapter.

Since most, if not all, of the tire data required for operation of the tire traction models is significantly dependent on inflation pressure, the data gathering procedures must be performed with the actual tire at the inflation pressure for which traction response simulation is desired.

Figure 22 arranges the collection of model input data required to characterize an actual tire according to the type of test (standing or rolling) required. The acquisition of each piece of tire characterizing data listed in Figure 22 will be described in the following sections. Data from an FR70-14 radial tire, whose footprint is shown in Figure 23, is used to illustrate the acquisition procedures.

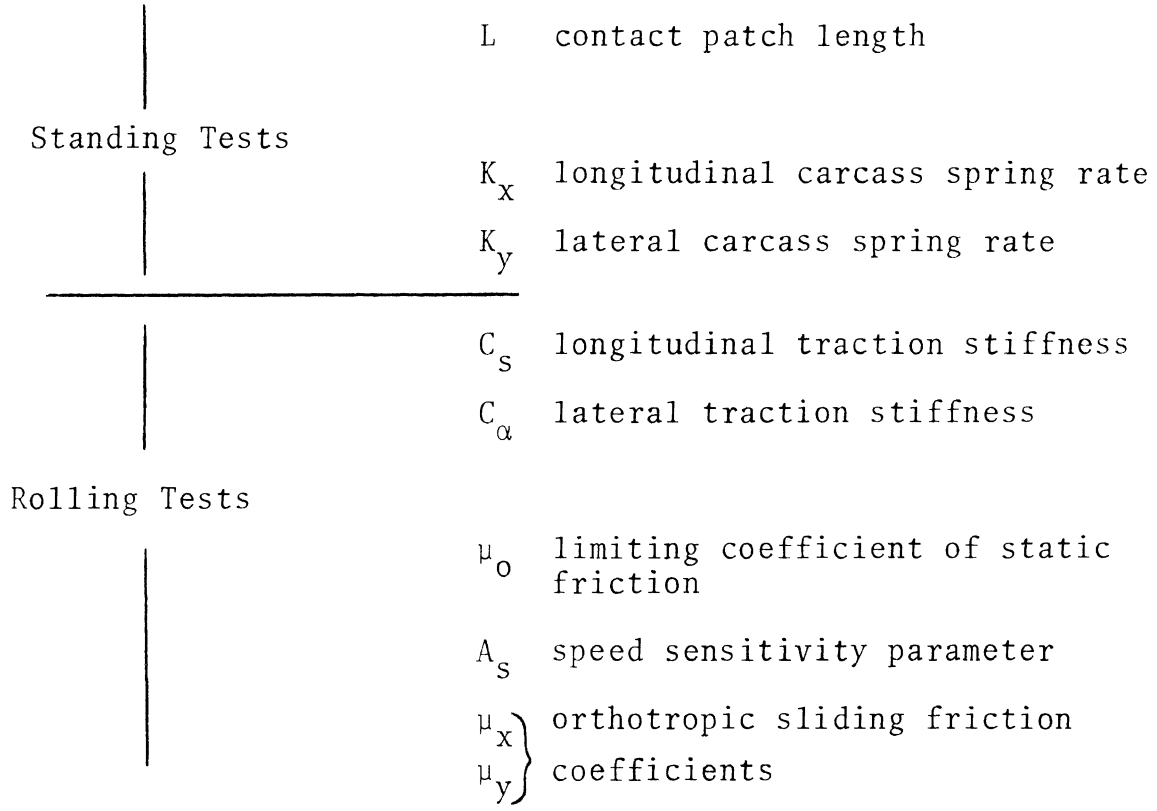

Figure 22. Tire and tire-road characterizing data for operation of tire traction models.

STANDING TIRE TESTS

The contact patch length and carcass spring rates are measured on the standing tire, statically loaded at the operating value of F_z. The HSRI Flat Bed Tire Tester [8] is used to obtain these measurements.

CONTACT PATCH LENGTH L. The patch length is measured on the tire footprint obtained by inking the tread with a stamp pad and deflecting the inked tread against a heavy sheet of graph paper. Figure 23 reproduces a print obtained in this manner with a

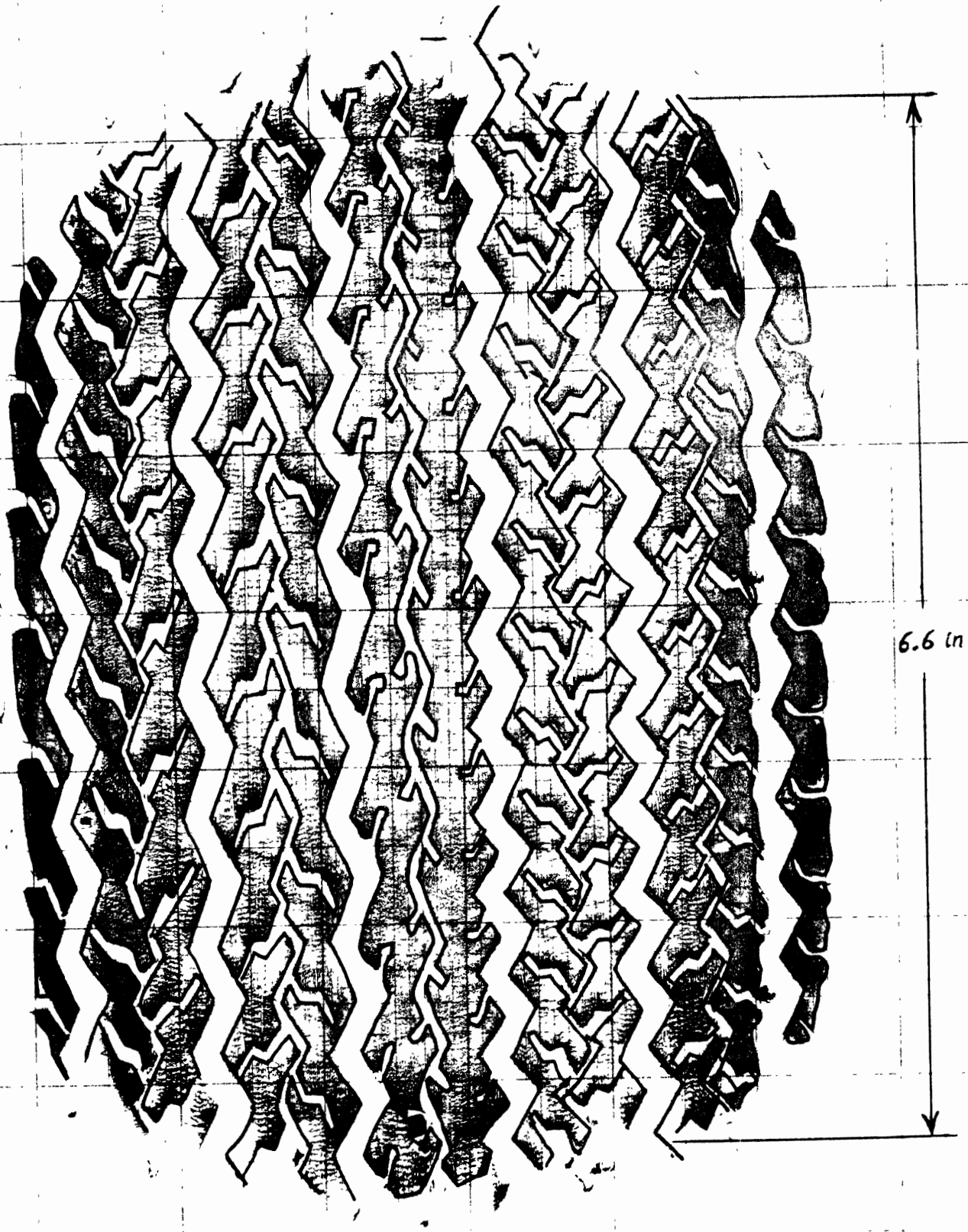

Figure 23. Inked tread footprint of a standing radial tire FR70-14 inflated to 24 psi and statically loaded at 1000 lb.

radial tire under a vertical load F_z = 1000 lb. As the contact perimeter generally deviates from the rectangular one assumed by tire models, a mean value is estimated (by eye) such that the rectangular area corresponds to the actual area.

The variation of the contact patch length with vertical load is shown in Figure 24. It is seen that linear interpolation can be used to obtain an approximation of the contact length L at other loads within the normal operating range of the tire.

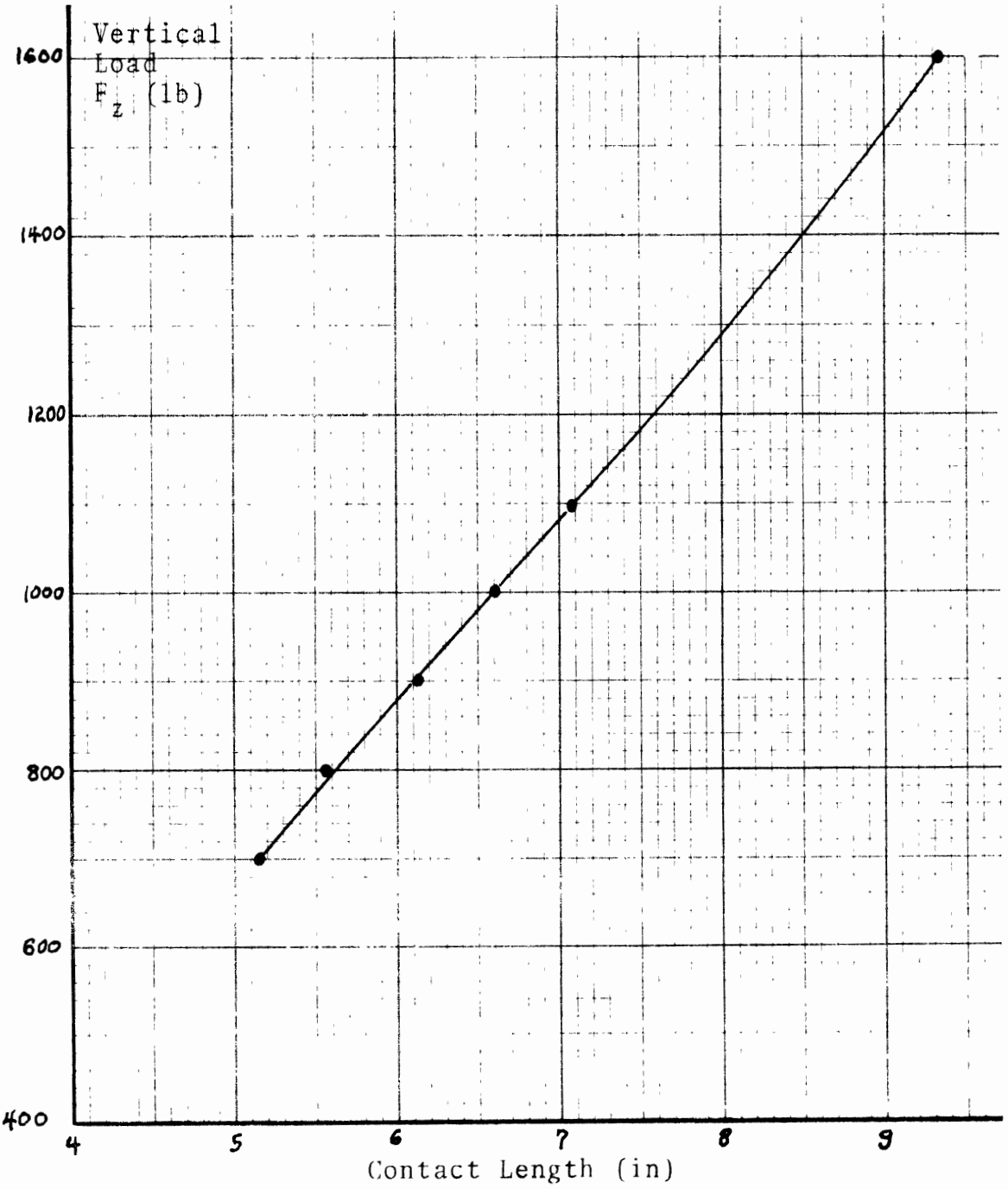

Figure 24. Variation of contact patch length with vertical load for a radial tire FR70-14 inflated to 24 psi.

LONGITUDINAL CARCASS SPRING RATE K_x. The load-deflection measurements leading to the longitudinal spring rate are made with the wheel plane in the direction of flat bed travel. The deflected tire is locked against the flat bed table which is manually moved in increments of .1 inch. Longitudinal force readings are taken at each displacement until the tire begins to slide. The onset of tire sliding is evident in the representative data for a radial tire shown in Figure 25. The longitudinal carcass spring rate is the

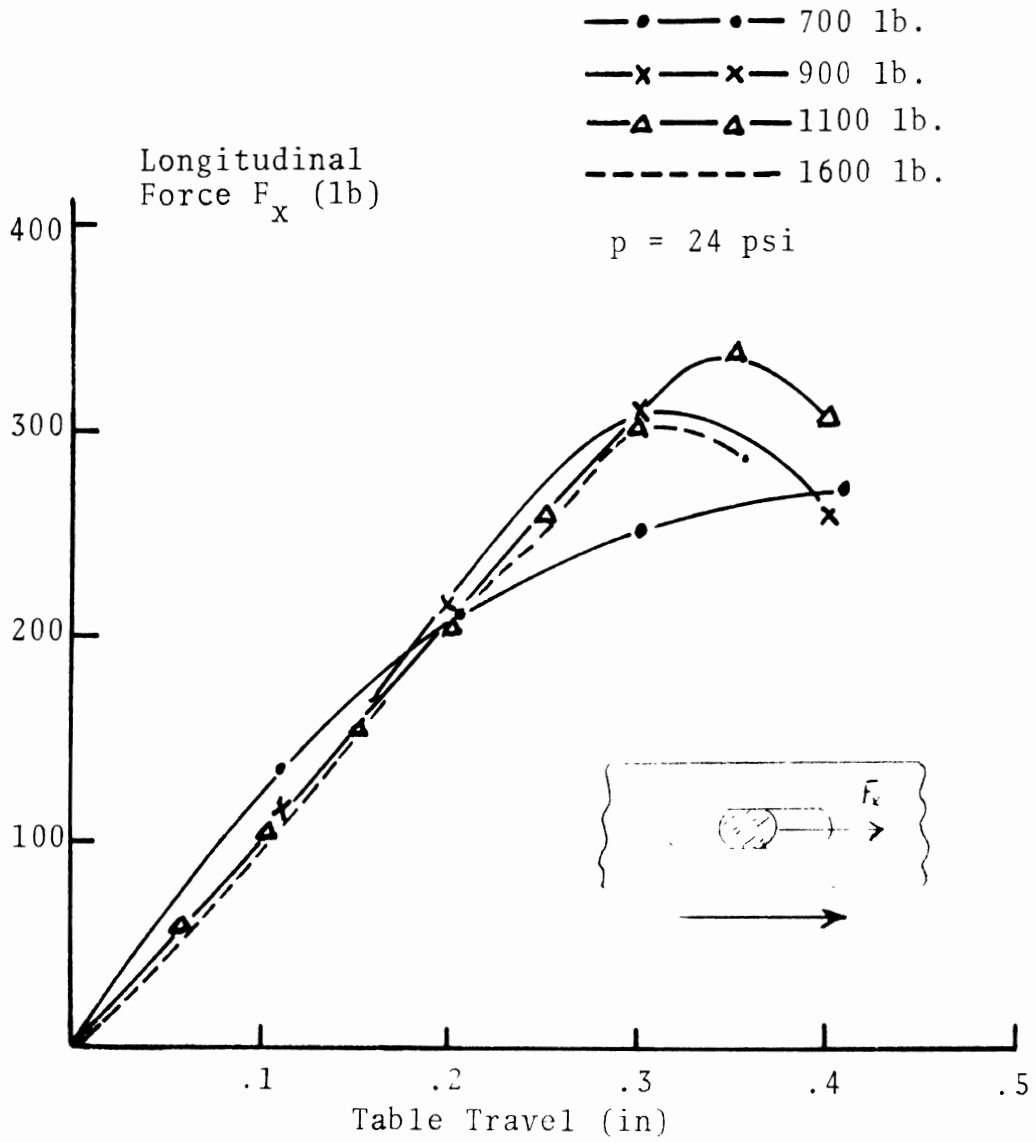

Figure 25. Longitudinal force (F_x) versus travel of flat bed table supporting a radial tire at the indicated vertical loads.

slope of the linear portion of the longitudinal load-deflection plot. As seen in Figure 25, the slope is essentially constant for the 900, 1100, and 1600 lb. vertical loads. The approximate value of K_x = 1000 lb/in is obtained at these loads.

LATERAL CARCASS SPRING RATE K_y. The lateral spring rate is obtained from load-deflection measurements made with the wheel plane perpendicular to the direction of flat bed travel. Lateral force measurements are made as the flat bed table is moved in small increments until the tire begins to slide. The lateral carcass spring rate is the slope of the linear portion of the resulting lateral load-deflection plot. As seen in Figure 26, tire vertical load has little influence on the lateral spring rate of a radial tire. The value of K_y = 500 lb/in is obtained from the data shown in Figure 26.

COMMENT ON CARCASS SPRING RATES. Since the hollow carcass structure is considerably more compliant than the solid tread structure (even with grooves), the lateral and longitudinal spring rates measured by the procedures described above are essentially those of the tire carcass. This argument would be supported by an experiment (not yet performed) whereby the carcass is rigidized in the deflected position and the procedures repeated to obtain the data shown in Figures 25 and 26. Substantially higher slopes would result for the tread spring rates K_x and K_y*. Recognition that the carcass-tread combination behaves elastically like springs

*Not to be confused with k_x and k_y which are spring constants of the hypothetical tread elements used to derive various models of traction response characteristics.

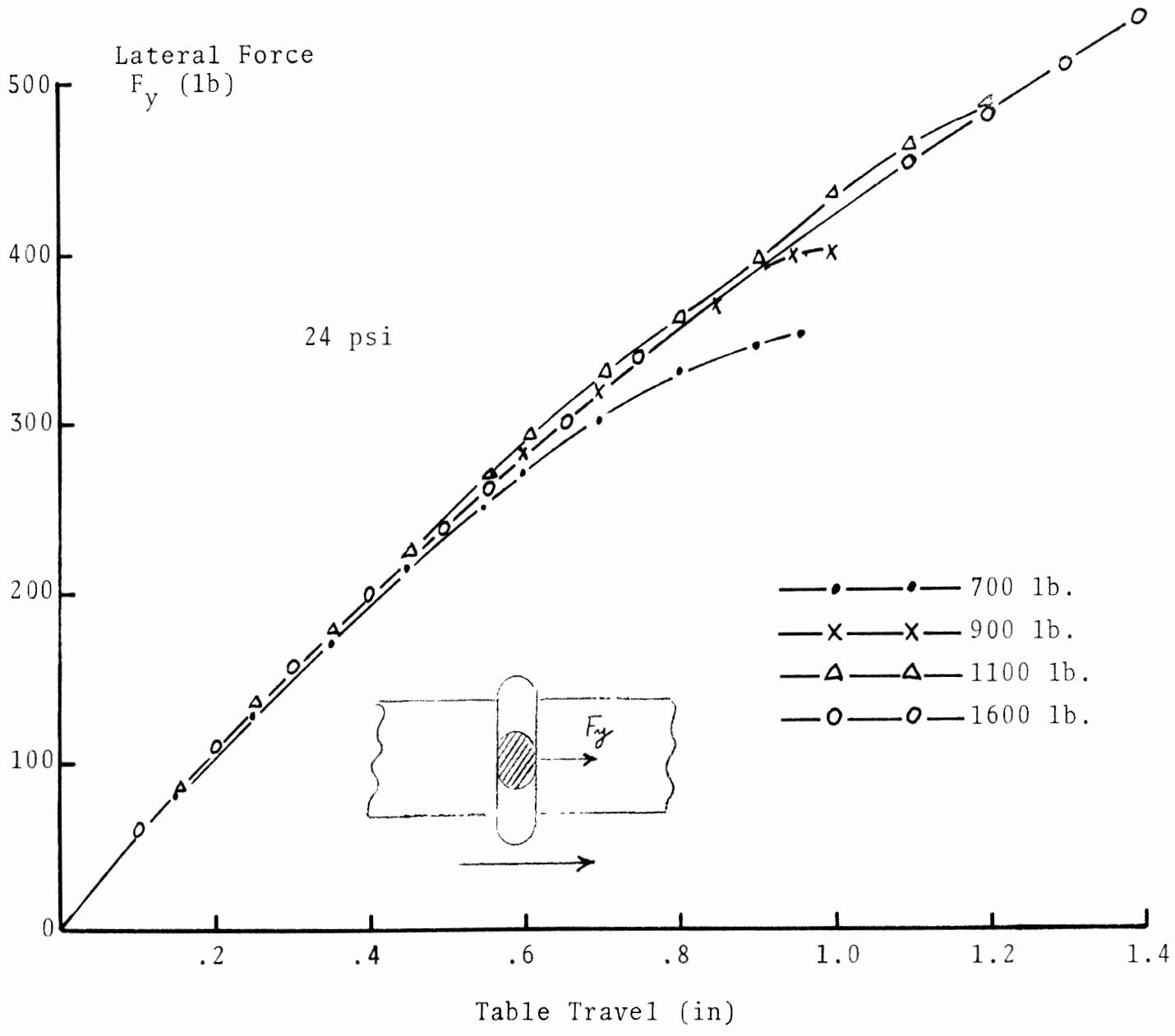

Figure 26. Lateral force (F_y) versus travel of flat bed table supporting a radial tire at the indicated vertical loads.

in series explains how the much softer carcass spring K_x dominates

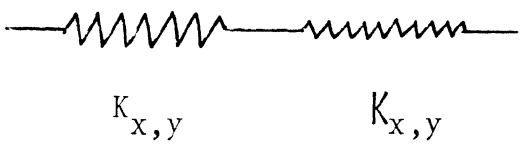

the data from these experiments which really measure the effective spring rate of the carcass-tread combination.

$$\frac{1}{K_{eff}} = \frac{1}{K_{x,y}} + \frac{1}{K_{x,y}}$$

ROLLING TIRE TESTS

LONGITUDINAL TRACTION STIFFNESS C_s. The longitudinal traction stiffness is defined by Equation (38), repeated below.

$$C_s \equiv \left.\frac{\partial F_x}{\partial s_x}\right|_{\substack{s_x = 0 \\ \alpha = 0}} \tag{38}$$

Graphically, this parameter is the slope at the origin of the longitudinal force (F_x) versus longitudinal slip (s_x) data measured in straight-ahead rolling. Figure 27 shows flat bed F_x versus s_x data for the FR70-14 radial tire operated at several loads. The slope through the origin of this data is seen to be nearly independent of tire load. The longitudinal traction stiffness for this tire, derived from the data shown in Figure 27, is approximated by

$$C_s = 20{,}000 \text{ lb/unit slip}$$

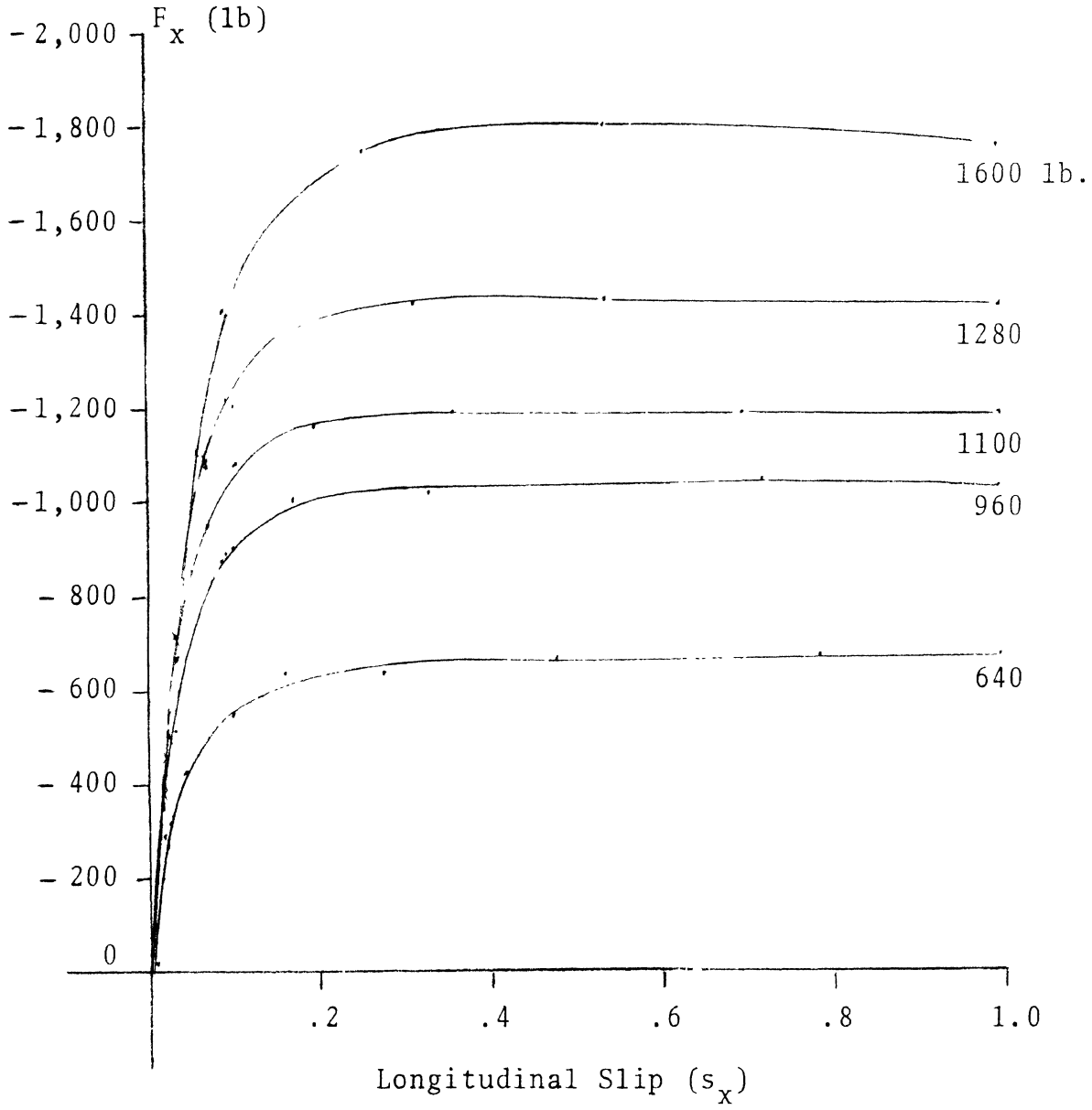

Figure 27. Longitudinal force (F_x) versus longitudinal slip (s_x) developed by a radial tire FR70-14 at the indicated tire loads and 24 psi.

LATERAL TRACTION STIFFNESS C_α. The lateral traction stiffness is defined by Equation (39), repeated below.

$$C_\alpha \equiv \left.\frac{\partial F_y}{\partial \alpha}\right|_{\substack{s_x = 0 \\ \alpha = 0}} \tag{39}$$

Graphically, this parameter is the slope at the origin of the lateral force (F_y) versus slip angle (α) data measured in free rolling. Figure 28 shows a carpet plot of flat bed F_y versus α and tire load (F_z) data for the FR70-14 radial tire. It is seen that the slope at the origin of each of the constant load curves are nearly equal to the slope at the origin of the F_z = 1100 lb curve which is found to be

$$C_\alpha = 10{,}300 \text{ lb/rad}$$

COMMENT ON TRACTION STIFFNESSES. The traction stiffnesses, C_s and C_α are measures of the traction force generating ability of a tire operated at small values of s_x and s_y (α). Although strictly valid only for traction forces which respond linearly to the operating variables s_x and α, i.e.,

$$F_x = -C_s s_x \qquad \text{and} \qquad F_y = -C_\alpha \alpha ,$$

the range of application is extended by the structure of the semi-empirical tire model. Thus the traction stiffnesses are employed in equations of the form

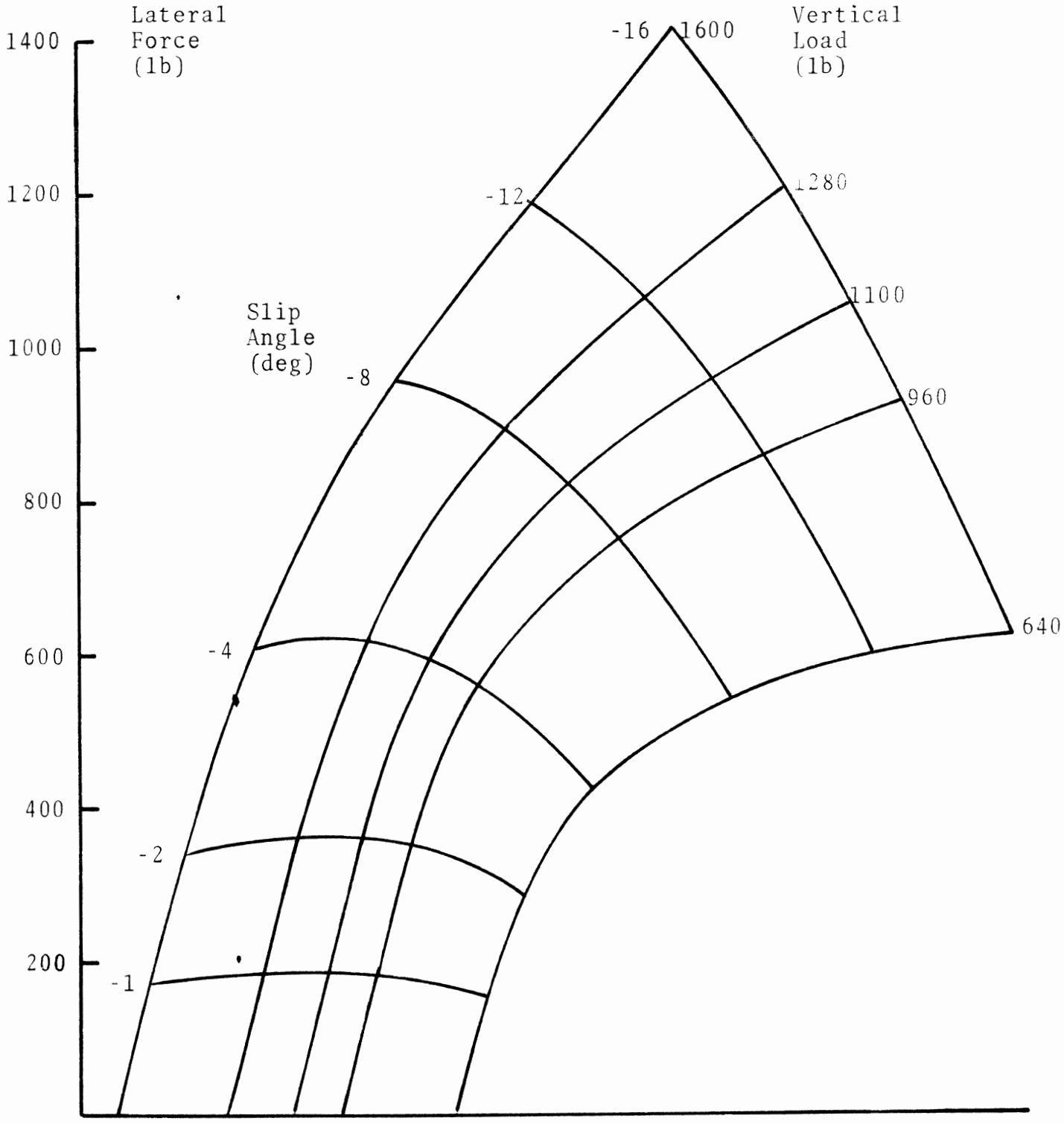

Figure 28. Lateral force (F_y) versus slip angle and vertical load. Radial tire FR70-14 at 24 psi.

$$F_x = - C_s \frac{s_x}{1-s_x} \qquad \text{and} \qquad F_y = - C_\alpha \frac{s_y}{1 - s_x}$$

which simulate the nonlinear response of F_x to s_x and the influence of s_x on the generation of lateral force F_y. The simulation is better at small values of s_x and s_y for which the rolling tire contact is mainly adhesive.

If the traction forces could be generated with completely adhesive contact, it would follow that C_s and C_α would be independent of tire-road friction properties and be measures solely of the influence of tire structure on traction force generation. Over-the-road experimental evidence, however, indicates that the traction stiffnesses do depend on road surface and contact contamination as well as tire load and velocity. Such dependencies are produced by a certain amount of sliding in the contact region.

Observing that over-the-road traction stiffnesses are generally somewhat less than flat bed traction stiffnesses, the values of

$$C_s = 16{,}000 \quad \text{lb/slip}$$

$$C_\alpha = 8{,}000 \quad \text{lb/rad}$$

which are 20% less than the flat bed stiffnesses found for the FR70-14 radial tire are taken as tire characterizing data for model comparison purposes.

TIRE-ROAD FRICTION PARAMETERS μ_o, A_s, μ_x, μ_y. The study of tire-road friction characteristics has not progressed to the stage where it is possible to define a procedure for determining the values of the friction characterizing parameters[10] appearing in Equation (30), repeated below.

$$\mu = \mu_o(1 - A_s V_s) \tag{30}$$

The current practice is to set the limiting static friction coefficient, μ_o, at some nominal value which will produce realistic peak traction forces F_x and F_y. The speed sensitivity factor, A_s, is then adjusted for optimum simulation of traction data at higher values of s_x and s_y (simulation when the sliding region becomes significant). As both μ_o and A_s influence the location of the adhesion limit, ξ_a, and consequently the magnitude of peak F_x and F_y, some iteration (a new adjustment of μ_o and then of A_s) may be necessary to set both parameters for optimum simulation of the complete traction force curves.

---

[10] The optimum form of the friction characterizing function (30) has not yet been determined. As explained in Reference [9], the assumption of a linear relationship (30) between friction and slip speed is largely pragmatic; being made in the absence of experimental data which would more closely define this very important relationship. It is believed that the linear approximation agrees sufficiently well with the qualitative aspects of experimental findings to justify its current adoption.

The orthotropic sliding friction coefficients, μ_x and μ_y, employed by the Sakai model, reflect speed sensitivity by taking a slightly lower value than the limiting coefficient of static friction μ_o.

The following values of μ_o, A_s, μ_x and μ_y were used in producing the model comparisons discussed in the next chapter.

$$\mu_o = 1.0$$

$$A_s = 0.0035$$

$$\mu_x = \mu_y = 0.9 \quad \text{(isotropic sliding friction)}$$

MODEL RESPONSE COMPARISONS

The tire model responses for the following comparisons were all calculated with FR70-14 radial tire characterizing data derived by the procedures discussed in the preceding chapter. The following model input data values were used.

L = 7.5 inches (contact length)

K_x = 1000 lb/in
K_y = 500 lb/in
} (carcass spring rates)

C_s = 16,000 lb/unit slip
C_α = 8,000 lb/radian
} (traction stiffnesses)

μ_o = 1.0 (static friction coefficient)

A_s = 0.0035 (speed sensitivity factor)

$\mu_x = \mu_y$ = 0.9 (isotropic sliding friction)

The tire load was set at F_z = 1000 lb and the traveling velocity at V = 25 ft/sec.

The tire models were operated over a range of s_x and s_y values covering driving and braking at slip angles varying from zero to 16 degrees. The computer-drawn plots in the following figures illustrate traction force and moment response as a continuous function of longitudinal slip, s_x. Each curve is calculated for the indicated slip angle α ($s_y = \tan\alpha$).

The HSRI tire models which assume uniform contact pressure do not show loss of adhesion until the wheel is locked ($s_x = 1$) or the slip angle is 90 degrees. The Goodyear and Sakai models, which assume parabolic contact pressure, show loss of adhesion at rather low values of longitudinal slip. This behavior is analyzed in Appendix III where upper bounds are derived for the slip parameter values which produce a finite adhesion region. With the assumption of a contact pressure distribution which vanishes at the entry and exit points, the upper bound on s_x, i.e., the value of s_x when adhesion is lost, depends on the slip angle α (s_y). For the parabolic contact pressure distribution, the upper bound on s_x is calculated with Equation (III-16) derived in Appendix III. Table 1 lists the upper bounds on s_x calculated for the FR70-14 radial tire characterizing data used in the model response comparisons. The maximum slip angle at which this tire could be

TABLE 1

Slip Angle α°	Lateral Slip Parameter $s_y = \tan\alpha$	Upper Bound s_x
0	0	.157
4	.070	.155
8	.141	.144
12	.213	.125
16	.286	.092

operated with retention of an adhesion region is approximately $\alpha = 20$ degrees.

The dashed lines on the following Goodyear and Sakai traction force and moment plots connect loss of adhesion points. The model response plots have been drawn for higher values of s_x although it is emphasized that the models have limited capability for simulating full sliding behavior as a function of longitudinal slip, s_x. To cite an example, the Goodyear traction force plots (Figs. 29c, 30c) appear to show a smooth transition from adhesion to full sliding, however, the Goodyear moment response (Fig. 33c) becomes unstable when loss of adhesion occurs.

TRACTION FORCE COMPARISONS

LONGITUDINAL TRACTION FORCE. Figure 29 presents the longitudinal traction force response of four models operated at five slip angles. The HSRI-NBS-I and II models assume a uniform contact pressure and thus carry the simulation out to the locked wheel condition ($s_x = 1$). The assumption of a tire-road friction coefficient which decreases with increasing slip speed, Equation (30), permits the HSRI-NBS-I and II models to show decreasing longitudinal traction force, F_x, after the peak is reached. This behavior is evident in the force curves at 0, 4, and 8 degrees slip angle (Fig. 29a,b). The decrease in F_x at lower values of the slip angle is confirmed by experimental evidence [10][11]. The Goodyear and Sakai models, which assume parabolic pressure, appear to show a slight peak in F_x at the zero degree slip angle (Fig. 29c, d) before adhesion is lost.

---

[11] The quantitative matching of model response to the referenced experimental data [10] has not yet been attempted. A quantitative validation study is planned.

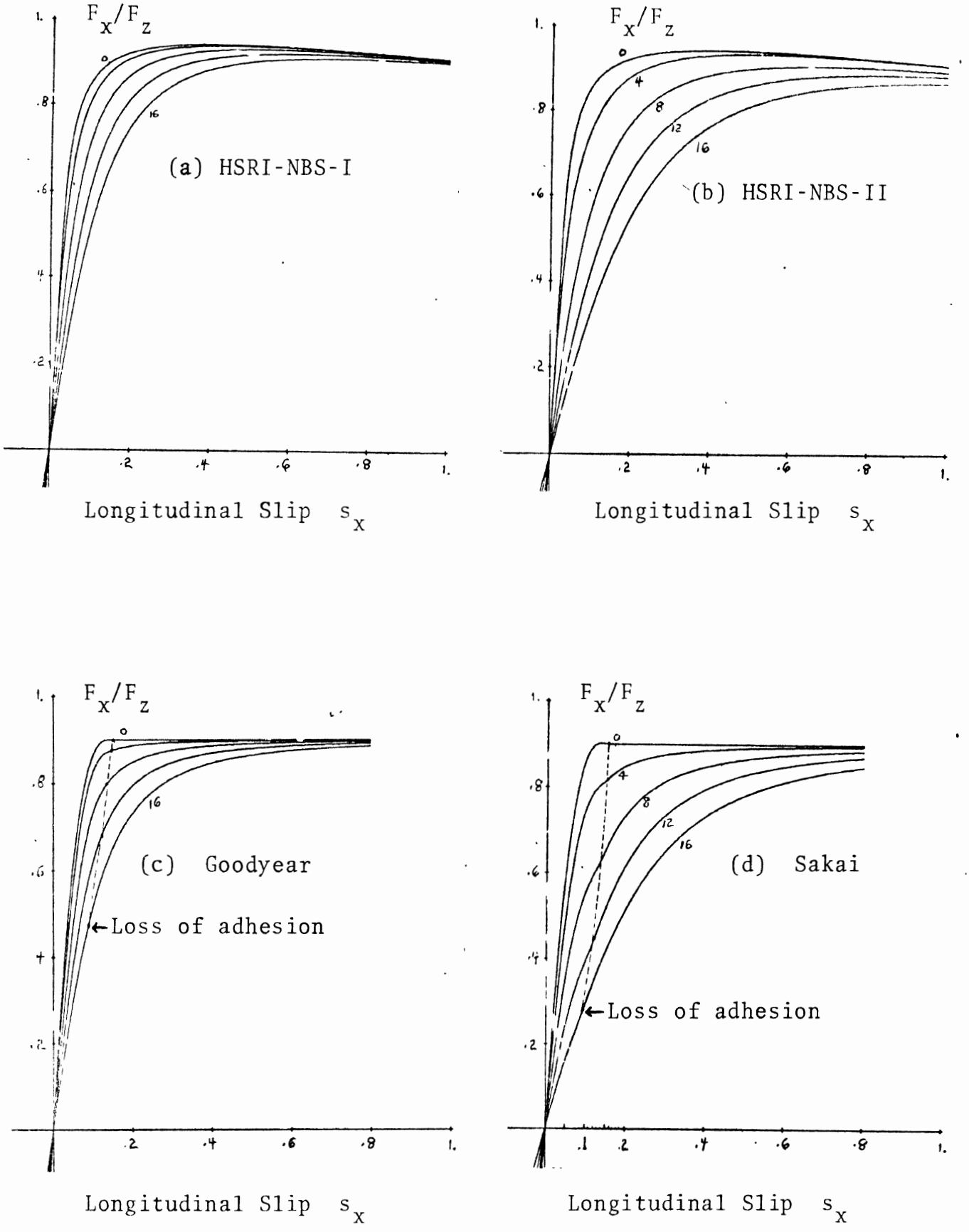

Figure 29. Comparison of longitudinal force (F_x/F_z) versus longitudinal slip (s_x) response of four tire traction models operated at the indicated slip angles. Radial tire FR70-14 data input.

Figure 30 compares the straight-ahead longitudinal traction force response of the five models analyzed in this document. The transition region apparently has little effect on straight-ahead longitudinal force generation as the HSRI-NBS-I and II models produce nearly the same curve. The HSRI models which assume a frictioncoefficient decreasing with slip speed, show F_x decreasing slightly as s_x increases after the peak while the Goodyear and Sakai models, which assume constant friction, show flat responses after the peak.

LATERAL TRACTION FORCE. Figure 31 presents the lateral traction force versus longitudinal slip response of four models operated at four slip angles. The lateral traction force curves from the HSRI-NBS-I and II, and the Goodyear models (Fig. 31a, b, c) all show peak lateral force at nearly zero longitudinal slip. The Sakai model (Fig. 31d) shows the lateral force peaks at noticeably higher values of longitudinal slip (s_x). The lateral force response of the Sakai model is qualitatively closer to experimental data which generally show peak lateral force tending to appear at smaller values of s_x as slip angle increases. The improved lateral force response of the Sakai model is attributed to the unique mechanism which this model contains for simulating the interaction of longitudinal force with the development of lateral force in the adhesion region.

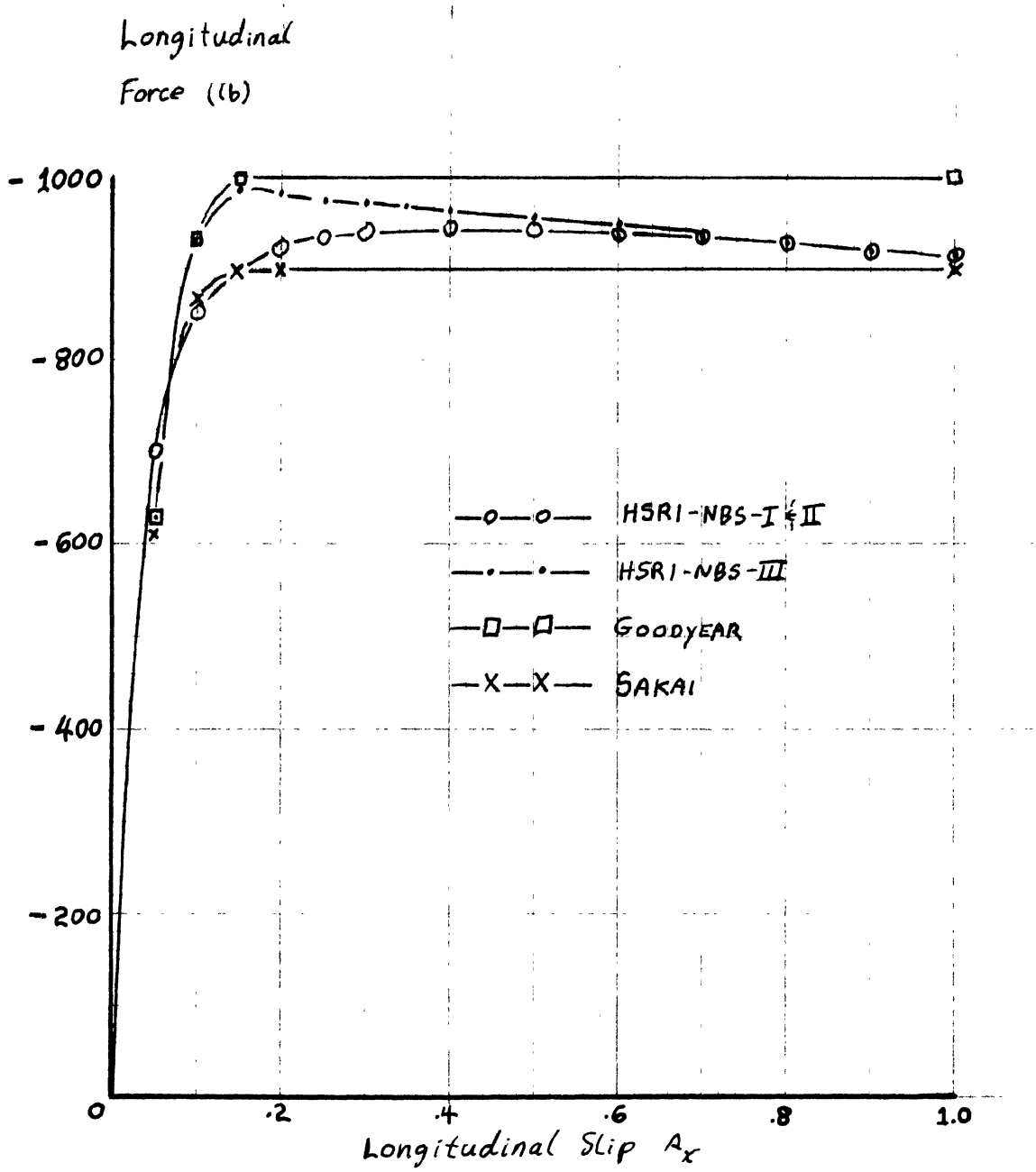

Figure 30. Comparison of the straight-ahead longitudinal force response of the five models analyzed in this document.

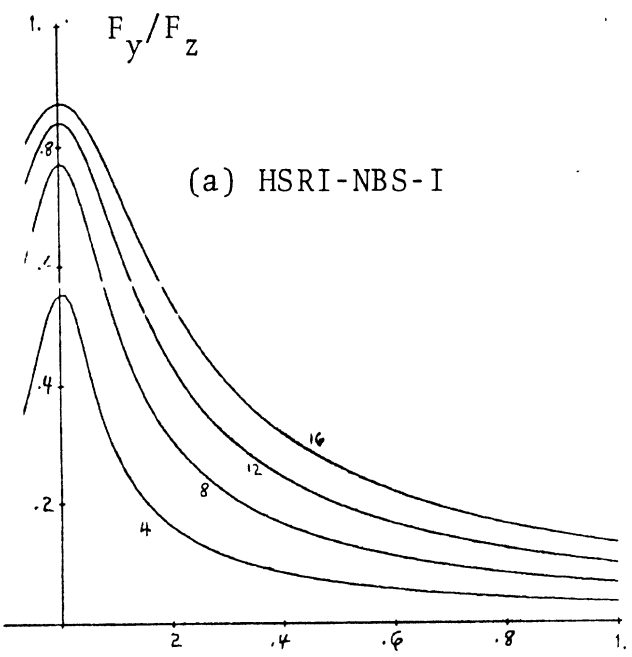

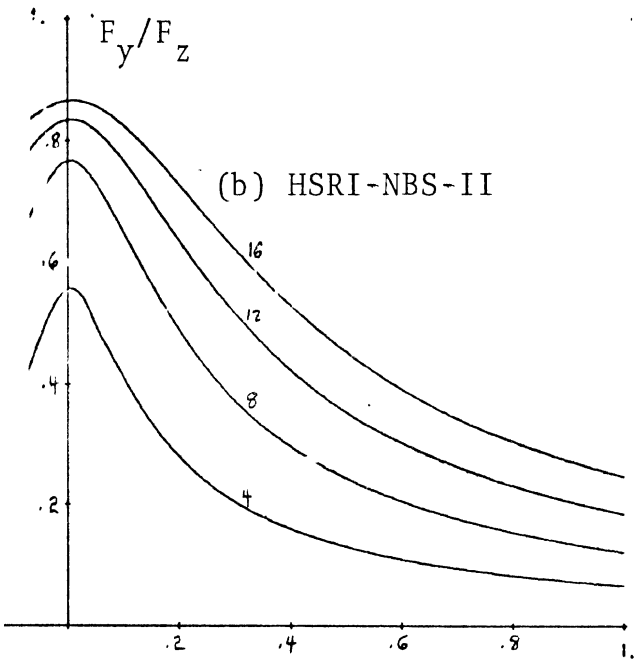

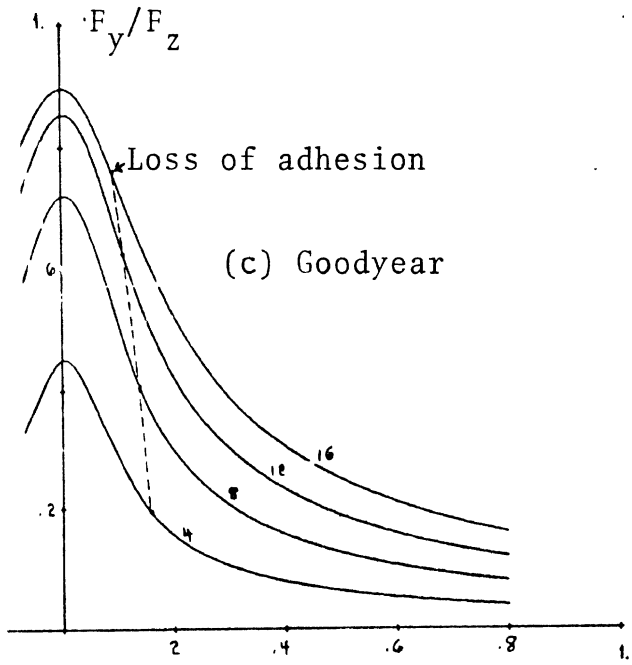

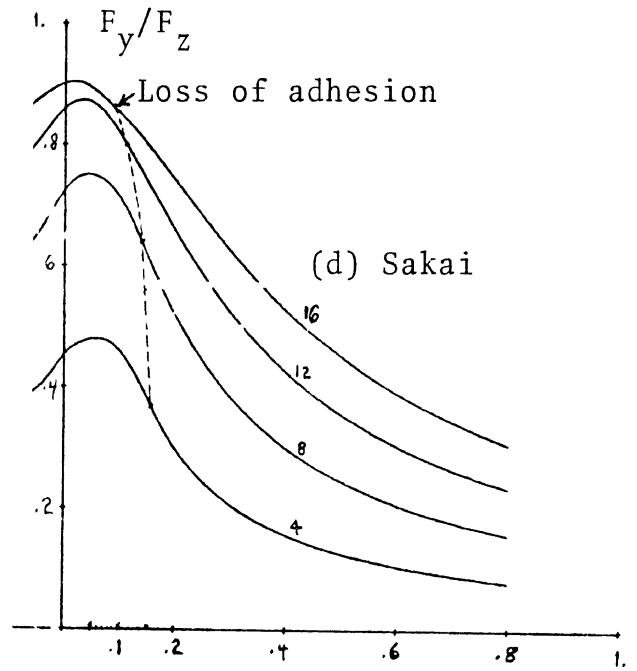

Figure 31. Comparison of lateral force (F_y/F_z) versus longitudinal slip (s_x) response of four tire traction models operated at the indicated slip angles. Radial tire FR70-14 data input.

The model comparisons of free-rolling lateral force response, Figure 32, show the HSRI-NBS-III model producing the same curve as the Goodyear model and nearly the same curve (at smaller slip angles) as the Sakai model. These models assume a parabolic contact pressure distribution. The HSRI-NBS-I and II models, which assume a uniform contact pressure distribution, produce a different curve. The adhesion region, which decreases with slip angle, is present at α = 16 degrees and contributed to the lateral force curves shown in Figure 32.

Figures 33 and 34 compare the simulation of the interaction of longitudinal force with lateral force. The HSRI-NBS-I and II models (Fig. 33) produce nearly identical plots. These HSRI models differ mainly in the treatment of the transition from adhesion to full sliding. Little traction force is apparently generated in the transition region for the operating conditions which produced these plots. Substantial differences are seen in the plots from the Goodyear and Sakai models. These differences are again attributed to the F_x-F_y interaction mechanism incorporated in the Sakai model. The comparison of the Goodyear plot, Figure 34a, with the HSRI-NBS-I plot, Figure 33a, indicates the effect of parabolic contact pressure vis à vis the effect of uniform contact pressure.

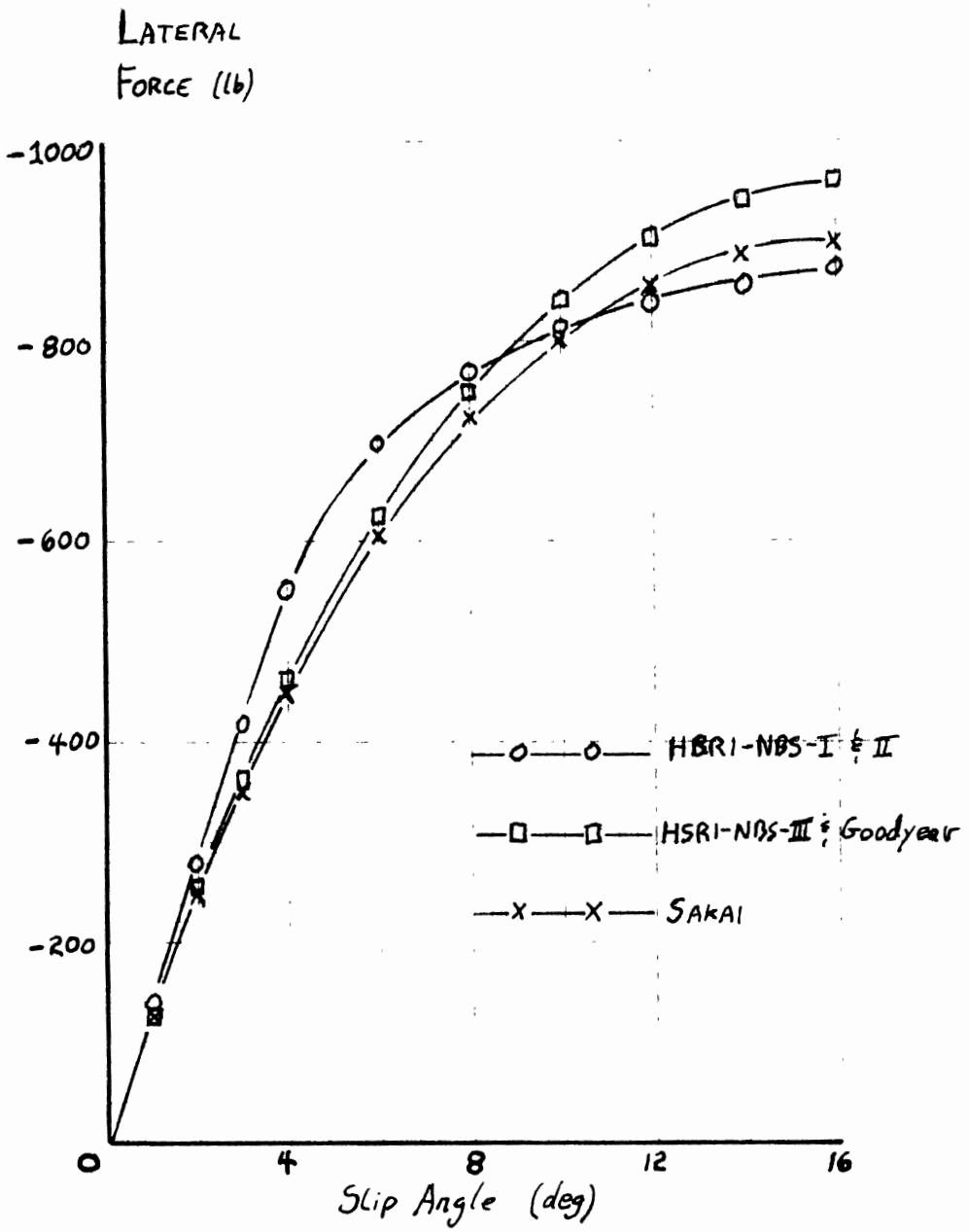

Figure 32. Comparison of the free-rolling lateral force response of the five models analyzed in this document.

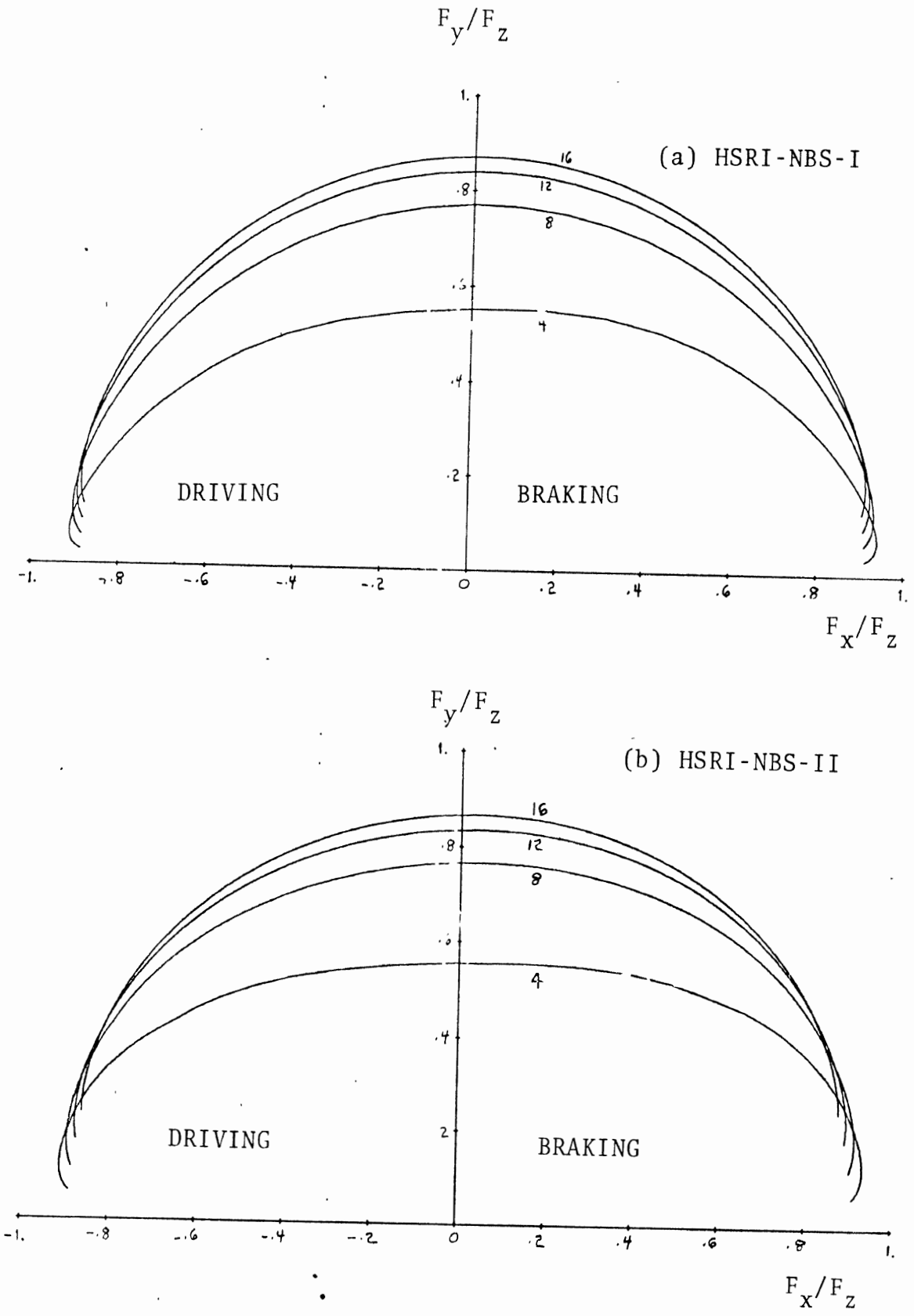

Figure 33. The interaction of longitudinal force (F_x/F_z) with lateral force (F_y/F_z) generated at the indicated slip angles. Radial tire FR70-14 data input to two tire traction models which assume uniform contact pressure.

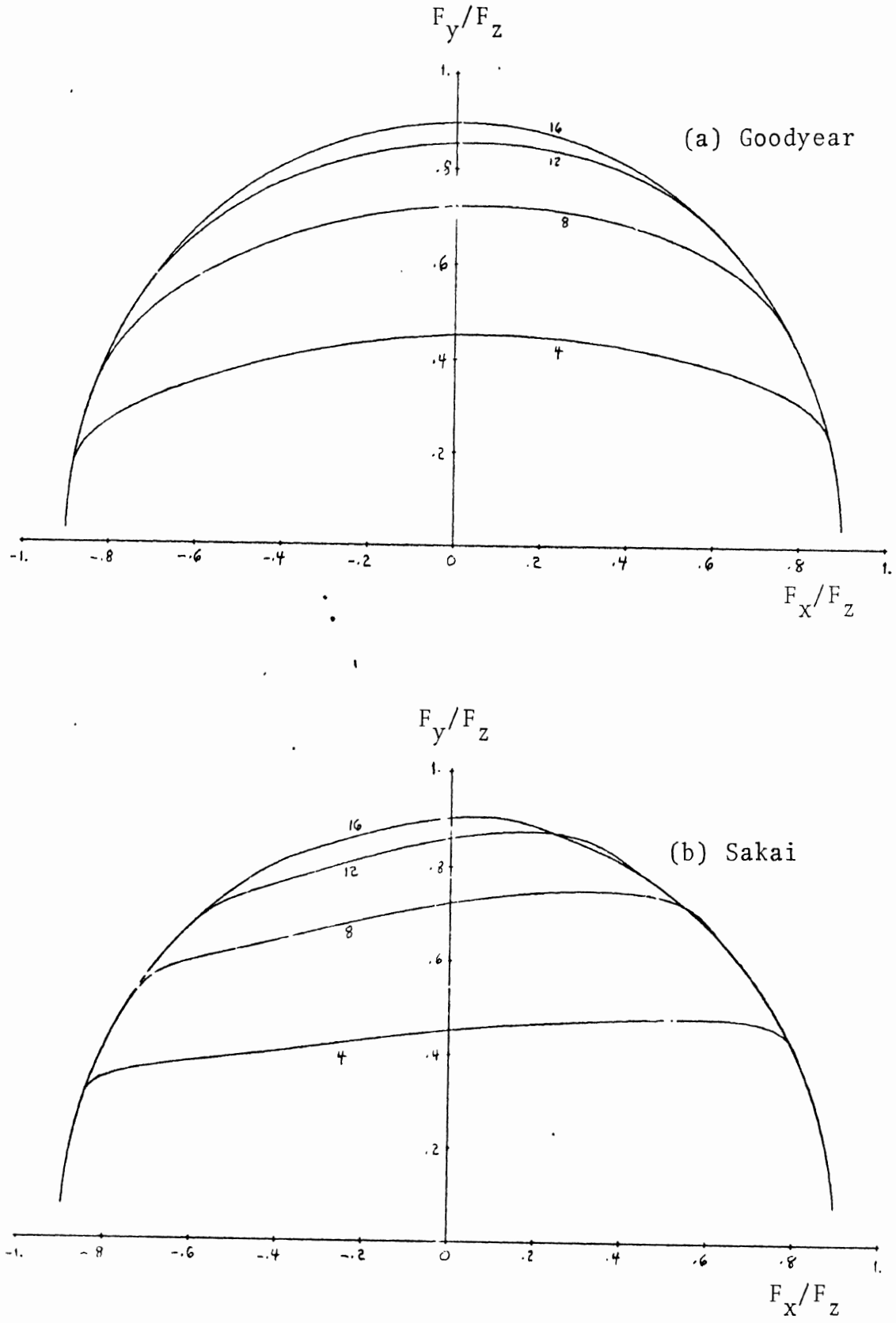

Figure 34. The interaction of longitudinal force (F_x/F_z) with lateral force (F_y/F_z) generated at the indicated slip angles. Radial tire FR70-14 data input to tire traction models which assume a parabolic distribution of contact pressure.

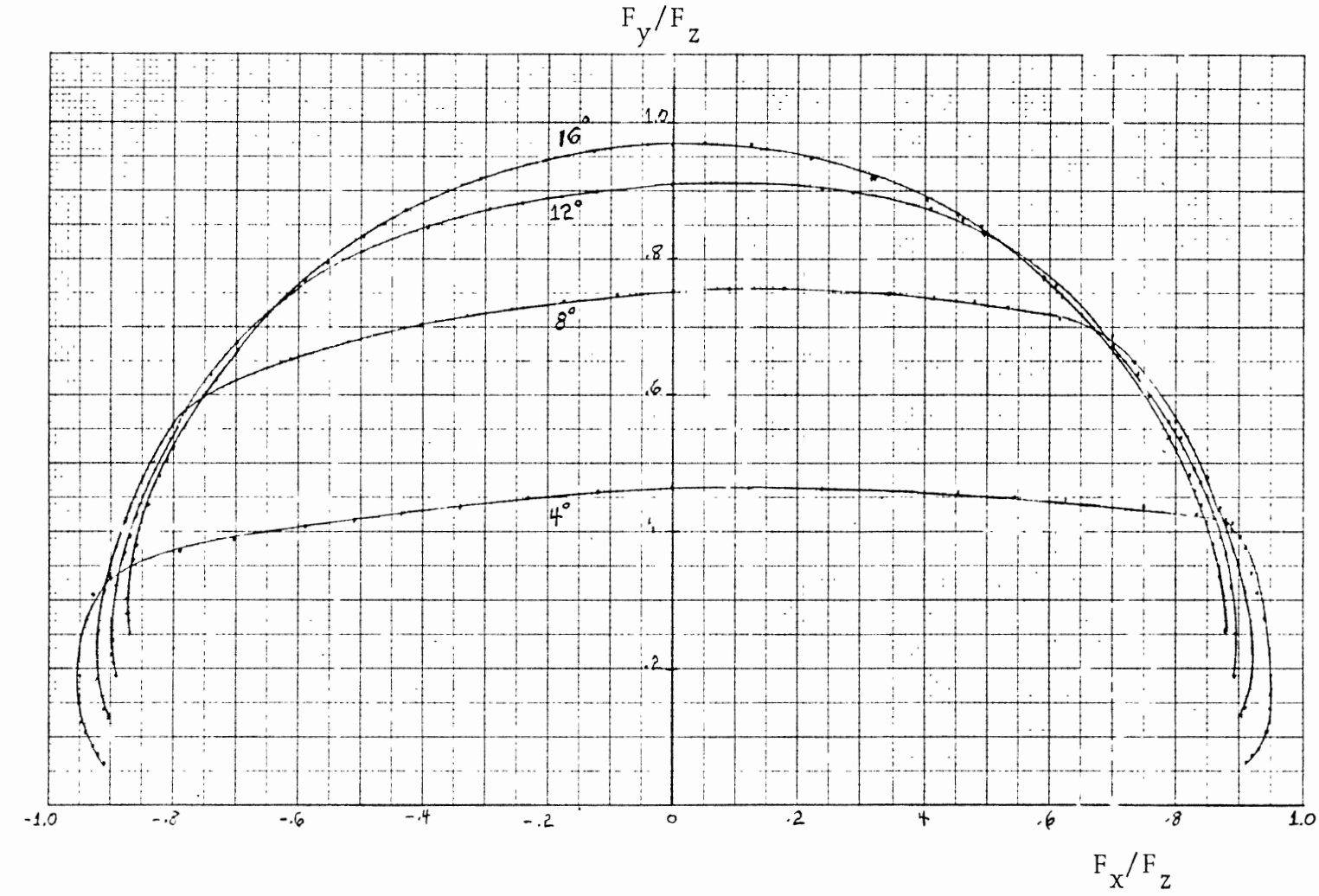

Figure 34(c). HSRI-NBS-III

The interaction of longitudinal force (F_x/F_z) with lateral force (F_y/F_z) generated at the indicated slip angles. Radial tire FR70-14 data input to the HSRI-NBS-III tire traction model which assumes a parabolic distribution of contact pressure.

ALIGNING MOMENT COMPARISONS

A more stringent test (than traction force response) of tire model realism is the capability for simulating aligning moment. Examination of Figure 35, comparing the aligning moment response of three tire models, reveals major differences in the simulations. Whereas the traction force simulations compared in Figures 29 and 31 are of essentially the same form and magnitude, the magnitude as well as the form of the aligning moment response plots show considerable variation. The Goodyear aligning moment response (Fig. 35c) has very low magnitude and is unstable after loss of adhesion. The Goodyear moment response when adhesion is present is shown on an expanded scale in Figure 35d.

Figure 36, comparing the free-rolling aligning moment response of the four models for which aligning moment equations were derived, shows the variation between the models. The exceedingly low amplitude of the Goodyear moment response may be attributed to lack of carcass flexibility. The other three models plotted utilize the carcass spring rates K_x and K_y.

Figure 37 illustrates the influence of carcass flexibility on aligning moment simulation. It appears that carcass flexiblity, described by the spring rates K_x and K_y, is essential for the magnitude of the aligning moment simulation to approach a realistic value. The lack of carcass flexibility in the Goodyear model partially explains the low magnitude of the aligning moment response. The carcass spring rates K_x and K_y, inasmuch as they are associated with uniform carcass translations, do not influence the generation of traction force (F_x and F_y).

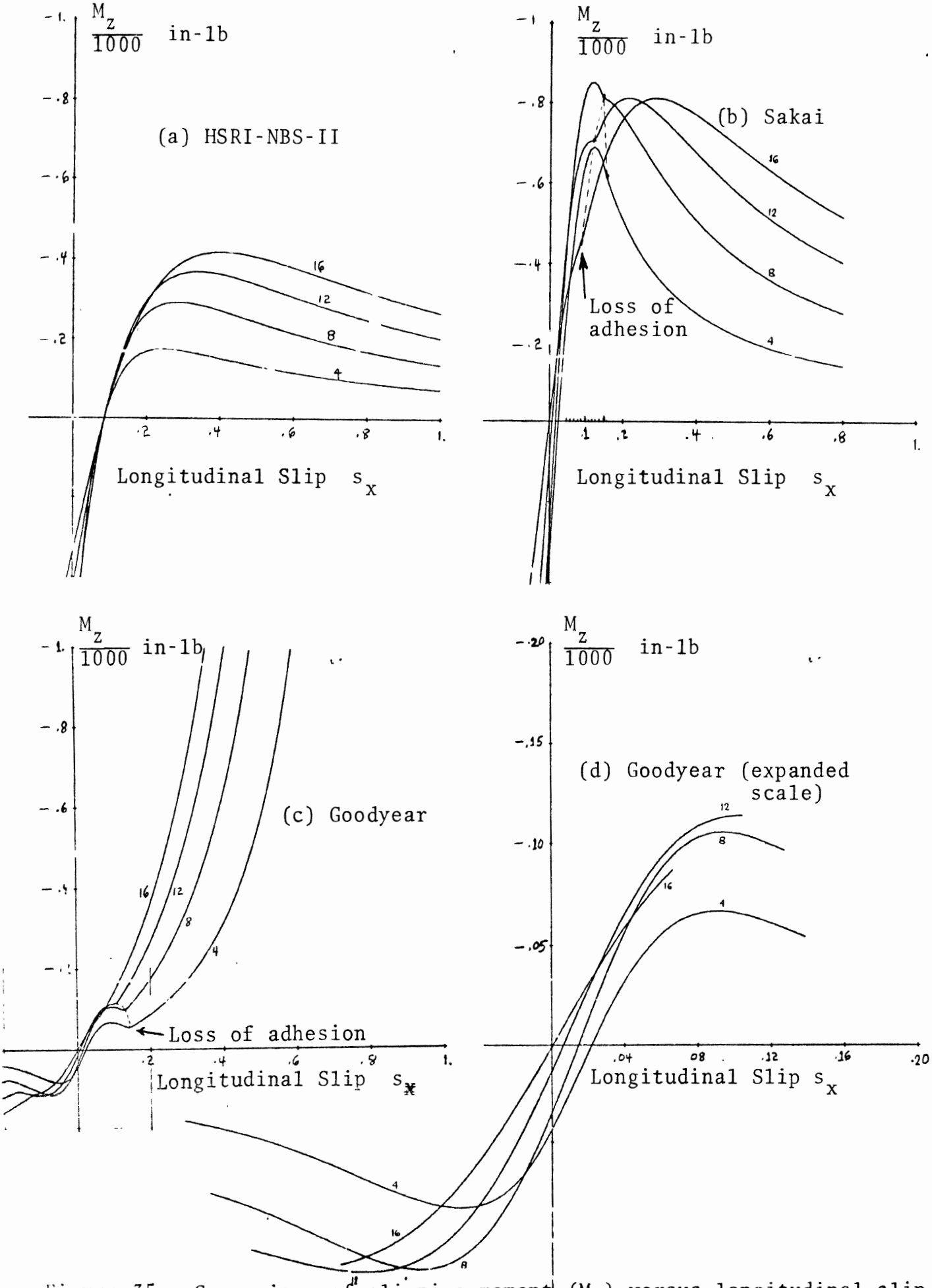

Figure 35. Comparison of aligning moment (M_z) versus longitudinal slip (s_x) response of three tire traction models operated at the indicated slip angles. Radial tire FR70-14 data input.

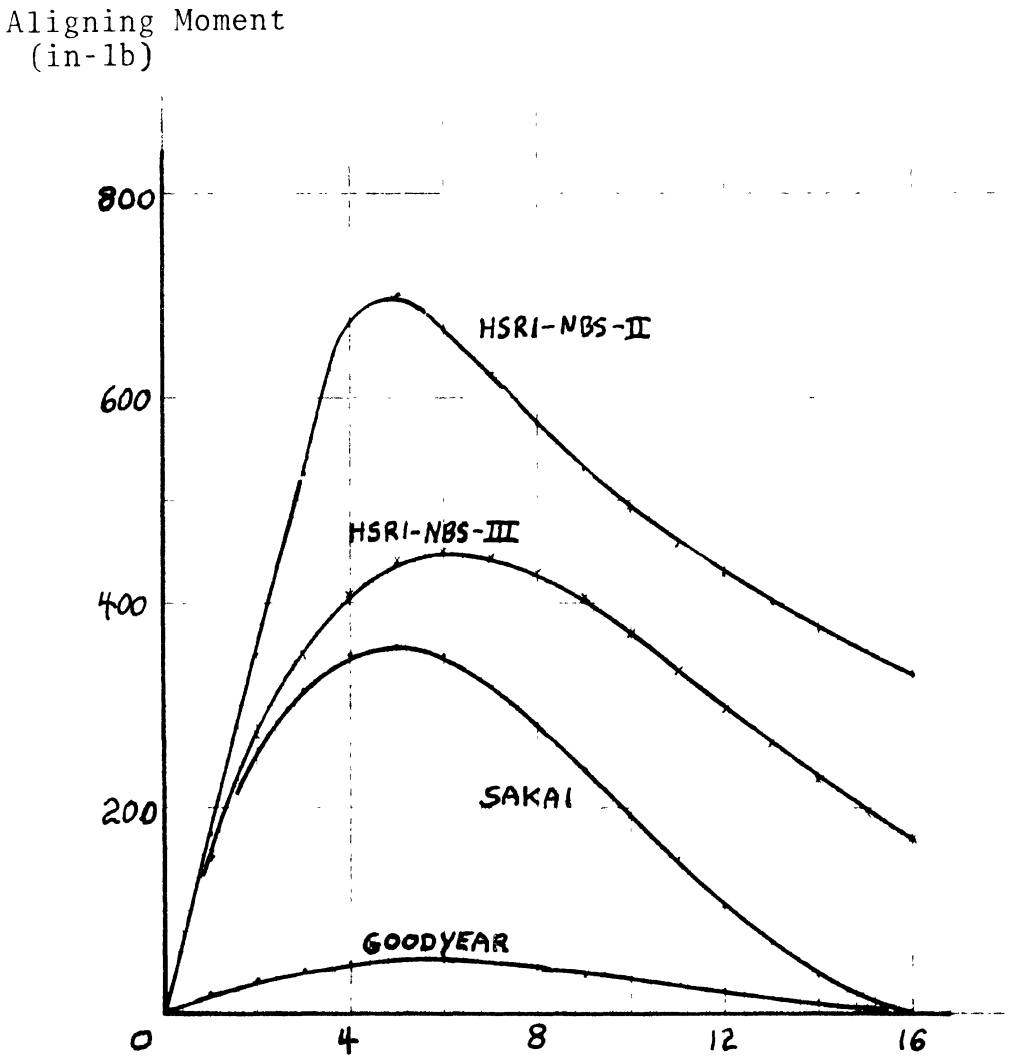

Figure 36. Comparison of the free-rolling aligning moment response from four traction models.

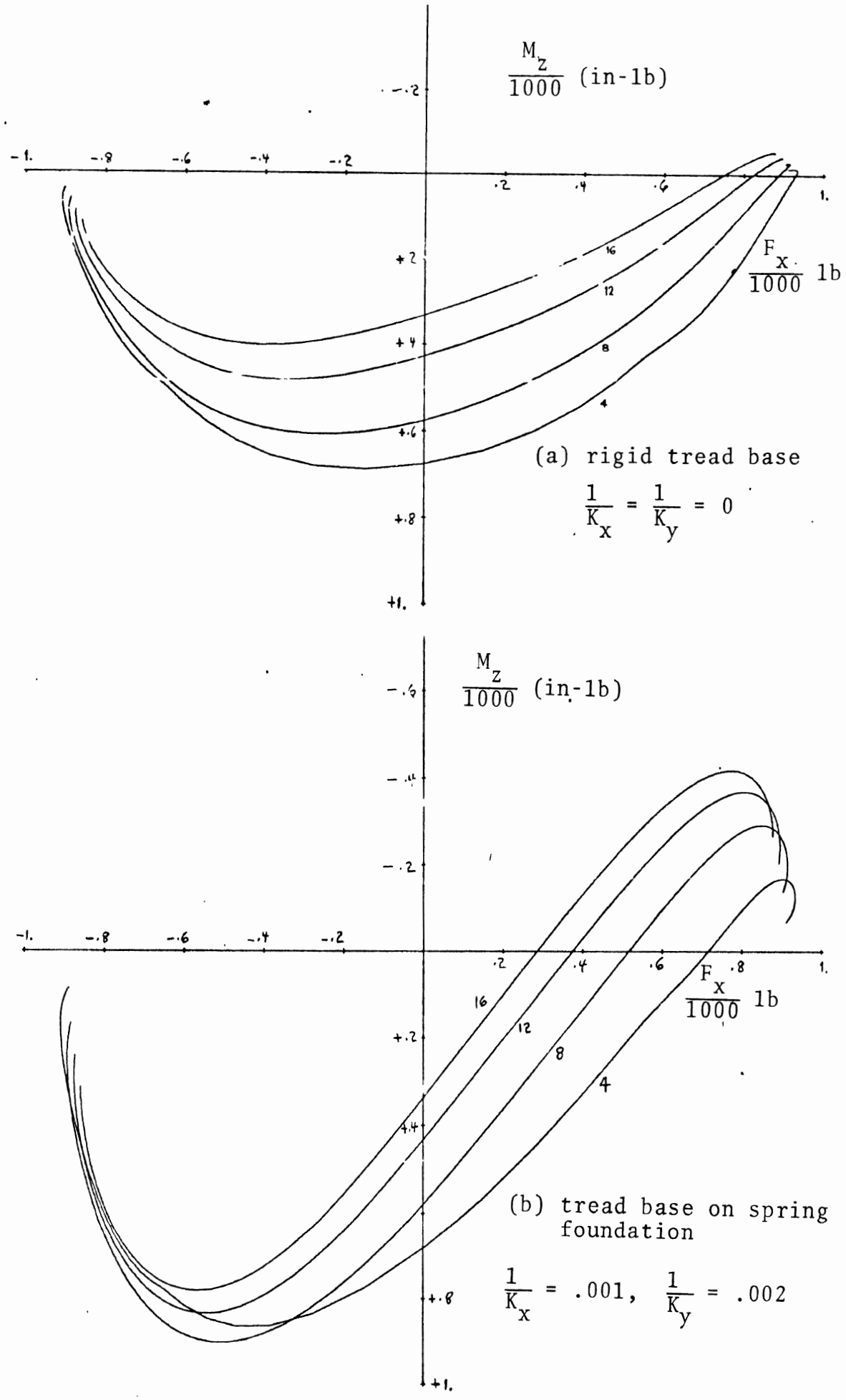

Figure 37. Comparison of the interaction of longitudinal force (F_x) with aligning moment (M_z) generated at the indicated slip angles using HSRI-NBS-II model with and without a tread base spring foundation.

REFERENCES

1. "Vehicle Dynamics Terminology," SAE Recommended Practice J670c, SAE Handbook Supplement J670c, January 1973.

2. Clark, S.K., ed., Mechanics of Pneumatic Tires, NBS Monograph 122, November 1971.

3. Dugoff, H., et al., "An Analysis of Tire Traction Properties and Their Influence on Vehicle Dynamic Performance," 1970 Inter. Auto. Safety Compendium, SAE, pp. 341-366. SAE Paper No. 700377.

4. Fancher, P.S., et al., Tire Traction Grading Procedures as Derived from the Maneuvering Characteristics of a Tire-Vehicle System (Volume II), Final Report, NBS Contract No. 1-35715, Highway Safety Research Institute, University of Michigan, Ann Arbor, June 13, 1972.

5. Livingston, D.I., and Brown, J.E., "Physics of the Slipping Wheel. II. Slip Under Both Tractive and Lateral Forces," Rubber Chemistry and Technology, Vol. 43, No. 2, 1970 (pp. 244-261).

6. Sakai, H., "Theoretical Study of the Effect of Tractive and Braking Forces on Cornering Characteristics of Tires," Safety Research Tour Paper No. 4, Oct-Nov. 1969, Stability and Control Committee, Society of Automotive Engineers of Japan.

7. Bergman, W., "Theoretical Prediction of the Effect of Traction on Cornering Force," SAE Transactions, Vol. 69, 1961 (pp. 614-640).

8. Tielking, J.T., et al., "Mechanical Properties of Truck Tires," SAE Paper No. 730138.

9. Dugoff, H., et al., Tire Performance Characteristics Affecting Vehicle Response to Steering and Braking Control Inputs, Final Report, NBS Contract No. CST-460, Highway Safety Research Institute, University of Michigan, Ann Arbor, August 1969.

10. Tielking, J.T., Construction and Profile Study, Part I: Tire Traction Data Measured by the HSRI Mobile Tire Tester, HSRI Project 329180, Tire Traction Characteristics Affecting Vehicle Performance," Interim Document 5, March 1973.

SYMBOLS AND TERMINOLOGY

A_s speed sensitivity factor

C_s braking/driving traction stiffness

C_α cornering traction stiffness

$C_{M\alpha}$ aligning traction stiffness

EI tread base bending stiffness

$\mathbf{F}$ Traction force vector

$F = |\mathbf{F}|$

F_s traction force saturation magnitude

F_x longitudinal tire traction force

- F_{xa} adhesion region contribution
- F_{xt} transition region contribution
- F_{xs} sliding region contribution

F_y lateral tire traction force

- F_{ya} adhesion region contribution
- F_{yt} transition region contribution
- F_{ys} sliding region contribution

F_z tire load

i, j unit vectors in x and y directions

K_x, K_y longitudinal and lateral carcass stiffnesses

k_x, k_y longitudinal and lateral tread element stiffnesses

L contact patch length (standing tire)

ℓ_x ℓ_y	longitudinal and lateral traction force offsets
M_z	aligning moment
	M_{za} adhesion region contribution
	M_{zt} transition region contribution
	M_{zs} sliding region contribution
$q = \|\sigma\|$	magnitude of shear force distribution vector
q_t	tangential tractive force (Sakai)
q_x, q_y	components of the shear force distribution vector
q_z	contact pressure distribution
R_e	effective rolling radius
$\mathbf{S}$	slip modulus vector (Goodyear)
$S = \|\mathbf{S}\|$	
S_s	slip modulus magnitude at traction force saturation
s_x, s_y	longitudinal and lateral slip parameters
t	time, transition region length
u, v	longitudinal and lateral tread element displacements
$\tilde{u}$, $\tilde{v}$	uniform longitudinal and lateral carcass translations
u_a, v_a	tread element displacements at the adhesion limit ξ_a
u_s, v_s	tread element displacements at the transition limit ξ_s
u_t, v_t	nonuniform displacements within the transition region
$\mathbf{V}$	traveling velocity vector

V_x, V_y	components of the traveling velocity vector
$\mathbf{V}_c$	slip velocity vector
V_{cx}, V_{cy}	components of the slip velocity vector
V_r	rolling velocity
$\mathbf{V}_s$	sliding velocity vector
w	contact patch width (standing tire)
x, y, z	tire coordinates
α	slip angle
γ	inclination angle
θ	slide angle
λ	parameter used in defining the transition region
μ	sliding friction coefficient
μ_o	limiting coefficient of static friction
μ_x, μ_y	orthotropic sliding friction coefficients
ξ, η	contact coordinates
ξ_a	limit of the adhesion region
ξ_s	limit of the transition region
σ	shear force distribution vector
Ω	rotational velocity of the wheel about the axle

APPENDIX I

MODEL RESUMES

The following five models were selected for analysis in this document because of their ability to simulate tire traction forces and moment in response to both lateral and longitudinal slip.* The salient features of each model are summarized in the following resumes.

MODEL	RESUME
HSRI-NBS-I [3]	Elastic tread blocks on rigid wheel, uniform contact pressure, uniform deformation in sliding region, tire-road friction decreasing linearly with slip speed. Aligning moment not simulated.
HSRI-NBS-II [4]	Elastic tread blocks on foundation allowed to translate uniformly, finite transition between adhesion and fully developed sliding, uniform contact pressure, distinction between static and dynamic friction which decreases linearly with slip speed.
Goodyear [5]	Elastic tread blocks on rigid wheel, parabolic or experimentally determined contact pressure, deformation in sliding region decreases with shear force, constant friction. Deformation discontinuity avoided by assuming sliding shear force to act in same direction as shear force in the adhesion region.
Sakai [6]	Elastic tread blocks on flexible elastically-supported beam carcass (subsequently reduced to rigid beam with uniform translation) with an artificial mechanism connecting longitudinal stiffness with lateral stiffness (but not vice-versa), parabolic contact pressure, distinction between static and sliding friction which is considered to be orthotropic. Prescribed stress in sliding region produces a displacement discontinuity for unequal longitudinal and lateral traction stiffnesses. Traction forces and moment computed by integrating

*The "classical" string and beam models treat the tire as free-rolling and are thus excluded.

	across a stress discontinuity which is more severe for bias tires than for radial tires.
HSRI-NBS-III	Parabolic contact pressure, otherwise identical to HSRI-NBS-II model.

APPENDIX II

SUMMARY OF FORMULAS

The adhesion limit equations and the traction force and moment equations associated with the five models are collected in this appendix. The digital computer programs listed in Appendix IV evaluate the force and moment equations as written here in terms of the slip parameters s_x and s_y.

HSRI-NBS-I [3]

Adhesion Limit

$$\frac{\xi_a}{L} = \frac{1}{2}\mu F_z(1 - s_x)[(s_x C_s)^2 + (s_y C_\alpha)^2]^{-1/2} \tag{45}$$

where

$$\mu = \mu_o(1 - A_s V_s); \quad V_s = \sqrt{s_x^2 + s_y^2}\,|V|\cos\alpha \tag{30}$$

Traction Modes

$\xi_a \geq L$ complete adhesion

$0 < \xi_a < L$ adhesion and sliding

$\xi_a = 0$ complete sliding (only at wheel lock)

Traction Forces

$$F_x = \begin{cases} -C_s \dfrac{s_x}{1 - s_x} & \xi_a \geq L \\ -C_s \dfrac{s_x}{1 - s_x} \dfrac{\xi_a}{L}\left(2 - \dfrac{\xi_a}{L}\right) & 0 < \xi_a < L \\ -C_s \mu F_z \left[C_s^2 + (s_y C_\alpha)^2\right]^{-1/2} & \xi_a = 0 \end{cases} \quad (42) \quad (46)$$

$$F_y = \begin{cases} -C_\alpha \dfrac{s_y}{1 - s_x} & \xi_a \geq L \\ -C_\alpha \dfrac{s_y}{1 - s_x} \dfrac{\xi_a}{L}\left(2 - \dfrac{\xi_a}{L}\right) & 0 < \xi_a < L \\ -C_\alpha s_y \mu F_z \left[C_s^2 + (s_y C_\alpha)^2\right]^{-1/2} & \xi_a = 0 \end{cases} \quad (43) \quad (47)$$

Adhesion Limit

$$\frac{\xi_a}{L} = \frac{1}{2}\mu_o F_z (1 - s_x)[(s_x C_s)^2 + (s_y C_\alpha)^2]^{-1/2}$$

Transition Limit

$$\frac{\xi_s}{L} = \frac{1}{2}\mu F_z (1 - s_x)(s_x^2 + s_y^2)^{-1/2}\left(\frac{1}{C_s} + \frac{1}{C_\alpha}\right)$$

where

$$\mu = \mu_o(1 - A_s V_s) \; ; \qquad V_s = \sqrt{s_x^2 + s_y^2}\;|V|\cos\alpha \qquad (30)$$

Traction Modes

$\xi_a \geq L$ complete adhesion

$\xi_a < \xi_s \geq L$ adhesion and transition

$\xi_a < \xi_s < L$ adhesion and transition and sliding

$\xi_s \leq \xi_a < L$ adhesion and sliding

$\xi_a = 0$ complete sliding (only at wheel lock)

Traction Forces

$$F_x = F_{xa} + F_{xt} + F_{xs} \qquad (64)$$

$$F_y = F_{ya} + F_{yt} + F_{ys} \qquad (65)$$

where

$$F_{xa} = -C_s \frac{s_x}{1 - s} \left(\frac{\xi_a}{L}\right)^2$$

$$F_{xt} = -\left[C_s \frac{s_x}{1 - s_x} \frac{\xi_a}{L} + \frac{1}{2} \mu F_z \frac{s_x}{\sqrt{s_x^2 + s_y^2}}\right] \left(\frac{\xi_s}{L} - \frac{\xi_a}{L}\right)$$

$$F_{xs} = -\mu F_z \frac{s_x}{\sqrt{s_x^2 + s_y^2}} \left(1 - \frac{\xi_s}{L}\right)$$

$$F_{ya} = -C_\alpha \frac{s_y}{1 - s_x} \left(\frac{\xi_a}{L}\right)^2$$

$$F_{yt} = -\left[C_\alpha \frac{s_y}{1 - s_x} \frac{\xi_a}{L} + \frac{1}{2} \mu F_z \frac{s_y}{\sqrt{s_x^2 + s_y^2}}\right] \left(\frac{\xi_s}{L} - \frac{\xi_a}{L}\right)$$

$$F_{ys} = -\mu F_z \frac{s_y}{\sqrt{s_x^2 + s_y^2}} \left(1 - \frac{\xi_s}{L}\right)$$

Aligning Moment

$$M_z = M_{za} + M_{zt} + M_{zs} + F_x F_y \left(\frac{1}{K_x} - \frac{1}{K_y}\right) \qquad (71)$$

where

$$M_{za} = -\frac{L}{3}\left[2(C_s - C_\alpha) \frac{s_x}{1 - s_x} \frac{\xi_a}{L} - \frac{1}{2} C_\alpha \left(4 \frac{\xi_a}{L} - 3\right)\right] \frac{s_y}{1 - s_x} \left(\frac{\xi_a}{L}\right)^2$$

$$M_{zt} = -\frac{L}{6}\left\{(C_s - C_\alpha)\left[4\,\frac{s_x s_y}{(1-s_x)^2}\left(\frac{\xi_a}{L}\right)^2 + \left(\frac{1}{C_s}+\frac{1}{C_\alpha}\right)\mu F_z\,\frac{s_y}{1-s_x}\,\frac{s_x}{\sqrt{s_x^2+s_y^2}}\,\frac{\xi_a}{L} + \frac{\mu^2 F_z^2}{C_s C_\alpha}\,\frac{s_x s_y}{s_x^2+s_y^2}\right]\right.$$

$$\left. - \left[C_\alpha\,\frac{s_y}{1-s_x}\,\frac{\xi_a}{L}\left(4\,\frac{\xi_a}{L} + 2\,\frac{\xi_s}{L} - 3\right) + \frac{1}{2}\,\mu F_z\,\frac{s_y}{\sqrt{s_x^2+s_y^2}}\left(2\,\frac{\xi_a}{L} + 4\,\frac{\xi_s}{L} - 3\right)\right]\right\}\left(\frac{\xi_s}{L} - \frac{\xi_a}{L}\right)$$

$$M_{zs} = -\frac{L}{2}\,\mu F_z\left[\left(\frac{1}{C_\alpha} - \frac{1}{C_s}\right)\mu F_z\,\frac{s_x}{\sqrt{s_x^2+s_y^2}} - \frac{\xi_s}{L}\right]\frac{s_y}{\sqrt{s_x^2+s_y^2}}\left(1 - \frac{\xi_s}{L}\right)$$

Note

F_{xa}, F_{ya}, M_{za} are terms contributed by the adhesion region which exists when $0 < \xi_a \leq L$.

F_{xt}, F_{yt}, M_{zt} are terms contributed by the transition region which exists when $0 < \xi_a < \xi_s \leq L$.

F_{xs}, F_{ys}, M_{zs} are terms contributed by the sliding region which exists when ξ_a, $\xi_s < L$.

GOODYEAR MODEL [5]

Adhesion Limit (for parabolic contact pressure)

$$\frac{\xi_a}{L} = 1 - \frac{\sqrt{(s_x C_s)^2 + (s_y C_\alpha)^2}}{3\mu_o F_z (1 - s_x)} \tag{85}$$

Traction Modes

$0 < \xi_a < L$ adhesion and sliding

$\xi_a = 0$ complete sliding (occurs before wheel lock)

Traction Forces

$$F_x = \begin{cases} -\frac{1}{3} C_s \frac{s_x}{1 - s_x} \left[1 + \frac{\xi_a}{L} + \left(\frac{\xi_a}{L}\right)^2\right] & 0 < \xi_a < L \\ -C_s s_x \mu_o F_z \left[(C_s s_x)^2 + (C_\alpha s_y)^2\right]^{-1/2} & \xi_a = 0 \end{cases} \tag{88}$$

$$F_y = \begin{cases} -\frac{1}{3} C_\alpha \frac{s_y}{1 - s_x} \left[1 + \frac{\xi_a}{L} + \left(\frac{\xi_a}{L}\right)^2\right] & 0 < \xi_a < L \\ -C_\alpha s_y \mu_o F_z \left[(C_s s_x)^2 + (C_\alpha s_y)^2\right]^{-1/2} & \xi_a = 0 \end{cases} \tag{89}$$

Aligning Moment

$$M_z = \begin{cases} -\frac{L}{6}\left\{\frac{2}{5}(C_s - C_\alpha)\left[1 + 2\frac{\xi_a}{L} + 3\left(\frac{\xi_a}{L}\right)^2 + 4\left(\frac{\xi_a}{L}\right)^3\right]\frac{s_x}{1 - s_x}\right. \\ \qquad \left. - C_\alpha\left(\frac{\xi_a}{L}\right)^3\right\}\frac{s_y}{1 - s_x} & 0 < \xi_a < L \quad (94) \\ -\frac{L}{15}(C_s - C_\alpha)\frac{s_x s_y}{(1 - s_x)^2} & \xi_a = 0 \quad (95) \end{cases}$$

SAKAI MODEL [6]

Adhesion Limit

$$\frac{\xi_a}{L} = 1 - \frac{\sqrt{(s_x C_s)^2 + (s_y C_\alpha)^2}}{3\mu_o F_z (1 - s_x)} \tag{105}$$

Traction Modes

$0 < \xi_a < L$ adhesion and sliding

$\xi_a = 0$ complete sliding (occurs before wheel lock)

Traction Forces

$$F_x = \begin{cases} -C_s \frac{s_x}{1 - s_x} \left(\frac{\xi_a}{L}\right)^2 - \mu_x F_z \frac{s_x}{\sqrt{s_x^2 + s_y^2}} \left[1 - 3\left(\frac{\xi_a}{L}\right)^2 + 2\left(\frac{\xi_a}{L}\right)^3\right] & 0 < \xi_a < L \\ -\mu_x F_z \frac{s_x}{\sqrt{s_x^2 + s_y^2}} & \xi_a = 0 \end{cases} \tag{111}$$

$$F_y = \begin{cases} -(C_\alpha + C_s s_x) \frac{s_y}{1 - s_x} \left(\frac{\xi_a}{L}\right)^2 - \mu_y F_z \frac{s_y}{\sqrt{s_x^2 + s_y^2}} \left[1 - 3\left(\frac{\xi_a}{L}\right)^2 + 2\left(\frac{\xi_a}{L}\right)^3\right] & 0 < \xi_a < L \\ -\mu_y F_z \frac{s_y}{\sqrt{s_x^2 + s_y^2}} & \xi_a = 0 \end{cases} \tag{112}$$

Aligning Moment

$$M_z = \begin{cases} -\frac{L}{6}\left[3(C_\alpha + C_s s_x) - 4\,C_\alpha \frac{\xi_a}{L}\right]\left(\frac{\xi_a}{L}\right)^2 \frac{s_y}{1 - s_x} \\ -\frac{L}{2}\left[\mu_x s_x\left(1 + 3\frac{\xi_a}{L}\right) - 3\mu_y \frac{\xi_a}{L}\right] F_z \frac{s_y}{\sqrt{s_x^2 + s_y^2}} \left(1 - \frac{\xi_a}{L}\right)^2 \frac{\xi_a}{L} \\ -F_x F_y / K_y \qquad 0 < \xi_a < L \qquad (117) \\ \hline -\frac{\mu_x \mu_y F_z^2 s_x s_y}{K_y\left(s_x^2 + s_y^2\right)} \qquad \xi_a = 0 \qquad (118) \end{cases}$$

Adhesion Limit

$$\frac{\xi_a}{L} = 1 - \frac{\sqrt{(s_x C_s)^2 + (s_y C_\alpha)^2}}{3\mu_o F_z (1 - s_x)} \tag{105}$$

Transition Limit

$$\frac{\xi_s}{L} = 1 - \left(\frac{C_s C_\alpha}{C_s + C_\alpha}\right) \frac{\sqrt{s_x^2 + s_y^2}}{3\mu F_z (1 - s_x)} \tag{119}$$

where

$$\mu = \mu_o(1 - A_s V_s) \; ; \qquad V_s = \sqrt{s_x^2 + s_y^2} \; |V| \cos\alpha \tag{30}$$

Traction Modes

$\xi_a < \xi_s < L$ adhesion and transition and sliding

$\xi_s \leq \xi_a < L$ adhesion and sliding

$\xi_a = 0$ complete sliding (occurs before wheel lock)

Traction Forces

$$F_x = F_{xa} + F_{xt} + F_{xs} \tag{64}$$

$$F_y = F_{ya} + F_{yt} + F_{ys} \tag{65}$$

where

$$F_{xa} = -C_s \frac{s_x}{1 - s_x} \left(\frac{\xi_a}{L}\right)^2$$

$$F_{xt} = -\left[\frac{1}{3} C_s \frac{s_x}{1 - s_x} \left(3 - 2\frac{\xi_a}{L} - \frac{\xi_s}{L}\right)\frac{\xi_a}{L} \Big/ \left(1 - \frac{\xi_a}{L}\right) + \mu F_z \frac{s_x}{\sqrt{s_x^2 + s_y^2}} \left(3 - 2\frac{\xi_s}{L} - \frac{\xi_a}{L}\right)\frac{\xi_s}{L}\right] \left(\frac{\xi_s}{L} - \frac{\xi_a}{L}\right)$$

$$F_{xs} = -\mu F_z \frac{s_x}{\sqrt{s_x^2 + s_y^2}} \left[1 - 3\left(\frac{\xi_s}{L}\right)^2 + 2\left(\frac{\xi_s}{L}\right)^3\right] \qquad (120)$$

$$F_{ya} = -C_\alpha \frac{s_y}{1 - s_x} \left(\frac{\xi_a}{L}\right)^2$$

$$F_{yt} = -\left[\frac{1}{3} C_\alpha \frac{s_y}{1 - s_x} \left(3 - 2\frac{\xi_a}{L} - \frac{\xi_s}{L}\right)\frac{\xi_a}{L} \Big/ \left(1 - \frac{\xi_a}{L}\right) + \mu F_z \frac{s_y}{\sqrt{s_x^2 + s_y^2}} \left(3 - 2\frac{\xi_s}{L} - \frac{\xi_a}{L}\right)\frac{\xi_s}{L}\right] \left(\frac{\xi_s}{L} - \frac{\xi_a}{L}\right)$$

$$F_{ys} = -\mu F_z \frac{s_y}{\sqrt{s_x^2 + s_y^2}} \left[1 - 3\left(\frac{\xi_s}{L}\right)^2 + 2\left(\frac{\xi_s}{L}\right)^3\right] \qquad (121)$$

Aligning Moment

$$M_z = M_{za} + M_{zt} + M_{zs} + F_x F_y \left(\frac{1}{K_x} - \frac{1}{K_y}\right) \qquad (71)$$

where

$$M_{za} = -\frac{L}{3}\left[2(C_s - C_\alpha)\frac{s_x}{1 - s_x}\frac{\xi_a}{L} - \frac{1}{2}C_\alpha\left(4\frac{\xi_a}{L} - 3\right)\right] \frac{s_y}{1 - s_x} \left(\frac{\xi_a}{L}\right)^2$$

$$M_{zt} = - s_y L \left[(C_s - C_\alpha) \left\{ \frac{s_x}{(1-s_x)^2} \left(\frac{\xi_a}{L}\right)^2 \frac{1}{15} \left[6\left(\frac{\xi_a}{L}\right)^2 + 3 \frac{\xi_a}{L} \frac{\xi_s}{L} \right.\right.\right.$$

$$\left. + \left(\frac{\xi_s}{L}\right)^2 - 15 \frac{\xi_s}{L} - 5 \frac{\xi_s}{L} + 10 \right] / \left(1 - \frac{\xi_a}{L}\right)^2$$

$$+ \frac{s_x \mu F_z}{(1-s_x)\sqrt{s_x^2 + s_y^2}} \left(\frac{1}{C_s} + \frac{1}{C_\alpha} \right) \frac{\xi_a}{L} \frac{\xi_s}{L} \frac{1}{10} \left[3\left(\frac{\xi_s}{L}\right)^2 \right.$$

$$\left. + 3\left(\frac{\xi_a}{L}\right)^2 + 4 \frac{\xi_a}{L} \frac{\xi_s}{L} - 10\left(\frac{\xi_a}{L} + \frac{\xi_s}{L}\right) + 10 \right] / \left(1 - \frac{\xi_a}{L}\right)$$

$$+ \frac{s_x \mu^2 F_z^2}{(s_x^2 + s_y^2) C_s C_\alpha} \frac{3}{10} \left[6\left(\frac{\xi_s}{L}\right)^2 + 3 \frac{\xi_a}{L} \frac{\xi_s}{L} + \left(\frac{\xi_a}{L}\right)^2 \right.$$

$$\left. \left. - 15 \frac{\xi_s}{L} - 5 \frac{\xi_a}{L} + 10 \right] \right\}$$

$$+ \frac{C_\alpha}{1-s_x} \frac{\xi_a}{L} \frac{1}{6} \left[3 - 3\frac{\xi_a}{L}\left(2 - \frac{\xi_a}{L}\right) - \frac{\xi_s}{L}\left(3 - \frac{\xi_s}{L}\right) + 2 \frac{\xi_a}{L} \frac{\xi_s}{L} \right] / \left(1 - \frac{\xi_a}{L}\right)$$

$$+ \frac{\mu F_z}{\sqrt{s_x^2 + s_y^2}} \frac{\xi_s}{L} \frac{1}{2} \left[3 - 3\frac{\xi_s}{L}\left(2 - \frac{\xi_a}{L}\right) - \frac{\xi_a}{L}\left(3 - \frac{\xi_a}{L}\right) \right.$$

$$\left. \left. + 2 \frac{\xi_a}{L} \frac{\xi_s}{L} \right] \right] \left(\frac{\xi_s}{L} - \frac{\xi_a}{L}\right)$$

$$M_{zs} = - s_y L \left\{ \left(\frac{1}{C_\alpha} - \frac{1}{C_s} \right) \frac{s_x (\mu F_z)^2}{s_x^2 + s_y^2} \frac{3}{5} \left[1 + 3\frac{\xi_s}{L} + 6\left(\frac{\xi_s}{L}\right)^2 \right] \left(1 - \frac{\xi_s}{L}\right)^2 \right.$$

$$\left. - \frac{\mu F_z}{\sqrt{s_x^2 + s_y^2}} \left[1 + \frac{\xi_s}{L} + \left(\frac{\xi_s}{L}\right)^2 \right] \right\} \left(1 - \frac{\xi_s}{L}\right) \qquad (124)$$

Note

F_{xa}, F_{ya}, M_{za} are terms contributed by the adhesion region which exists when $0 < \xi_a < L$.

F_{xt}, F_{yt}, M_{zt} are terms contributed by the transition region which exists when $0 < \xi_a < \xi_s < L$.

F_{xs}, F_{ys}, M_{zs} are terms contributed by the sliding region which always exists when a parabolic pressure distribution is presumed.

It is interesting to note that all of the expressions summarized in this appendix can be normalized (dimensionless) with respect to F_z and L by the following substitutions.

$$\overline{C}_s = \frac{C_s}{F_z}$$

$$\overline{C}_\alpha = \frac{C_\alpha}{F_z}$$

$$\overline{K}_x = \frac{K_x L}{F_z}$$

$$\overline{K}_y = \frac{K_y L}{F_z}$$

Therefore,

$$\overline{F}_x = \frac{F_x}{F_z}$$

$$\overline{F}_y = \frac{F_y}{F_z}$$

$$\overline{M}_z = \frac{M_z}{F_z \cdot L}$$

$$\overline{F}_z = \frac{F_z}{F_z} = 1.$$

$$\overline{L} = \frac{L}{L} = 1.$$

This procedure is particularly useful in computer implementation of the models as explained in Appendix IV.

APPENDIX III

LOCI OF ADHESION LIMIT POINTS

The adhesion limit point, $\xi = \xi_a$, depends upon the contact pressure distribution $q_z(\xi)$ as well as the slip parameters s_x and s_y. The shape of the contact pressure distribution produces certain values (upper bounds) of the slip parameters which initiate full sliding operation of the linear tire models* discussed in this document. The upper bounds on the slip parameters are determined by considering the loci of the adhesion limit points for the pressure distribution function assumed. Two contact pressure distributions, uniform and parabolic, will be analyzed in this appendix.

UNIFORM CONTACT PRESSURE $\qquad q_z = F_z/wL$

Equation (20), solved for the adhesion limit in terms of slip parameters and traction stiffnesses, becomes

$$\xi_a = \frac{1}{2}\,\mu_o F_z L\,\frac{(1 - s_x)}{\sqrt{(C_s s_x)^2 + (C_\alpha s_y)^2}} \qquad \text{(III-1)}$$

The tread element deformation, u_a and v_a, at the adhesion limit, are given by Equations (18) and (19) written in terms of slip parameters.

$$u_a = \frac{s_x}{1 - s_x}\,\xi_a \qquad \text{(III-2)}$$

$$v_a = \frac{s_y}{1 - s_x}\,\xi_a \qquad \text{(III-3)}$$

---

*The term 'linear tire model' is applied to those models which consider contact shear stress as a linear function of shear deformation.

Equation (III-1) may be solved for s_y and used to eliminate s_y from (III-3). The result expresses v_a in terms of s_x and ξ_a.

$$v_a = \frac{1}{C_\alpha}\sqrt{\left(\frac{1}{2}\mu_o F_z L\right)^2 - \left(C_s \frac{s_x}{1 - s_x}\xi_a\right)^2} \qquad \text{(III-4)}$$

The coordinates, u_a and v_a, of the adhesion limit point, A (Fig. III-1), have now been written independent of s_y. The locus of the adhesion limit points, as the adhesion limit moves back from the contact entry point, is given by

$$\eta(\xi_a + u_a) = v_a(\xi_a)$$

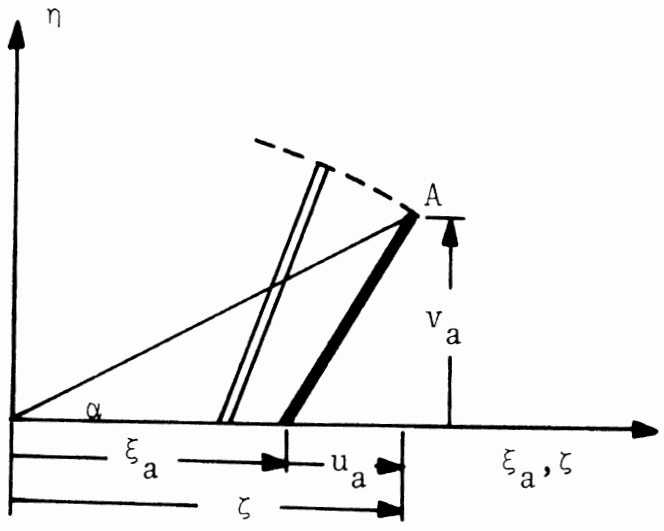

Figure III-1. Coordinates of the adhesion limit point A .

For analyzing the locus of points A, it is convenient to define a new independent variable ζ such that

$$\zeta = \xi_a + u_a = \frac{1}{1 - s_x} \xi_a \qquad \text{(III-5)}$$

The locus of adhesion limit points, for uniform contact pressure, may now be written as

$$\eta(\zeta) = \frac{1}{C_\alpha} \sqrt{\left(\tfrac{1}{2}\mu_o F_z L\right)^2 - \left(C_s s_x \zeta\right)^2} \qquad \text{(III-6)}$$

The uniform pressure locus (III-6) is found to be elliptical with lateral semi-axis independent of s_x. The elliptical locus, which occurs for $s_x < 1$, is shown as a dashed line in Figure III-2.

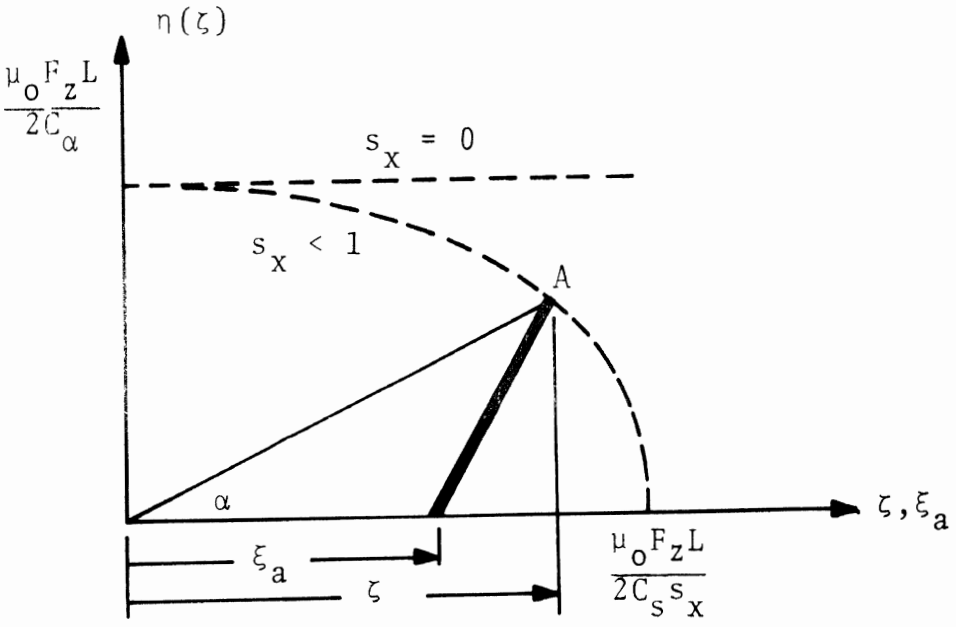

Figure III-2. Loci of adhesion limit points (A) for uniform contact pressure.

The adhesion limit for a free-rolling tire with uniform contact pressure is at

$$\zeta = \xi_a = \frac{\mu_o F_z L}{2C_\alpha s_y}$$

and the locus of adhesion limit points is the horizontal straight line

$$\eta(\zeta) = v_a = \frac{\mu_o F_z L}{2C_\alpha}$$

shown in Figures III-2 and III-3.

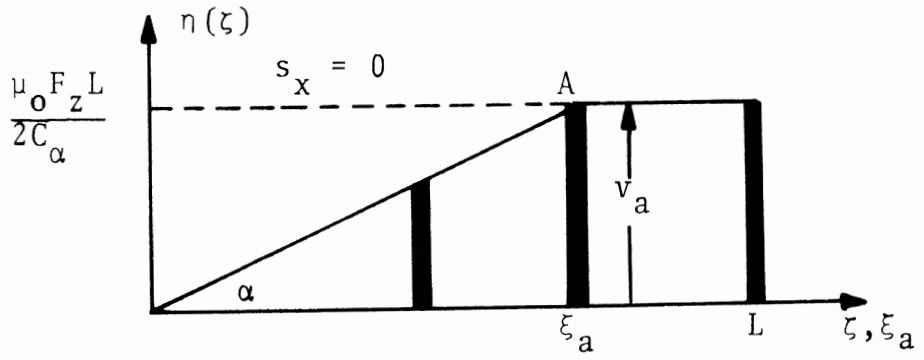

Figure III-3. Locus of adhesion limit points (A) for a free-rolling tire with uniform contact pressure.

The preceding study of adhesion limit point loci reveals the following slip parameter ranges producing an adhesion region in a linear tire model with the assumption of uniform contact pressure.

Since Equation (III-1) shows the adhesion limit ξ_a to vanish only for $s_x = 1$, the adhesion operating range of s_x is

$$-\infty < s_x \leq 1 \qquad \text{(III-7)}$$

Figure III-2 shows that for all $s_x \neq 1$, the adhesion limit will vanish only for $\alpha = 90°$ ($s_y = \infty$). The adhesion operating range of s_y is

$$0 \leq s_y < \infty \qquad \text{(III-8)}$$

PARABOLIC CONTACT PRESSURE $\qquad q_z(\xi) = \frac{6F_z}{wL}\left(1 - \frac{\xi}{L}\right)\frac{\xi}{L}$

For a parabolic contact pressure distribution evaluated at $\xi = \xi_a$, Equation (20), solved for the adhesion limit in terms of slip parameters and traction stiffnesses, becomes

$$\xi_a = L\left[1 - \frac{\sqrt{(C_s s_x)^2 + (C_\alpha s_y)^2}}{3\mu_o F_z (1 - s_x)}\right] \qquad \text{(III-9)}$$

Solving Equation (III-9) for s_y and using the result in (III-3) allows v_a to be written in terms of s_x and ξ_a.

$$v_a = \frac{1}{C_\alpha}\sqrt{\left[3\mu_o F_z(1 - s_x)(1 - \frac{\xi_a}{L})\right]^2 - (C_s s_x)^2}\ \left(\frac{\xi_a}{1 - s_x}\right) \quad \text{(III-10)}$$

The coordinates of the adhesion limit point, A (Fig. III-1), are u_a given by (III-2) and v_a given by (III-10) above. These coordinates are independent of s_y and allow the limit point locus to be expressed as an explicit function of ξ_a (or ζ). The locus of adhesion limit points, for parabolic contact pressure, is

$$\eta(\zeta) = \frac{1}{C_\alpha}\sqrt{\left[3\mu_o F_z(1 - s_x)(1 - \frac{1-s_x}{L}\zeta)\right]^2 - (C_s s_x)^2}\ \zeta \quad \text{(III-11)}$$

where ζ is the independent variable defined by (III-5). The parabolic pressure locus (III-11) is found to be lemniscatic with finite slope at the origin. The analysis of (III-11) is facilitated by rewriting it in the following form.

$$\eta^2 = \left[\left(\frac{3\mu_o F_z(1-s_x)^2}{C_\alpha L}\right)^2\left(\zeta - \frac{L}{1-s_x}\right)^2 - \left(\frac{C_s}{C_\alpha}s_x\right)^2\right]\zeta^2 \quad \text{(III-12)}$$

For a particular value of s_x, Equation (III-12) has the functional form

$$\eta^2 = [A^2(\zeta - B)^2 - C^2]\,\zeta^2 \quad \text{(III-13)}$$

where A, B, and C are constants depending on s_x. Nonzero adhesion limits exist when $B > C/A$, for which Equation (III-13) exhibits the two curves whose essential features are shown in Figure III-4.

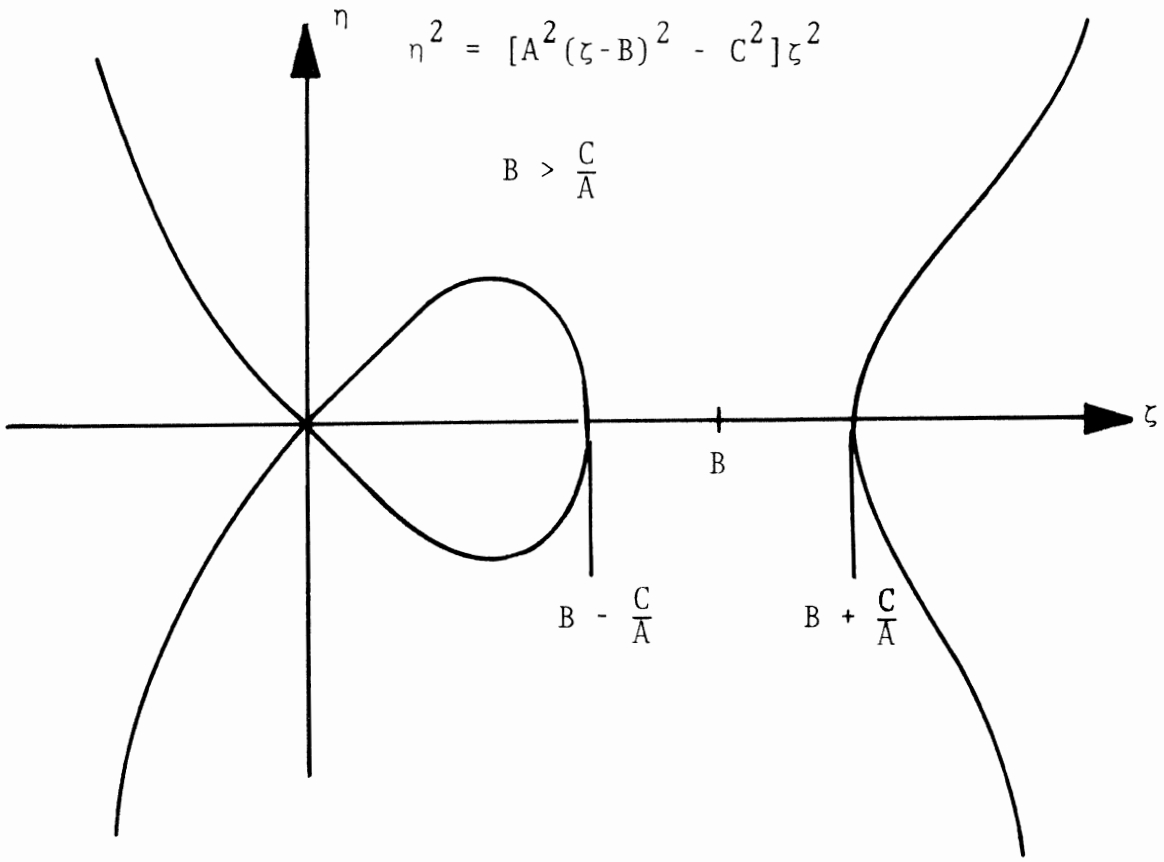

Figure III-4. Sketch of adhesion limit locus equation (III-13).

The adhesion limit locus is confined to the upper half of the lemniscatic loop in the region $0 \leq \zeta \leq (B - C/A)$. Recognizing that the adhesion limit locus exists only for $(B - C/A) > 0$ determines the upper bound for s_x at

$$B - C/A = 0$$

$$\frac{L}{1-s_x} - \frac{C_s}{C_\alpha} s_x \frac{C_\alpha L}{3\mu_o F_z (1-s_x)^2} = 0$$

$$s_x = \frac{3\mu_o F_z}{3\mu_o F_z + C_s} \qquad \text{(III-14)}$$

The adhesion limit vanishes for straight-ahead braking when s_x attains the value given by Equation (III-14). For braking at a slip angle, the adhesion limit vanishes somewhat before the s_x value given by (III-14).

The adhesion limit locus for s_x below the upper bound is shown in Figure III-5. The lemniscatic nature of the locus is retained as s_x drops to zero for the free-rolling tire. At $s_x = 0$, the locus becomes a parabola crossing the axis at the contact exit point ($\zeta = \frac{L}{1-s_x}$).

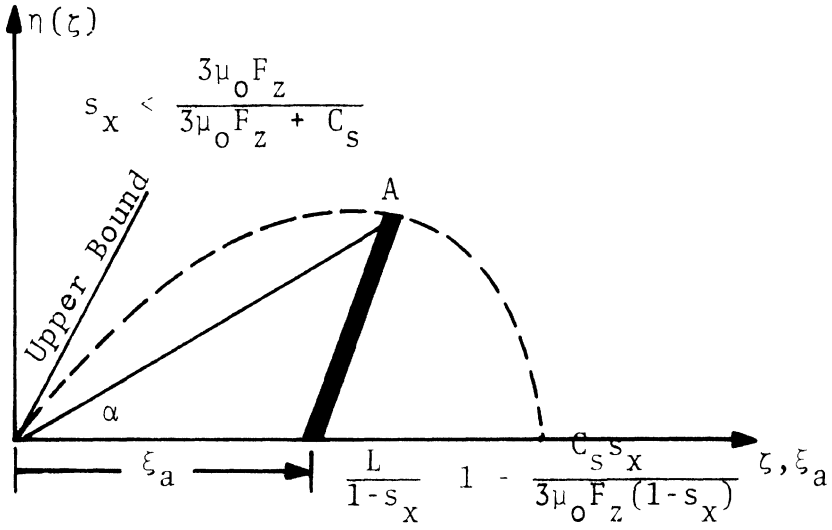

Figure III-5. Locus of adhesion limit points for parabolic contact pressure.

As the slip angle α is increased from zero, the adhesion point A moves forward in the contact patch until it reaches the contact entry point at $\xi_a = \zeta = 0$. As seen in Figure III-5, the upper bound for the slip angle (and the parameter s_y) occurs at the finite slope of the adhesion limit locus passing through the origin. The first derivative of Equation (III-13), evaluated at the origin, is

$$\frac{d\eta}{d\zeta} = \sqrt{A^2B^2 - C^2}$$

Introducing the constants A, B, and C from (III-12) yields the upper bound to the slip angle α as the limit slope s_y.

$$s_y = \frac{1}{C_\alpha}\sqrt{[3\mu_o F_z(1-s_x)]^2 - (C_s s_x)^2} \qquad \text{(III-15)}$$

Solving Equation (III-15) for s_x gives the upper bound to s_x when a slip angle is present.

$$s_x = \frac{(3\mu_o F_z)^2 - \sqrt{(3\mu_o F_z)^2 C_s^2 + s_y^2[(3\mu_o F_z)^2 - C_s^2]C_\alpha^2}}{(3\mu_o F_z)^2 - C_s^2} \qquad \text{(III-16)}$$

A slightly lower limiting value for s_x results for nonzero s_y. When $s_y = 0$, Equation (III-16) reduces to Equation (III-14).

The adhesion limit for a free-rolling tire with parabolic contact pressure is obtained by setting $s_x = 0$ in Equation (III-9).

$$\zeta = \xi_a = L\left[1 - \frac{C_\alpha s_y}{3\mu_o F_z}\right]$$

As predicted by the above and Equation (III-15), the free-rolling adhesion limit vanishes when

$$s_y = \frac{3\mu_o F_z}{C_\alpha} \qquad \text{(III-17)}$$

Setting $s_x = 0$ in Equation (III-11) results in the parabolic locus of adhesion limit points

$$\eta(\zeta) = \frac{3\mu_o F_z}{C_\alpha}\left(1 - \frac{\zeta}{L}\right)\zeta \qquad \text{(III-18)}$$

$$\eta(\zeta) = \mu_o q_z(\xi)$$

shown in Figure III-6. The locus is proportional to the parabolic contact pressure.

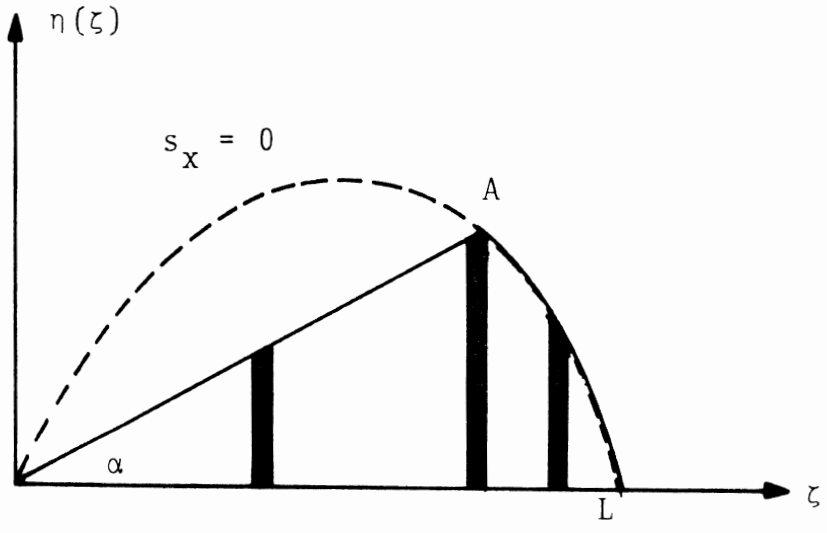

Figure III-6. Locus of adhesion limit points for a free-rolling tire with parabolic contact pressure.

As the slip angle increases, the sliding region contact points will follow the adhesion limit locus. This is a special case. In general, the sliding contact points will not follow the adhesion limit locus which terminates inside the contact region (except for $s_x = 0$).

The preceding analysis has determined the following slip parameter ranges producing an adhesion region in a linear tire model with the assumption of parabolic contact pressure.

For straight-ahead braking, the upper bound on s_x is given by Equation (III-14) and the adhesion operating range of s_x is

$$0 \leq s_x \leq \frac{3\mu_o F_z}{3\mu_o F_z + C_s} \qquad \text{(straight-ahead)} \qquad \text{(III-19)}$$

In the presence of a slip angle ($s_y > 0$), the upper bound on s_x is reduced to the value given by Equation (III-16).

In free-rolling cornering, the upper bound on s_y is given by Equation (III-17) and the adhesion operating range of s_y is

$$0 \leq s_y \leq \frac{3\mu_o F_z}{C_\alpha} \qquad \text{(free-rolling)} \qquad \text{(III-20)}$$

In the presence of braking ($s_x > 0$), the upper bound on s_y is reduced to the value given by Equation (III-15).

APPENDIX IV

DIGITAL COMPUTER PROGRAMS

The digital computer programs described and listed in this appendix are written in FORTRAN IV for execution on the HSRI PDP 11/45 computer with 64K (bytes) of core memory. The traction response plots were drawn by a Calcomp 565 digital plotter controlled by the PDP 11/45.

TIRE MODEL SUBROUTINES

The five tire models, whose descriptive equations are summarized in Appendix II, have been programmed as FORTRAN subroutines. The programming has employed the normalization scheme described at the end of Appendix II. Thus, the computed traction forces FX and FY should be multiplied by the tire load FZ to obtain the dimensional values. The computed aligning moment MZ should be multiplied by FZ·L to obtain the dimensional value.

The tire model subroutines are identified by a five-character name and a model code number as listed in Table 2.

TABLE 2

TIRE MODEL SUBROUTINE NAMES AND CALLING CODE NUMBERS

Subroutine Name	Tire Model	Calling Code
NMHS1	HSRI-NBS-I	1
NMHS2	HSRI-NBS-II	2
NMHS3	HSRI-NBS-III	3
NMSK1	SAKAI	4
NMGDR	GOODYEAR	5

The tire model subroutines may be called from either of two main programs, NMDGT1 and NMDGT2, developed to exercise the models.

MAIN PROGRAMS

Two main programs were developed for the purposes of obtaining the comprehensive traction response of a specific tire model (NMDGT1) and to compare the traction response of all five tire models in either free-rolling or straight-ahead operation (NMDGT2).

NMDGT1. This main program calls a specific tire model identified by the calling code input datum IMODE. The value of the input datum ISW1 selects the slip variable (α or s_x) to be swept at discrete values of the nonswept variable (s_x or α) assigned by a DATA initialization statement. The nonswept variable is called the path variable. Subroutine PATH1 is called by NMDGT1 if an α-path is to be taken (ISW1=1). Subroutine PATH2 is called if an s_x path is to be taken (ISW1=2). Subroutines PATH1 and PATH2 both call subroutine MODEL which, in turn, calls the specific tire model subroutine to be exercised. A subroutine calling flow chart is shown in Figure IV-1.

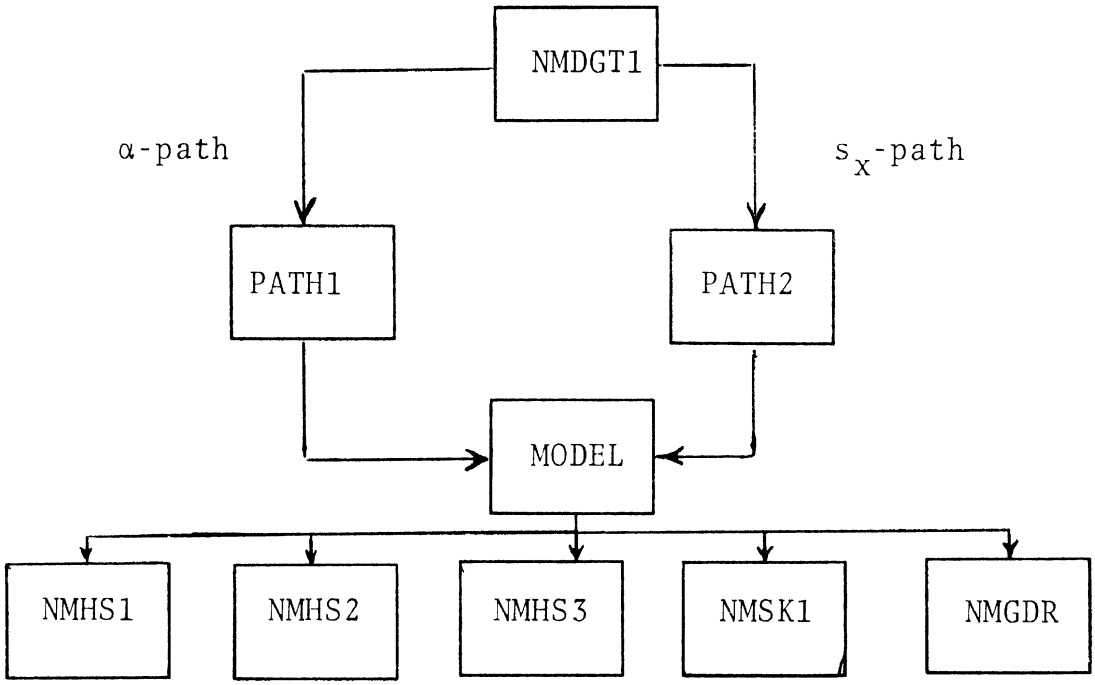

Figure IV-1. Flow chart for subroutine calling when main program NMDGT1 is used.

NMDGT2. This main program calls all of the tire model subroutines directly. The value of input datum ISW1 selects straight-ahead (ISW1=1: α=0) or free-rolling (ISW1=2: s_x=0) operation. As with main program NMDGT1, the swept variable, s_x or α, is increased according to the initial value, step interval, and number of steps specified by the input data. Print or plot output is selected by ISW2.

The main programs read the following input data:

ISW1	Selects variable, s_x or α, to be swept	
ISW2	Selects output mode, plot or print	
IMODE	Tire model calling number	NMDGT1 only
NAME	Name of the tire model called (12 char.)	NMDGT1 only
MUO	Static coefficient of friction, μ_o	
AS	Speed sensitivity parameter, A_s	
V	Traveling velocity	
MUX	Longitudinal coefficient of sliding friction, μ_x	
MUY	Lateral coefficient of sliding friction, μ_y	
CS	Longitudinal traction stiffness, C_s	
CALFA	Lateral traction stiffness, C_α	
KX	Longitudinal carcass stiffness, K_x	
KY	Lateral carcass stiffness, K_y	
BX	Longitudinal patch point relocation factor, β_x (set=1.)	
BY	Lateral patch point relocation factor, β_y (set=1.)	

L	Contact patch length, L
FZ	Tire load, F_z
SX11	Initial value of s_x for s_x sweep
DSX	Step interval in s_x sweep
N	Number of steps, or points, in s_x sweep
ALF11	Initial value of α for α sweep
DALFA	Step interval in α sweep
M	Number of steps, or points, in α sweep

The following parameters are assigned by a DATA initialization statement in NMDGT1:

ALF1	Fixed values of α for which an s_x sweep will be conducted.
SX1	Fixed values of s_x for which an α sweep will be conducted.

SUBROUTINE MODEL

When main program NMDGT1 is used, the tire model subroutines are called from subroutine MODEL which employs the following input and output arguments.

Input Arguments (MODEL)

SX	longitudinal slip parameter, s_x
ALFA	slip angle α (degrees)
IMODE	calling code number (Table 2)

Output Arguments (MODEL)

FX	normalized longitudinal force F_x/F_z
FY	normalized lateral force F_y/F_z
XMZ	normalized aligning moment $M_z/(F_z \cdot L)$
XIA	adhesion limit fraction ξ_a/L
XIS	transition limit fraction ξ_s/L

It should be noted that argument XIS is relevant only for the HSRI-NBS-II and HSRI-NBS-III models as these are the only models which include a transition region between adhesive and sliding contact.

PLOTTING SUBROUTINES

The plotting subroutines NMGR2, NMPL2, NMPL3 are not included in this appendix as they are highly dependent on the particular computing and plotting equipment utilized.

```
FORTRAN V06.13                    13:16:20    10-JAN-74   PAGE    1

      C*NMDGT1.....MAIN PROGRAM FOR DIGITAL TIRE MODELS.....
      C     ------------------------------------------------------------
      C
0001        REAL MUO,MUX,MUY,KX,KY,L
0002        DIMENSION ALF2(5),SX2(5)
0003        COMMON IPR,IRD,IWR,IKEY
0004        COMMON    ALF1(5),SX1(5)
0005        COMMON SX11,IMODE,XIA,XIS,DSX,ISW2
0006        COMMON  ISW1 ,SXI,ALFAI,N,M,J1,J2
0007        COMMON  XORG(5),YORG(5),XLEN(5),YLEN(5),XMIN(5),XMAX(5),
           +        YMIN(5),YMAX(5),NXDIV(5),NYDIV(5),SCALX(5),SCALY(5)
0008        COMMON  X(205),FX(205),FY(205),XMZ(205),NAME(6)
0009        COMMON MUO,AS,V,MUX,MUY
0010        COMMON CS,CALFA
0011        COMMON KX,KY,BX,BY
0012        COMMON L,FZ
0013        COMMON DALFA
0014        DATA  ALF2/0.,.4,.8,1.2,1.6/,SX2/0.,.05,.1,.15,.2/
0015        IPR=5
0016        IRD=8
0017        IWR=6
0018        IKEY=6
0019        DO 1  I=1,5
0020        ALF1(I)=ALF2(I)
0021      1 SX1(I)=SX2(I)
0022        XIS=0.
0023        NMAX=5
      C     . . . . . .
      C     ------------------------------------------------------------
      C
0024        READ(IRD,1201)ISW1,ISW2
      C ***** ISW1 DESIGNATES WHICH PATH THE PROGRAM IS TO TAKE .....
      C ******  1 = ALPHA PATH
      C ******  2 = SX PATH
      C
      C ***** ISW2 DESIGNATES PRINTOUT OR PLOT
      C *****   1 = PRINTOUT
      C *****   2 = PLOT
      C
0025        READ(IRD,1200)IMODE,NAME
0026        READ(IRD,1100)MUO,AS,V,MUX,MUY
0027        READ(IRD,1100)CS,CALFA
0028        READ(IRD,1100)KX,KY,BX,BY
0029        READ(IRD,1100)L,FZ
0030        READ(IRD,1000)SX11,DSX,N
0031        READ(IRD,1000)ALF11,DALFA,M
      C     . . . . . .
      C     ------------------------------------------------------------
      C
0032        WRITE(IPR,5000)
0033        WRITE(IPR,7000)NAME,MUO,MUX,MUY,V,AS,CS,CALFA
0034        WRITE(IPR,7100)KX,KY,BX,BY,FZ,L
0035        CS=CS/FZ
0036        CALFA=CALFA/FZ
0037        KX=KX/FZ
```

```
0038          KY=KY/FZ
0039       10 N1=1
0040          N2=1
0041          GO TO (50,60),ISW1
      C
      C     ------------------------------------------------------------
      C
      C
0042       50 GO TO (51,52),ISW2
0043       51 CONTINUE
0044          WRITE(IPR,5000)
0045          WRITE(IPR,6000)
0046       52 CONTINUE
0047          ALFAI=ALF1(N1)
0048          X(1)=SX11
0049          CALL PATH1
0050          GO TO (71,72),ISW2
0051       72 CONTINUE
0052          IF(ALFAI)150,160,150
0053      160 CALL NMGR2
0054      150 CALL NMPL2
0055       71 CONTINUE
0056          N1=N1+1
0057          IF(N1-NMAX)50,50,100
      C
      C     ------------------------------------------------------------
      C
      C
0058       60 GO TO (61,62),ISW2
0059       61 CONTINUE
0060          WRITE(IPR,5000)
0061          WRITE(IPR,6000)
0062       62 CONTINUE
0063          SXI=SX1(N2)
0064          X(1)=ALF11
0065          CALL PATH2
0066          GO TO (101,102),ISW2
0067      102 CONTINUE
0068          IF(SXI)130,140,130
0069      140 CALL NMGR2
0070      130 CALL NMPL2
0071      101 CONTINUE
0072          N2=N2+1
0073          IF(N2-NMAX)60,60,100
0074      100 CALL EXIT
      C
      C     ------------------------------------------------------------
      C
      C
0075     1000 FORMAT(2F4.0,I3)
0076     1100 FORMAT(5E8.3)
0077     1200 FORMAT(I1,6A2)
0078     1201 FORMAT(2I1)
0079     5000 FORMAT(1H1)
0080     6000 FORMAT(10X,'SLIP ANGLE     LONG. SLIP     FORCE-LONG     FORCE-L
     +,       MOMENT'/11X,7H(ALPHA),10X,4H(SX),11X,4H(FX),11X,4H(FY),
     +11X,4H(MZ)/11X,7HDEGREES,8X,7HPERCENT,8X,8H1000 LB.,7X,8H1000 LB
     +6X,10H1000 LB-IN/10X,'----------     ----------     ----------
     + ----------     ----------'/' ')
```

```
FORTRAN V06.13                    13:16:20    10-JAN-74   PAGE    3

0081      7000 FORMAT(5X,'TIRE MODEL  ',6A2///,
     +            5X,'MUO=',F4.2,4X,'MUX=',F4.2,4X,'MUY=',F4.2//,
     +            5X,'V   =',F4.2,4X,'AS =',F5.3//,
     +            5X,'CS =',F4.1,4X,'CALFA=',F4.1/)
0082      7100 FORMAT(5X,'KX =',F4.2,4X,'KY =',F4.2,4X,
     +            'BX =',F5.3,3X,'BY =',F5.3//,
     +            5X,'FZ =',F4.2,4X,'L  =',F5.3//)
          C
          C     ------------------------------------------------------------
          C
0083            END

          ROUTINES CALLED:
          PATH1 , NMGR2 , NMPL2 , PATH2 , EXIT

          OPTIONS =/ON,/OP:3

          BLOCK        LENGTH
          MAIN.   901     (003412)*
          .$$$$.  1827    (007106)

          **COMPILER ----- CORE**
             PHASE       USED  FREE
          DECLARATIVES  00622 14243
          EXECUTABLES   01335 13530
          ASSEMBLY      01585 17920
```

```
FORTRAN V06.13                  11:39:36    10-JAN-78   PAGE    1

      C*** LINK PATH1 OF MAIN LINK NMDGT
0001          SUBROUTINE PATH1
0002          REAL MUO,MUX,MUY,KX,KY,L
0003          COMMON IPR,IRD,IWR,IKEY
0004          COMMON     ALF1(5),SX1(5)
0005          COMMON SX11,IMODE,XIA,XIS,DSX,ISW2
0006          COMMON  ISW1 ,SXI,ALFAI,N,M,J1,J2
0007          COMMON  XORG(5),YORG(5),XLEN(5),YLEN(5),XMIN(5),XMAX(5),
     +                YMIN(5),YMAX(5),NXDIV(5),NYDIV(5),SCALX(5),SCALY(5)
0008          COMMON  X(205),FX(205),FY(205),XMZ(205),NAME(6)
0009          COMMON MUO,AS,V,MUX,MUY
0010          COMMON CS,CALFA
0011          COMMON KX,KY,BX,BY
0012          COMMON L,FZ
0013          COMMON DALFA
0014          DO 70 I=1,N
0015          CALL MODEL(X(I),ALFAI,FX(I),FY(I),XMZ(I),XIA,XIS,IMODE)
0016          GO TO (80,90),ISW2
0017       80 WRITE(5,8000)I,ALFAI,X(I),FX(I),FY(I),XMZ(I),  XIA,XIS
0018       90 X(I+1)=X(I)+DSX
0019     8000 FORMAT(I5,5X,F6.2,10X,F6.3,1X,7F15.4)
0020       70 CONTINUE
0021          RETURN
0022          END

      ROUTINES CALLED:
      MODEL

      OPTIONS =/ON,/OP:3

      BLOCK       LENGTH
      PATH1   151     (000456)*
      .$$$$.  1827    (007106)

      **COMPILER ----- CORE**
         PHASE       USED  FREE
      DECLARATIVES 01255 13610
      EXECUTABLES  01183 13682
      ASSEMBLY     01297 18208
```

```
FORTRAN V06.13                    11:40:01    10-JAN-74   PAGE    1

      C**** LINK PATH2 OF MAIN LINK NMDGT
0001          SUBROUTINE PATH2
0002          REAL MUO,MUX,MUY,KX,KY,L
0003          COMMON IPR,IRD,IWR,IKEY
0004          COMMON     ALF1(5),SX1(5)
0005          COMMON SX11,IMODE,XIA,XIS,DSX,ISW2
0006          COMMON  ISW1 ,SXI,ALFAI,N,M,J1,J2
0007          COMMON  XORG(5),YORG(5),XLEN(5),YLEN(5),XMIN(5),XMAX(5),
             +        YMIN(5),YMAX(5),NXDIV(5),NYDIV(5),SCALX(5),SCALY(5)
0008          COMMON  X(205),FX(205),FY(205),XMZ(205),NAME(6)
0009          COMMON MUO,AS,V,MUX,MUY
0010          COMMON CS,CALFA
0011          COMMON KX,KY,BX,BY
0012          COMMON L,FZ
0013          COMMON DALFA
0014          DO 100 I=1,M
0015          CALL MODEL(SXI,X(I),FX(I),FY(I),XMZ(I),XIA,XIS,IMODE)
0016          GO TO (110,120),ISW2
0017      110 WRITE(5,8000)I,X(I),SXI,FX(I),FY(I),XMZ(I),  XIA,XIS
0018     8000 FORMAT(I5,5X,F6.2,10X,F6.3,1X,7F15.4)
0019      120 X(I+1)=X(I)+DALFA
0020      100 CONTINUE
0021          RETURN
0022          END

      ROUTINES CALLED:
      MODEL

      OPTIONS =/ON,/OP:3

      BLOCK        LENGTH
      PATH2    154     (000464)*
      .$$$$.   1827    (007106)

      **COMPILER ----- CORE**
         PHASE       USED  FREE
      DECLARATIVES 01255 13610
      EXECUTABLES  01183 13682
      ASSEMBLY     01297 18208
```

```
C*MODEL.......... TIRE SHEAR FORCE ROUTINES.
C     ================================================================
C
0001        SUBROUTINE MODEL(SX,ALFA,FX,FY,XMZ,XIA,XIS,IMODE)
C
C     ================================================================
C
0002        COMMON IBUFF(1827)
0003        XIS=0.
C
0004        GO TO (10,20,30,40,50),IMODE
C
0005     10 CALL NMHS1(SX,ALFA,FX,FY,XMZ,XIA)
0006        GO TO 999
C
0007     20 CALL NMHS2(SX,ALFA,FX,FY,XMZ,XIA,XIS)
0008        GO TO 999
C
0009     30 CALL NMHS3(SX,ALFA,FX,FY,XMZ,XIA,XIS)
0010        GO TO 999
C
0011     40 CALL NMSKI(SX,ALFA,FX,FY,XMZ,XIA)
0012        GO TO 999
C
0013     50 CALL NMGDR(SX,ALFA,FX,FY,XMZ,XIA)
C     ================================================================
C
0014    999 RETURN
0015        END

ROUTINES CALLED:
NMHS1 , NMHS2 , NMHS3 , NMSKI , NMGDR

OPTIONS =/ON,/CO,/OP:3

BLOCK       LENGTH
MODEL   210     (000644)*
.$$$$.  1827    (007106)

**COMPILER ----- CORE**
   PHASE       USED  FREE
DECLARATIVES 00802 14063
EXECUTABLES  00966 13899
ASSEMBLY     01053 18452
```

```
      C*NMDGT2.....MAIN PROGRAM FOR DIGITAL TIRE MODELS.
      C     ------------------------------------------------------------
      C
0001        REAL MUO,MUX,MUY,KX,KY,L
0002        COMMON IPR,IRD,IWR,IKEY
0003        COMMON     ALF1(5),SX1(5)
0004        COMMON SX11,IMODE,XIA,XIS,DSX,ISW2
0005        COMMON  ISW1 ,SXI,ALFAI,N,M,J1,J2
0006        COMMON  XORG(5),YORG(5),XLEN(5),YLEN(5),XMIN(5),XMAX(5),
     +          YMIN(5),YMAX(5),NXDIV(5),NYDIV(5),SCALX(5),SCALY(5)
0007        COMMON  X(205),FX(205),FY(205),XMZ(205),NAME(6)
0008        COMMON MUO,AS,V,MUX,MUY
0009        COMMON CS,CALFA
0010        COMMON KX,KY,BX,BY
0011        COMMON L,FZ
0012        COMMON DALFA
      C     . . . . . .
      C     ------------------------------------------------------------
      C
0013        IRD=8
0014        IPR=5
0015        IKEY=6
0016        IWR=6
0017        READ(IRD,1201)ISW1,ISW2
0018        READ(IRD,1100)MUO,AS,V,MUX,MUY
0019        READ(IRD,1100)CS,CALFA
0020        READ(IRD,1100)KX,KY,BX,BY
0021        READ(IRD,1100)L,FZ
0022        READ(IRD,1000)SX11,DSX,N
0023        READ(IRD,1000)ALF11,DALFA,M
      C     . . . . . .
      C     ------------------------------------------------------------
      C
0024        WRITE(IPR,5000)
0025        WRITE(IPR,7000)      MUO,MUX,MUY,V,AS,CS,CALFA
0026        WRITE(IPR,7100)KX,KY,BX,BY,FZ,L
0027        CS=CS/FZ
0028        CALFA=CALFA/FZ
0029        KX=KX/FZ
0030        KY=KY/FZ
0031        GO TO (50,60),ISW1
      C     . . . . . .
      C     ------------------------------------------------------------
      C
0032     50 GO TO (51,52),ISW2
0033     51 CONTINUE
0034        WRITE(IPR,5000)
0035        WRITE(IPR,6000)
0036     52 CONTINUE
0037        ALFAI=0.
0038        X(1)=SX11
0039        DO 71 IMODE=1,5
0040        DO 70 I=1,N
0041        GO TO (201,202,203,204,205),IMODE
0042    201 CALL NMHS1(X(I),ALFAI,FX(I),FY(I),XMZ(I),XIA)
```

```
0043          GO TO 206
0044       202 CALL NMHS2(X(I),ALFAI,FX(I),FY(I),XMZ(I),XIA,XIS)
0045          GO TO 206
0046       203 CALL NMHS3(X(I),ALFAI,FX(I),FY(I),XMZ(I),XIA,XIS)
0047          GO TO 206
0048       204 CALL NMSKI(X(I),ALFAI,FX(I),FY(I),XMZ(I),XIA)
0049          GO TO 206
0050       205 CALL NMGDR(X(I),ALFAI,FX(I),FY(I),XMZ(I),XIA)
0051       206 CONTINUE
0052          GO TO (80,90),ISW2

0053        80 WRITE(5,8000)I,ALFAI,X(I),FX(I),FY(I),XMZ(I),  XIA,XIS
0054        90 X(I+1)=X(I)+DSX
0055        70 CONTINUE
0056          GO TO (71,72),ISW2
0057        72 CONTINUE
0058          IF(IMODE-1)160,160,150
0059       160 CALL NMGR2
0060       150 CALL NMPL3
0061        71 CONTINUE
0062          GO TO 2000
           C  . . . . . .
           C  ============================================================
           C
0063        60 GO TO (61,62),ISW2
0064        61 CONTINUE
0065          WRITE(IPR,5000)
0066          WRITE(IPR,6000)
0067        62 CONTINUE
0068          SXI=0.
0069          X(1)=ALFI1
0070          DO 101 IMODE=1,5
0071          DO 100 I=1,M
0072          GO TO (207,208,209,210,211),IMODE
0073       207 CALL NMHS1(SXI,X(I),FX(I),FY(I),XMZ(I),XIA)
0074          GO TO 212
0075       208 CALL NMHS2(SXI,X(I),FX(I),FY(I),XMZ(I),XIA,XIS)
0076          GO TO 212
0077       209 CALL NMHS3(SXI,X(I),FX(I),FY(I),XMZ(I),XIA,XIS)
0078          GO TO 212
0079       210 CALL NMSKI(SXI,X(I),FX(I),FY(I),XMZ(I),XIA)
0080          GO TO 212
0081       211 CALL NMGDR(SXI,X(I),FX(I),FY(I),XMZ(I),XIA)
0082       212 CONTINUE
0083          GO TO (110,120),ISW2
0084       110 WRITE(IPR,8000)I,X(I),SXI,FX(I),FY(I),XMZ(I),  XIA,XIS
0085       120 X(I+1)=X(I)+DALFA
0086       100 CONTINUE
0087          GO TO (101,102),ISW2
0088       102 CONTINUE
0089          IF(IMODE-1)140,140,130
0090       140 CALL NMGR2
0091       130 CALL NMPL3
0092       101 CONTINUE
0093      2000 CALL EXIT
           C
```

```
C     ------------------------------------------------------------------
C
0094   1000 FORMAT(2F4.0,I3)
0095   1100 FORMAT(5F8.3)
0096   1200 FORMAT(I1,6A2)
0097   1201 FORMAT(2I1)
0098   5000 FORMAT(1H1)
0099   6000 FORMAT(10X,'SLIP ANGLE     LONG. SLIP     FORCE-LONG     FORCE-L
      +,      MOMENT'/11X,7H(ALPHA),10X,4H(SX),11X,4H(FX),11X,4H(FY),
      +11X,4H(MZ)/11X,7HDEGREES,8X,7HPERCENT,8X,8H1000 LB.,7X,8H1000 LB
      +6X,10H1000 LB-IN/10X,'----------     ----------     ----------
      + ----------     ----------'/' ')
0100   8000 FORMAT(I3,5X,F6.2,10X,F6.3,1X,7F15.4)
0101   7000 FORMAT(5X,'MUO=',F4.2,4X,'MUX=',F4.2,4X,'MUY=',F4.2//,
      +       5X,'V  =',F4.2,4X,'AS =',F5.3//,
      +       5X,'CS =',F4.1,4X,'CALFA=',F4.1/)
0102   7100 FORMAT(5X,'KX =',F4.2,4X,'KY =',F4.2,4X,
      +       'BX =',F5.3,3X,'BY =',F5.3//,
      +       5X,'FZ =',F4.2,4X,'L  =',F5.3//)
C     ------------------------------------------------------------------
C     ------------------------------------------------------------------
C
0103       END

      ROUTINES CALLED:
      NMHS1 , NMHS2 , NMHS3 , NMSKT , NMGDR , NMGR2 , NMPL3
      EXIT

      OPTIONS =/ON,/OP:3

      BLOCK        LENGTH
      MAIN.    1331    (005146)*
      .$$$$.   1827    (007106)

      **COMPILER ----- CORE**
         PHASE       USED  FREE
      DECLARATIVES 00622 14243
      EXECUTABLES  01335 13530
      ASSEMBLY     01805 17700
```

```
      C*NMHS1.........HSRI / NBS TIRE MODEL - FIRST (DOC. 6, REF. 3).....
      C     ************************************************************
0001        SUBROUTINE NMHS1(SX,ALFA,FX,FY,MZ,XIA)
      C
      C.....COMPLETE SLIDING POSSIBLE ONLY AT WHEEL LOCK.
      C     MOMENT IS NOT COMPUTED.
      C     WHEEL LOCK FORCES ARE COMPUTED.
      C     NO TRANSITION FROM ADHESION TO SLIDING.
      C     ..... ... ... ... ... ... ... ... ... ... ... ... ... ... ...
      C     ************************************************************
      C
0002        REAL MU,MUX,MUY,MZ,KX,KY,L,MUO
0003        COMMON IBUFF(1799)
0004        COMMON MUO,AS,V,MUX,MUY
0005        COMMON CS,CALFA
0006        COMMON KX,KY,BX,BY
0007        COMMON L,FZ
      C     ..... ... ... ... ... ... ... ... ... ... ... ... ... ... ...
      C     ************************************************************
      C
0008        MZ=0.
0009        ALF=ALFA*.0174533
0010        SY=SIN(ALF)/COS(ALF)
0011        IF(SX)21,23,21
0012     23 IF(SY)21,22,21
0013     22 FX=0.
0014        FY=0.
0015        XIA=1.
0016        GO TO 30
0017     21 CONTINUE
0018        IF(SX-1.)20,20,80
0019     80 SX=1.
0020     20 VS=V*COS(ALF)*SQRT(ABS(SX)**2.+ABS(SY)**2.)
0021        MU=MUO*(1.-AS*VS)
0022        TEMP=SQRT(ABS(SX*CS)**2.+ABS(SY*CALFA)**2.)
      C
      C.....DETERMINE ADHESION RANGE.
      C
0023        IF(SX-1.)40,10,22
0024     40 XIA=.5*MU*(1.-SX)/TEMP
0025        IF(1.-XIA)50,50,60
0026     50 XIAP=1.
0027        GO TO 70
0028     60 XIAP=XIA
      C
      C.....ADHESION AND SLIDING.
      C
0029     70 FX=CS*SX/(1.-SX)*XIAP*(2.-XIAP)
0030        FY=CALFA*SY/(1.-SX)*XIAP*(2.-XIAP)
0031        GO TO 30
      C
      C.....COMPLETE SLIDING (WHEEL LOCK).
      C
0032     10 XIA=0.
0033        TEMP=SQRT(ABS(SX*CS)**2.+ABS(SY*CALFA)**2.)
```

```
0034            FX=CS*MU/TEMP
0035            FY=CALFA*MU*SY/TEMP
          C
          C.....MULTIPLY BY FZ.
          C
0036         30 FX=FX*FZ
0037            FY=FY*FZ
          C
          C     ----------------------------------------------------------------
          C
0038            RETURN
0039            END

          ROUTINES CALLED:
          SIN    , COS    , SQRT   , ABS

          OPTIONS =/ON,/OP:3

          BLOCK        LENGTH
          NMHS1    410     (001464)*
          .$$$$.   1825    (007102)

          **COMPILER ----- CORE**
             PHASE        USED  FREE
          DECLARATIVES  00622 14243
          EXECUTABLES   00967 13898
          ASSEMBLY      01185 18320
```

```
      C*NMHS2.....HSRI / NBS TIRE MODEL - SECOND (DOC, 6, REF, 4)
      C     ------------------------------------------------------------
      C
0001        SUBROUTINE NMHS2(SX,ALFA,FX,FY,MZ,XIA,XIS)
      C     ------------------------------------------------------------
      C     ------------------------------------------------------------
      C
      C.....COMPLETE SLIDING POSSIBLE ONLY AT WHEEL LOCK.
      C     WHEEL LOCK FORCES ARE COMPUTED.
      C     TRANSITION FROM ADHESION TO SLIDING.
      C     UNIFORM VERTICAL PRESSURE DISTRIBUTION
      C     ------------------------------------------------------------
      C     ------------------------------------------------------------
      C
0002        REAL MU,MUO,MZ,MZA,MZT,MZS,MZP,KY,KX,L,MUX,MUY
0003        COMMON IBUFF(1799)
0004        COMMON MUO,AS,V,MUX,MUY
0005        COMMON CS,CALFA
0006        COMMON KX,KY,BX,BY
0007        COMMON L,FZ
      C     ------------------------------------------------------------
      C     ------------------------------------------------------------
      C
0008        ALF=ALFA*.0174533
0009        SY=SIN(ALF)/COS(ALF)
0010        IF(SX)21,23,21
0011     23 IF(SY)21,22,21
0012     22 FX=0.
0013        FY=0.
0014        MZ=0.
0015        XIA=1.
0016        XIS=1.
0017        GO TO 40
0018     21 CONTINUE
0019        IF(SX-1.)10,10,20
0020     20 SX=1.
0021     10 SP=SQRT((ABS(SX)**2.)+(ABS(SY)**2.))
0022        VS=V*COS(ALF)*SP
0023        MU=MUO*(1.-AS*VS)
0024        IF(SX-1.)30,15,22
      C
      C.....COMPLETE SLIDING (WHEEL LOCK).
      C
0025     15 XIA=0.
0026        XIS=0.
0027        XIAP=0.
0028        XISP=0.
0029        SXP=0.
0030        SYP=0.
0031        GO TO 100
      C
      C.....DETERMINE ADHESION AND TRANSITION LIMITS.
      C
0032     30 SXP=SX/(1.-SX)
0033        SYP=SY/(1.-SX)
```

```
0034          TEMP=SQRT((ABS(SX*CS)**2.)+(ABS(SY*CALFA)**2.))
0035          XIA=.5*MUO*(1.-SX)/TEMP
0036          XIS=.5*MU*(1.-SX)*(1./CS+1./CALFA)/SP
0037          IF(1.-XIA)50,50,60
0038       50 XIAP=1.
0039          XISP=1.
0040          GO TO 100
0041       60 IF(XIS-XIA)70,70,80
0042       70 XIAP=XIA
0043          XISP=XIA
0044          GO TO 100
0045       80 IF(1.-XIS)90,90,110
0046       90 XIAP=XIA
0047          XISP=1.
0048          GO TO 100
0049      110 XIAP=XIA
0050          XISP=XIS
          C
          C.....DETERMINE FORCES IN CONTACT PATCH.
          C
0051      100 FXA=CS*SXP*XIAP**2.
0052          FXT=(CS*SXP*XIAP+.5*MU*SX/SP)*(XISP-XIAP)
0053          FXS=MU*SX/SP*(1.-XISP)
0054          FX=FXA+FXT+FXS
          C
0055          FYA=CALFA*SYP*XIAP**2.
0056          FYT=(CALFA*SYP*XIAP+.5*MU*SY/SP)*(XISP-XIAP)
0057          FYS=MU*SY/SP*(1.-XISP)
0058          FY=FYA+FYT+FYS
          C
0059          MZA=(.66666*SXP*(CS-CALFA)*XIAP-.16666*CALFA*(4.*XIAP-3.))*SYP*X
             1IP**2.
0060          MZT=.66666*((CS-CALFA)*(SYP*SXP*XIAP*XIAP+.25*(1./CALFA+1./CS)*M
             1SYP*SX/SP*XIAP+.25*MU**2./(CS*CALFA)*SX*SY/SP**2.)-.25*(CALFA*SY
             2XIAP*(4.*XIAP+2.*XISP-3.)+.5*MU*SY/SP*(2.*XIAP+4.*XISP-3.)))*(XI
             3-XIAP)
0061          MZS=.5*MU*SY/SP*(SX/SP*MU*(1./CALFA-1./CS)-XISP)*(1.-XISP)
0062          MZP=-(BX/KX-BY/KY)*FX*FY
0063          MZ=MZA+MZT+MZS+MZP/L
          C
          C.....MULTIPLY BY FZ AND L.
          C
0064          FX=FX*FZ
0065          FY=FY*FZ
0066          MZ=MZ*FZ*L
          C     . . . . . .
          C     ----------
          C
0067       40 RETURN
0068          END

          ROUTINES CALLED:
          SIN    , COS    , SQRT   , ABS

          OPTIONS =/ON,/OP:3

          BLOCK        LENGTH
          NMHS2    797     (003072)*
          .$$$$.   1825    (007102)
```

```
      C*NMHS3.....HSRI/NBS TIRE MODEL III
      C     ------------------------------------------------------------
      C
0001        SUBROUTINE NMHS3(SX,ALFA,FX,FY,MZ,XIA,XIS)
      C     ------------------------------------------------------------
      C
      C.....COMPLETE SLIDING POSSIBLE ONLY AT WHEEL LOCK.
      C     WHEEL LOCK FORCES ARE COMPUTED.
      C     TRANSITION FROM ADHESION TO SLIDING.
      C     PARABOLIC VERTICAL PRESSURE DISTRIBUTION.
      C     ------------------------------------------------------------
      C
0002        REAL MU,MUO,MZ,MZA,MZT,MZS,MZP,KY,KX,L,MUX,MUY
0003        COMMON IBUFF(1799)
0004        COMMON MUO,AS,V,MUX,MUY
0005        COMMON CS,CALFA
0006        COMMON KX,KY,BX,BY
0007        COMMON L,FZ
      C     ------------------------------------------------------------
      C
0008        ALF=ALFA*.0174533
0009        SY=SIN(ALF)/COS(ALF)
0010        IF(SX)21,23,21
0011     23 IF(SY)21,22,21
0012     22 FX=0.
0013        FY=0.
0014        MZ=0.
0015        XIA=1.
0016        XIS=1.
0017        GO TO 999
0018     21 CONTINUE
0019        IF(SX-1.)10,10,20
0020     20 SX=1.
0021     10 SP=SQRT(SX*SX+SY*SY)
0022        VS=V*COS(ALF)*SP
0023        MU=MUO*(1.-AS*VS)
0024        IF(SX-1.)30,15,22
      C
      C.....COMPLETE SLIDING (WHEEL LOCK).
      C
0025     15 XIA=0.
0026        XIS=0.
0027        XIAP=0.
0028        XISP=0.
0029        SXP=0.
0030        SYP=0.
0031        GO TO 120
      C
      C.....DETERMINE ADHESION AND TRANSITION LIMITS.
      C
0032     30 SXP=SX/(1.+SX)
0033        SYP=SY/(1.+SX)
```

```
0034            TEMP=SQRT((ABS(SX*CS)**2.)+(ABS(SY*CALFA)**2.))
0035            XIA=1.-TEMP/(3.*MUO*(1.-SX))
0036            XIS=1.-CS*CALFA/(CS+CALFA)*SP/(3.*MU*(1.-SX))
        C
0037            IF(XIS)35,35,40
0038         35 XIAP=0.
0039            XISP=0.
0040            GO TO 120
        C
0041         40 IF(XIA)45,45,50
0042         45 XIAP=0.
0043            XIA=0.
0044            GO TO 90
        C
0045         50 IF(1.-XIA)60,60,70
0046         60 XIAP=1.
0047            XISP=1.
0048            GO TO 120
        C
0049         70 IF(XIS-XIA)80,80,90
0050         80 XIAP=XIA
0051            XISP=XIAP
0052            GO TO 120
0053         90 IF(1.-XIS)100,100,110
0054        100 XIAP=XIA
0055            XISP=1.
0056            GO TO 120
0057        110 XIAP=XIA
0058            XISP=XIS
        C
        C.....COMPUTATION OF TRACTION FORCE.
        C
0059        120 FXA=CS*SXP*XIAP**2.
0060            FXT=(1./3.*CS*SXP*(3.-2.*XIAP-XISP)*XIAP/(1.-XIAP)+
               +MU*SX/SP*(3.-2.*XISP-XIAP)*XISP)*(XISP-XIAP)
0061            FXS=MU*SX/SP*(1.-3.*XISP**2.+2.*XISP**3.)
0062            FX= FXA+FXT+FXS
        C
        C.....COMPUTATION OF CORNERING FORCE.
        C
0063            FYA=CALFA*SYP*XIAP**2.
0064            FYT=(1./3.*CALFA*SYP*(3.-2.*XIAP-XISP)*XIAP/(1.-XIAP)+
               +MU*SY/SP*(3.-2.*XISP-XIAP)*XISP)*(XISP-XIAP)
0065            FYS=MU*SY/SP*(1.-3.*XISP**2.+2.*XISP**3.)
0066            FY= FYA+FYT+FYS
        C
        C.....COMPUTATION OF ALIGNING MOMENT.
        C
0067            MZA=2./3.*SXP*SYP*(CS-CALFA)*XIAP**3.-1./6.*SYP*CALFA
               +    *(4.*XIAP**3.-3.*XIAP**2.)
0068            MZT=SY*(CS-CALFA)*(SX/((1.-SX)**2.)*XIAP**2./((1.-XIAP)**2.)
               +**1./15.*(6.*XIAP**2.+3.*XIAP*XISP+XISP**2.-15.*XIAP-5.*XISP+10.)
               +*(XISP-XIAP)
0069            MZT=MZT+SY*(CS-CALFA)*(SXP*MU/SP*(1./CS+1./CALFA)*XIAP*XISP/(1.-
               +XIAP)*.1*(3.*XISP**2.+3.*XIAP**2.+4.*XIAP*XISP-10.*(XIAP+XISP)+
               +10.))*(XISP-XIAP)
```

```
0070          MZT=MZT+SY*(CS-CALFA)*(SX*MU**2./(SP**2.*CS*CALFA)*.3*(6.*XISP**
             ++3.*XIAP*XISP+XIAP**2.-15.*XISP-5.*XIAP+10.))*(XISP-XIAP)
0071          MZT=MZT+SY*CALFA/(1.-SX)*XIAP/(1.-XIAP)*1./6.*(3.-3.*XIAP*(2.-XI
             +)-XISP*(3.-XISP)+2.*XISP*XIAP)*(XISP-XIAP)
0072          MZT=MZT+SY*MU*XISP/SP*.5*(3.-3.*XISP*(2.-XIAP)-XIAP*(3.-XIAP)+2.
             ++XIAP*XISP)*(XISP-XIAP)
0073          MZS=MU*SY/SP*(.6*MU*SX/SP*(1./CALFA-1./CS)
             +     *(1.-10.*XISP**3.+15.*XISP**4.-6.*XISP**5.)
             +     -1.5*(XISP**2.-2.*XISP**3.+XISP**4.))
0074          MZP=-(BX/KX-BY/KY)*FX*FY
0075          MZ= MZA+MZT+MZS+MZP/L
              C
              C.....MULTIPLY BY FZ AND L.
              C
0076          FX=FX*FZ
0077          FY=FY*FZ
0078          MZ=MZ*FZ*L
              C     . . . . . .
              C     ----------
              C
0079        999 RETURN
0080          END

              ROUTINES CALLED:
              SIN    , COS    , SQRT   , ABS

              OPTIONS =/ON,/CO,/OP:3

              BLOCK        LENGTH
              NMHS3   1140    (000350)*
              .$$$$.  1825    (007102)

              **COMPILER ----- CORE**
                 PHASE       USED  FREE
              DECLARATIVES 00802 14063
              EXECUTABLES  01387 13478
              ASSEMBLY     01393 18112
```

```
      C
0001          SUBROUTINE  NMSKI(SX,ALFA,FX,FY,MZ,XIA)
      C
      C     ------------------------------------------------------------
      C
      C....COMPLETE SLIDING POSSIBLE WITHOUT WHEEL LOCK.
      C     WHEEL LOCK (SX=1.) CAN BE SPECIFIED.
      C     NO TRANSITION FROM ADHESION TO SLIDING.
      C
      C     ------------------------------------------------------------
      C
0002          REAL MUO,MUX,MUY,MZ,KY,L,KX
0003          COMMON IBUFF(1799)
0004          COMMON MUO,AS,V,MUX,MUY
0005          COMMON CS,CALFA
0006          COMMON KX,KY,BX,BY
0007          COMMON L,FZ
      C
      C     ------------------------------------------------------------
      C
0008          ALF=ALFA * 3.1416/180.
0009          SY=SIN(ALF)/COS(ALF)
0010          IF(SX-1.)10,17,17
0011       17 XIA=0.
0012          SX=1.
0013          SP=SQRT((ABS(SX)**2.)+(ABS(SY)**2.))
0014          GO TO 40
0015       10 IF(SX)16,11,16
0016       11 IF(SY)16,15,16
0017       15 FX=0.
0018          FY=0.
0019          MZ=0.
0020          XIA=1.
0021          GO TO 20
0022       16 CONTINUE
0023          SXP=SX/(1.-SX)
0024          SYP=SY/(1.-SX)
0025          SP=SQRT((ABS(SX)**2.)+(ABS(SY)**2.))
      C
      C.....DETERMINE ADHESION LIMIT.
      C
0026          XIA=1.-SQRT((ABS(SX*CS)**2.)+(ABS(SY*CALFA)**2.))/(3.*MUO*(1.-SX
0027          IF(XIA)40,40,50
0028       50 IF(1.-XIA)60,60,70
      C
      C.....COMPLETE ADHESION
      C
0029       60 FX=CS*SXP
0030          FY=(CALFA+CS*SX)*SYP
0031          MZ=.1666*SYP*(3.*CS*SX-CALFA)+FX*FY/(KY*L)
0032          GO TO 20
      C
      C.....ADHESION AND SLIDING
```

```
      C
0033     70 FX=CS*SXP*XIA**2.+MUX*(SX/SP)*(1.-XIA)**2.*(1.+2.*XIA)
0034        FY=(CALFA+CS*SX)*SYP*XIA**2.+MUY*(SY/SP)*(1.-XIA)**2.*(1.+2.*XIA
0035        MZ=.1666*SYP*(3.*CS*SX+CALFA*(3.-4.*XIA))*XIA**2.
           +    +.5*(SY/SP)*(MUX*SX*(1.+3.*XIA)-3.*MUY*XIA)*(1.-XIA)**2.*XIA
           +    +FX*FY/(KY*L)
0036        GO TO 20
      C
      C.....COMPLETE SLIDING
      C
0037     40 FX=MUX*SX/SP
0038        FY=MUY*SY/SP
0039        MZ=FX*FY/(KY*L)
      C
      C.....MULTIPLY BY FZ AND L.
      C
0040     20 FX=FX*FZ
0041        FY=FY*FZ
0042        MZ=MZ*FZ*L
      C     . . . . . . . . . . . . . . . . . . . . . . . . . . . . . . . .
      C     ================================================================
      C
0043        RETURN
0044        END

      ROUTINES CALLED:
      SIN    , COS    , SQRT   , ABS

      OPTIONS =/ON,/CO,/OP:3

      BLOCK        LENGTH
      NMSKT    575     (002176)*
      .$$$$.   1825    (007102)

      **COMPILER ----- CORE**
         PHASE        USED  FREE
      DECLARATIVES  00802 14063
      EXECUTABLES   01227 13638
      ASSEMBLY      01217 18288
```

```
      C*NMGDR.....GOODYEAR TIRE MODEL (DOC.6, REF.5)
      C     ------------------------------------------------------------
      C
0001        SUBROUTINE NMGDR(SX,ALFA,FX,FY,MZ,XIA)
      C     ------------------------------------------------------------
      C
      C
      C....COMPLETE SLIDING POSSIBLE WITHOUT WHEEL LOCK.
      C     WHEEL LOCK (SX=1.) SHOULD NOT BE SPECIFIED.
      C     NO TRANSITION FROM ADHESION TO SLIDING.
      C
      C     ------------------------------------------------------------
      C
0002        REAL MUO,MUX,MUY,MZ,KY,L,KX
0003        COMMON IBUFF(1799)
0004        COMMON MUO,AS,V,MUX,MUY
0005        COMMON CS,CALFA
0006        COMMON KX,KY,BX,BY
0007        COMMON L,FZ
      C     ------------------------------------------------------------
      C
0008        ALF=ALFA*.0174533
0009        SY=SIN(ALF)/COS(ALF)
0010        IF(SX-1.)10,12,15
0011     15 FX=0.
0012        FY=0.
0013        MZ=0.
0014        XIA=1.
0015        GO TO 20
0016     12 SX=.95
0017     10 IF(SX)16,11,16
0018     11 IF(SY)16,15,16
0019     16 CONTINUE
0020        SXP=SX/(1.-SX)
0021        SYP=SY/(1.-SX)
0022        TEMP=SQRT(ABS(SX*CS)**2.+ABS(SY*CALFA)**2.)
      C
      C.....DETERMINE ADHESION LIMIT.
      C
0023        XIA=1.-TEMP/(MUO*(1.-SX)*3.)
0024        IF(XIA)40,40,50
0025     50 IF(1.-XIA)60,60,70
      C
      C.....COMPLETE ADHESION
      C
0026     60 FX=CS*SXP
0027        FY=CALFA*SYP
0028        MZ=-.16666*CALFA*SYP+.66666*(CS-CALFA)*SXP*SYP
0029        GO TO 20
      C
      C.....ADHESION AND SLIDING
      C
0030     70 TEMP1=1.+XIA+XIA**2.
0031        FX=.33333*CS*SXP*TEMP1
```

```
0032            FY=.33333*CALFA*SYP*TEMP1
0033            MZ=-.16666*SYP*XIA**3.+.066666*(CS-CALFA)*SXP*SYP*(1.+2.*XIA+3.*
               2A**2.+4.*XIA**3.)
0034            GO TO 20
          C
          C.....COMPLETE SLIDING
          C
0035         40 FX=CS*MUO*SX/TEMP
0036            FY=CALFA*MUO*SY/TEMP
0037            MZ= .066666*(CS-CALFA)*SXP*SYP
          C
          C.....MULTIPLY BY FZ AND L.
          C
0038         20 FX=FX*FZ
0039            FY=FY*FZ
0040            MZ=MZ*FZ*L
          C     ------------------------------------------------------------
          C
0041            RETURN
0042            END

          ROUTINES CALLED:
          SIN    , COS    , SQRT   , ABS

          OPTIONS =/ON,/CO,/OP:3

          BLOCK        LENGTH
          NMGDR   438     (001554)*
          .$$$$.  1825    (007102)

          **COMPILER ----- CORE**
             PHASE       USED  FREE
          DECLARATIVES 00802 14063
          EXECUTABLES  01227 13638
          ASSEMBLY     01205 18300
```